UNIVERSITY OF
BIRMINGHAM

Design and Analysis of a 9 DOF Hybrid Parallel Robot

By

Hamid Rakhodaei

A thesis submitted to
The University of Birmingham
for the degree of
DOCTOR OF PHILOSOPHY

School of Mechanical Engineering
University of Birmingham
Birmingham, United Kingdom

October 2013

To Sedigheh and Abdolmohammad for all patience and supports.

Abstract

The research presented in this thesis discusses the design of a new configuration of a hybrid parallel robot with nine degrees of freedom. The robot contains a hexapod and a tripod, which are connected serially to one another. Parallel robots have been studied due to their high stiffness and accuracy rather than serial robots. However, parallel mechanisms have not been widely used in industry due to the lack of workspace and singularities of their structure. A major advantage of the proposed hybrid parallel robot is to increase the work volume while the stiffness of the system remains suitable for a range of industrial applications. Inverse kinematic of the system is the primary formulation used in the majority of this research. The inverse kinematic is calculated by combining the translation and rotation matrices that the robot could create while the position and orientation of the end effector are the input of the formula. The stiffness formulation developed in the research considered the materials of the components, force direction and the kinematics of the system. Finite element analysis is used to compare displacement and stiffness of the system with the theoretical approach. Novel dynamic formulations have been developed by using Newton Euler and inverse kinematics in order to identify the best configurations based on stiffness and velocity of system in any particular position. Three degrees of freedom of the tripod allows the system to reach the same position with a different configuration. The developed program determines the velocity and stiffness of the system for each configuration. The accuracy of the system is analyzed by a CAD model that receives the actuator size and calculates in the kinematic program through the use of an interface program. A physical robot prototype based on the proposed design was built and used to test the developed theoretical model. The control strategies of the robot were developed and tested based on both point to point control and continuous path applications. The path between two points was selected based on the stiffness of the system in a particular position and orientation. A robotic ankle rehabilitation application was successfully used to verify the design of the proposed hybrid parallel robot.

Acknowledgments

I would like to express my gratitude to my supervisor Dr. Mozafar Saadat, whose attitude and guidance inspired me for this project. Without his persistent help this dissertation would not have been possible. Everything represented in this thesis is the result of his guidance and efforts.

I would like to express my deepest appreciation to my loving parents, Sedigheh Moradi Pari and Abdolmohammad Rakhodaei whose words of encouraging and push for tenacity assist me throughout the process.

I would like to thank Che Zulkhairi Abdullah, who was my good colleague, was always willing to help and give his best suggestion. It would be just a lonely lab without him. I also thank my friends, Mohammad Hosein Zulfaghari and Hamed Rowshandel who helped me through my research. In addition, there are some names that I have to thank them, Alireza Rastegarpanah, Guivani Jules and other researcher in laboratory of Dr Saadat.

Finally I would also thank Mohammad Hossein Naghashian for all of his excitement and willingness to provide feedback made the completion of this research.

Table of Contents

Abstract II

Acknowledgments III

List of illustrations IX

List of Tables IX

Chapter 1 Introduction 1

1.1 Parallel Robots Design and Applications 1

1.2 Aim and Objectives 2

1.3 Thesis Layout 5

Chapter 2 Literature Review 7

2.1 Introduction 7

2.2 Kinematic and Stiffness Review 7

2.3 Dynamics Review 11

2.4 Path Planning Review 12

Chapter 3 Inverse Kinematic and Workspace Analysis 16

3.1 Introduction 16

3.2 Kinematic Mapping Motion 17

3.3 Workspace Analysis 20

3.4 Verification of Kinematic 24

3.4.1 Parametric Sweep Modeling 25

3.4.2 Boolean Logic Search Control 26

3.4.2.4 Case 4: Boolean Method for Data Slicing Analysis 35

3.5 Results 37

3.6 Conclusion 38

Chapter 4 Dynamics Analysis 40

4.1 Introduction 40

4.2 Methodology 40

4.3 Dynamics formulation 42

4.4 Optimization Motion 45

4.5 Control Strategy 49

4.6 Results and Discussion 51

4.7 Conclusion 54

Chapter 5 Robot Modeling and stiffness Analysis 55

5.1 Introduction 55

5.2 Designing Hybrid Parallel Robot 56

5.3 Stiffness Calculation 58

5.4 FEA Analysis and Case Studies 64

5.5 Dynamic Stiffness 68

5.6 Dynamic Simulation 71

5.7 Control Simulation Results 74

5.8 Conclusion 76

Chapter 6 Physical Prototype Building 78

6.1 Introduction 78

6.2 Physical Model Components 78

6.3 Static Experimentation and Results 80

6.4 Dynamic Experimentation and Results 85

6.6 Conclusion 92

Chapter 7 Path Planning and Control Strategy 93

7.1 Introduction 93

7.2 Singularity Analysis 94

7.3 Singularity-free Path Planning Approach 97

7.3.1 Initial Polynomial Paths for End-effector 98

7.3.2 Serial Optimization Method 100

7.3.3 Detour Optimization Method 102

7.3.4 Time Determing Method 103

7.4 Results and Discussion 104

7.5 Optimum Methodology 112

7.5.1 Bezier Curve 112

7.5.2 Simulation Results 116

7.5.3 Results of the Optimum Method 120

7.6 Conclusion 121

Chapter 8 Path Planning for Rehabilitation Application 123

8.1 Introduction 123

8.2 Methodology 123

8.2.1 Analysis of Experiment Data 124

8.2.2 Singularity and Limitation 128

8.3 Simulation Results 134

8.4 Theoretical Results of Ankle Motions simulation 139

8.5 Methodology of Dynamics Experimentation 142

8.6 Force Analysis 144

8.7 Simulation Results 146

8.8 Results and Discussion 149

8.9 Conclusion 154

Chapter 9 Conclusion 156

9.1 Introduction 156

9.1 Developed Methodologies and Main Results 157

9.2 Contribution of this Thesis 160

9.3 Future Direction 161

References 162

Appendices 168

Appendix A: Stiffness Development 168

Appendix B: Simulation Results of the HPKM 170

Appendix C: Sensors Calibration 176

Appendix D: Interfacing Program for MATLAB and SOLIDWORKS 181

Appendix E: Drawing of Designed Components 182

List of Illustrations

Figure 3-1: CAD Model and Kinematic Mapping 18

Figure 3-2: Workspace Results of Tripod 22

Figure 3-3: Workspace Results of Hexapod 23

Figure 3-4: Workspace Results of Hybrid Parallel Robot 23

Figure 3-5: 1D Array Network 28

Figure 3-6: Work Volume Outside the Two Obstacles Volumetric Region 34

Figure 3-7: Boolean Method Search Avoiding Obstacles 35

Figure 3-8: Interpolation between Slices 36

Figure 3-9: 1D Path between the 3 Data Slices 36

Figure 3-10: End Effector Tracking Position 37

Figure 4-1: Hybrid Parallel Robot System 41

Figure 4-2: Enhancing the system performance case 1 47

Figure 4-3: Enhancing the system performance case 2 48

Figure 4-4: Functional schematic of Control Model 50

Figure 4-5: Ideal Force of Actuators through the Motion Case 1 52

Figure 4-6: Ideal Force of Actuator through the Motion Case 2 52

Figure 4-7: Velocity Profile of Platform E Case 1 53

Figure 4-8: Acceleration Results of End-Effector for Case 1 53

Figure 5-1: Components of Hybrid Parallel Robot in Assembly 58

Figure 5-2: Stiffness Distribution in Z=50 63

Figure 5-3: FEA Results on Hybrid Parallel Robot 66

Figure 5-4: FEA Results of System in Initial Position 66
Figure 5-5: Deformation for Translational Motion 70
Figure 5-6: Deformation of Rotational Motions 70
Figure 5-7: Force of actuator through the motion Case 1 72
Figure 5-8: Force of actuator through the motion Case 2 72
Figure 5-9: Velocity Profile Case 2 73
Figure 5-10: Position Error of End Effector in X-axis 75
Figure 5-11: Position Error of End effector in Y-axis 75
Figure 5-12: Position Error of End effector in Z-axis 76
Figure 6-1: Results of Deformation for Theoretical and Simulation Methods 80
Figure 6-2: Prototype and Experimentation Model 81
Figure 6-3: Force on Actuators of Tripod 82
Figure 6-4: Applied Force on Actuators on Hexapod 83
Figure 6-5: Force on the Actuators based on the Size of Stroke 84
Figure 6-6: Comparison of Theoretical and Experimental Results 84
Figure 6-7: Motor Force for Experimental Result Case 1 86
Figure 6-8: Experimental Results of Actuator Force of Case1 86
Figure 6-9: Prototyped Hybrid Parallel Robot for Dynamic Test 87
Figure 6-10: Prototyped Hybrid Parallel Robot for Dynamic Test 87
Figure 6-11: Force Comparison on the Actuator in Case 1 88
Figure 6-12: Force Comparison on the Actuator in Case 1 88
Figure 6-13: Force Comparison on the Actuator in Case 1 89
Figure 6-14: Experimental Results of Actuator Force Case 2 90
Figure 6-15: Experimental Results of Actuator Force Case 1 90

Figure 6-16: Comparison of Experimental and Simulation Result Case2 91

Figure 7-1: Flowchart of the MATLAB Program 105

Figure 7-2: Singularity of the Original and Optimized Path 107

Figure 7-3: Motion of Platform A in X-Axis 108

Figure 7-4: Motion of Platform A in Y-Axis 109

Figure 7-5: Motion of Platform A in Z-Axis 109

Figure 7-6: Motion of Platform E in X-Axis 110

Figure 7-7: Motion of Platform E in Y-Axis 111

Figure 7-8: Motion of Platform E in Z-Axis 111

Figure 7-9: The Developed Bezier Curve for End-effectors 114

Figure 7-10: Machining Application for Hybrid Parallel Robot Using the Bezier Curve . 115

Figure 7-11: The Bezier Patch Data 116

Figure 7-12: Applied Force on the Hexapod's Actuators through the Motion Path1 117

Figure 7-13: Applied Force on the Tripod's Actuators through Motion Path1 118

Figure 7-14: Applied Force on the Hexapod's Actuators Path 2 118

Figure 7-15: Applied Force on the Tripod's Actuators path 2 119

Figure 7-16: Theoretical and Simulation Results Comparison of Path 1 120

Figure 7-17: Theoretical and Simulation Results Comparison of Path 2 121

Figure 8-1: Vicon Software Simulation 126

Figure 8-2: Hexapod Motion in Z-Axis for Activity 1 134

Figure 8-3: Hexapod Motion in Z-Axis for Activity 1 135

Figure 8-4: Hexapod Motion in Z-Axis for Activity 1 135

Figure 8-5: Program Modeled for Hybrid parallel robot 136

Figure 8-6: Hybrid Motion in X-axis Activity 1 137

Figure 8-7: Hybrid Motion in Y-axis Activity 1 138
Figure 8-8: Hybrid Motion in Z-axis Activity 1 138
Figure 8-9: Hybrid Parallel Robot and Hexapod Path for Activity 1 140
Figure 8-10: Hybrid Parallel Robot and Hexapod Path for Activity 2 140
Figure 8-11: Hybrid Parallel Robot and Hexapod Path for Activity 3 141
Figure 8-13: Comparison of Experiment and Simulation X-axis 148
Figure 8-12: Program Modeled for Hybrid Parallel Robot 147
Figure 8-14: Comparison of Experiment and Simulation Y-axis 148
Figure 8-15: Comparison of Experiment and Simulation Z-axis 149
Figure 8-16: Obtained Path Motion of Theory and Experimental Data 150
Figure 8-17: Applied Force on the Tripod's Actuators 151
Figure 8-18: Applied Force on the Hexapod's Actuators 151
Figure 8-19: Error of the Motion in X Direction 153
Figure 8-20: Error of the Motion in Y Direction 153
Figure 8-21: Error of the Motion in Z Direction 154
Figure A-1: The Stiffness Comparisons of Two Configuration of Hybrid Robot 171
Figure A-2: FEA Results of the HPKM 6-3-3 with Different Stroke Sizes from 30mm-200mm 172
Figure A-3: FEA Results of the HPKM 3-3-3 with Different Stroke Sizes from 30mm-200mm 173
Figure A-4: Hexapod with a Stroke Size of 100mm FEA Results 174
Figure A-5: Hexapod with a Stroke Size of 200mm FEA Results 174
Figure A-6: Tripod with a Stroke Size of 100mm FEA Results 175
Figure A-7: Results for Calibration of Sensor 1 176

Figure A-8: Results for Calibration of Sensor 2 177
Figure A-9: Results for Calibration of Sensor 3 177
Figure A-10: Results for Calibration of Sensor 4 178
Figure A-11: Results for Calibration of Sensor 5 178
Figure A-12: Results for Calibration of Sensor 6 179
Figure A-13: Results for Calibration of Sensor 7 179
Figure A-14: Results for Calibration of Sensor 8 180
Figure A-15: Results for Calibration of Sensor 9 180
Figure A-16: GUID Control Model with Interface Program 181

List of Tables

Table 1: Parametric Sweep Performance for Case 1 26

Table 2: Random Generator for 3D Interpolation 33

Table 3: Applied Motions to Hybrid Parallel Robot 47

Table 4 : Optimum Motions 48

Table 5: Size of Components of Assembled Cad Model..... 65

Table 6: Lengths of Actuators and End-Effector Position 65

Table 7: Results of Translation Motion Effect on Stiffness in Theory and Simulation 67

Table 8: Applied Motions to Hybrid Parallel Robot 71

Table 9: Fixture Position of the FEA Simulation 170

Table 10: Load Position on Platform..... 170

Table 11: Mesh Information 171

Chapter 1

Introduction

1.1 Parallel Robots Design and Applications

The robots have significant effects on intelligent automation manufacturing. The robots using for industries mostly are fixed with manipulator and end-effector (Serial Robots). The robots were the reason of accuracy and productivity of industries such as car production, packing, building electronics board.

Improving in manufacturing technology required more accuracy and force mobility for applications and parallel robot was one of the solutions. Parallel robots are close kinematic chain mechanisms. Limbs connect the two platforms that each limb contains at least one joint. Number and type of joints in a structure are depending on the required number of degrees of freedom. Usually, in parallel robots, spherical, universal and prismatic joints are used [1].

High accuracy and stiffness are two important factors for a number of industrial robotic applications such as operations involving automated aerospace assembly. Parallel Kinematic

Mechanisms (PKM) have been considered for these applications due to their high load mobility and accuracy. However, this kind of robots has not been widely used in industry due to the lack of the workspace, as compared to serial robots. The hybrid parallel robots (Truss robots) contain two are more parallel robots that are serially connected to each other. Truss robots have larger workspace rather than the conventional structures of parallel robots such as the hexapod or the tripod.

In this project a new configuration of hybrid parallel robot is investigated. Hybrid parallel kinematic mechanisms (HPKM) (Truss configuration) support more work volume while the stiffness is decreased. The proposed model is investigated in terms of force mobility and control methodology. The system includes a six degrees of freedom robot as the base, and a three degrees of freedom at the top. The added tripod increases the capability of the system in translation and rotational motion. The design of the hybrid system has to be considered in conjunction with a minimum loss in overall stiffness of the system.

1.2 Aim and Objectives

The aim of this project is to develop a 9 DOF reconfigurable hybrid parallel robot for industrial applications that require larger work volumes than conventional parallel robots, while providing higher stiffness compared with serial robots. The focus of the research is the development of the robot system's kinematics, stiffness and dynamic analysis.

The objectives of the project are as follow:

- Development and verification of inverse kinematic of hybrid parallel robot

The first step is to investigate kinematic relations of different configurations of parallel robot, such as the Stewart platform and 3-DOF in order to develop the inverse kinematics of the hybrid parallel robot. Developing inverse kinematics of the system is a required step to calculate workspace, stiffness and dynamics of the model.

- Development of dynamics analysis of the system

The developed methodology of dynamics of the system is used to determine the required actuators' force and velocity of the end-effector for different motions. The dynamics of the system will be required for the robot's control strategy development.

- Design of CAD model and analysis of robot stiffness

The overall structure of the model including all components assembly is designed for static and dynamic simulations of the system. The results will be used to validate system's dynamic and stiffness.

- Build physical prototype and perform static and dynamic experimentation

The design of the hybrid parallel robot is prototyped, in order to test the robot and validate the proposed dynamics and stiffness formulation. The provided force sensors determine the applied force on the actuators in a static state and through the motions. The experimentation rig is used to test the control strategy developed for the system.

- Development of control strategy and algorithm

The results of inverse kinematics and dynamics of the theory are used to control the motion actuators and end-effector. The developed methodologies help increase the performance of the system for different applications.

- Systems verification through an industrial application

The robotic ankle rehabilitation application is used to test the developed control model of the hybrid parallel robot. Path planning of ankle motions are applied to the system to validate accuracy of the required force for this application.

1.3 Thesis Layout

Chapter 1 gives and introduction to the thesis and presents the research aim and objectives. Chapter 2 provides a literature review on stiffness, kinematics, dynamics and control models for parallel robots.

Inverse kinematics of a hybrid parallel robot is developed in chapter 3. The joints' positions and actuators' position vectors are identified by using the developed transformation matrix for end-effector. The obtained positions of end-effector by using theoretical method are compared with results of a Python simulation.

Chapter four explains the inverse dynamics methodology of hybrid parallel robot by using Euler-Newton approach in order to calculate the velocity and applied force on the actuators as well as velocity and acceleration of end-effector. The motions of the hybrid parallel robot are simulated with SOLIDSIMULATION software in order to investigate applied force on the actuators for two considered motions.

Chapter five introduces the 3D CAD model of hybrid parallel robot in order to apply finite element analysis on the system. This is then used to verify the theoretical development. The 3D model of the platforms will later assist to build a physical prototype of the model.

Chapter six explains the processes of prototyping of physical model. Here the components of the robot are introduced. Force sensors obtain the applied forces on the actuators in static and dynamic situations. The results are then compared against the simulation and theoretical values.

Chapter seven discusses the free singularity path planning methodology of the hybrid parallel robot by using point to point control strategy. In this method, limitations of joints and singularities of the system are identified in order to enhance the efficiency of the motions Bezier curves applied to control strategy.

Chapter eight introduces the path planning for a robotic ankle rehabilitation application. The foot motions are obtained by using experimental method.

Chapter nine provides a conclusion of this project. A summary of design methodologies and main results, including the research contributions of the project are presented.

Chapter 2

Literature Review

2.1 Introduction

This chapter addresses the review of the published work on parallel robot mechanisms. The review begins with the kinematics and stiffness analysis of the different configuration of parallel robots existing in the market. The dynamics and control methods of the models are investigated and compared in order to identify the suitable method to control hybrid parallel robot.

2.2 Kinematic and Stiffness Review

Stiffness and accuracy are the most important characteristics making parallel mechanisms suitable for applications such as machine tools. However, serial robots are preferable for use in industry for pick and place, due to the small workspace and singularities of parallel robots [1]. The focus of the investigation is to develop the parallel mechanism for jigging airplane wings for aerospace industry. The system contains a three degrees of freedom robot attached

to the top of a hexapod's moving platform. Delta and hexapod are the most well-known structures of parallel robots, which have been investigated for decades, analyzing stiffness and workspace. Stiffness of a tripod and hexapod were previously investigated by calculating the deformation caused by external force on the end effector. Therefore, the developed model depends on the material properties and length of the actuators [2]. Stiffness of a parallel robot can be developed by considering different parameters such as joints and platforms' positions, structural architecture and its end effector's position and orientation [3]. Different researchers have developed the stiffness of parallel robots based on a developed Jacobean matrix for different configurations [4-7].

Inverse Kinematic is the method that was used in different studies to find the workspace of the parallel mechanism [8-11]. Shi Yan and Lu Yi found a method to demonstrate the workspace in CAD software for a particular model [12]. Zhongfei obtained a new general and parametric formulation of a parallel manipulator's workspace for different geometries [13]. Daniel Lazard obtained a different arrangement of the hexapod's configurations [14]. Combinational parallel mechanism was designed and kinematic and dynamic formulations were calculated based on kinematic change in models [15-17]. Saglia added the redundant actuator to the hexapod for a stiffer structure [18]. Due to the limited workspace of the parallel robots, new configurations were investigated for surgery application [19]. However, the stiffness of parallel robots for industry application was studied using 5-axis machines and a 6-DOF manipulator [20, 21]. The hybrid and planner 3DOF parallel manipulators are a new configuration of parallel robots which were investigated in terms of stiffness [22, 23]. Hybrid

parallel robot structures improved the limited workspace of a 6-DOF. This made the hybrid parallel robot more efficient to use for industry for structural component assembly applications [24-25].

The stiffness of the different structures of hybrid parallel robots was investigated for elastic deformation [26]. The formulation of stiffness for HPKM in a multi-dimensional vibration isolator was developed [27]. The parallel robots could be defined as closed loop mechanisms with higher accuracy and stiffness rather than their serial counterparts. A dangerous problem with parallel robots is the singularity points in the workspace due to the limitation of the joints' motion and orientation of the moving platform. Typically square, spherical or hemispherical grid systems are used to determine the workspace for parallel robots [28, 29]. Various workspaces such as constant orientation or translation workspace, which are application-specific search methodologies and require low-to-medium computational time, are presented [30]. The other workspace types, including maximal, inclusive, total orientation, dextrous and reduced total orientation, require an orientation check for a specific task or region, or other advanced searches. The computational process of finding the workspace is complex and more factors needed to be checked such as Grassman vector, stiffness, and cost factor [31]. The conventional geometrical grid search is not useful for coplex workspace calculation [32]. There are different methods to search the workspace of system suck as constant position and various orientations which is required for some industries [33].

In order to reduce the time of search process, the geometrical shape (Hemisphere, cube) of data designed to be input of search methodology. This method positioned the end-effector in the edge of shape to make the actuators to reach to their maximum stroke. The angles of the joints, actuator size needed to be check to verify the data in workspace [34]. The described methodology to find work volume is called ‘parametric sweep’ [35].

Another method which is called Boolean Logic was investigated. This method uses the maximum and minimum size of actuators and joins’ angle limitation as input of algorithm. The position vectors of actuators are used in order to find singularities in the workspace. The concept of this method using combination of AND, NAND and NOR logics to check the conditions. The described conditions are useful to create the factors of search. However this method just could be used for limited applications [36].

Boolean search method is optimized in order to reduce the redundant process of search. Although the time of process is reduced, the method was not accurate to identify the all singular points through the workspace. The method uses the mesh surfaces to create the workspace then checks for the redundancy. The algorithm is used to increase resolution and accuracy of search and reducing the process time. [37, 38]. Slicing method assists the investigation of any slices in workspace of system. This method could improve the efficiency of searching and investigation. [39].

2.3 Dynamics Review

The parallel robots are closed loop mechanical chains having properties such as high mobility and accuracy compare to serial robots [40]. Complex kinematic and non-linear dynamic equations for different configurations of parallel robot have been investigated for an accurate controlling system. Stewart platform and delta are the most famous structures which have been investigated to develop the dynamic equations. The developed configuration of a parallel robot for aerospace application contains delta connecting serially to the hexapod. The developed methodology for the dynamic of the proposed system is expanding the hexapod structure to calculate the end-effector motions having three degrees of freedom [41]. The inverse dynamic of a hexapod and other configurations have been investigated for years [42-44]. The first step of developing the dynamic equation is mapping the inverse kinematic of the system for 3-DOF PKM [45]. The inverse dynamic of a tripod parallel robot was developed by using inverse kinematic [46]. The developed formulation calculated the dived force need for the actuators. Based on the type of actuators, such as pneumatic and hydraulic, the dynamic of the actuators was investigated in different research [47,48].

Besides the inverse kinematic, different methods were considered for the dynamic of a 6-DOF parallel robot; such as the forward dynamic calculated by Lagrange principles and the Newton-Euler method [49-50].

Dynamic equations are key factors for developing the PID controller [51]. In order to enhance the speed of transferring data, the Jacobian matrix was developed for dynamic formulations of 3-DOF and 6-DOF configurations [52-54]. Calculating the linear equation for the real time controlling application system (RTOS) called Xoberon, is another developed method for 6-DOF parallel robots [55]. The acceleration formulation of a rigid body was applied on a robotic dynamic model [56]. The position analysis of joints and the end-effector, based on the kinematic of a robot, was developed to enhance performance of two 3-DOF hybrid parallel robots [57]. However, the dynamic model of 6-DOF parallel robot and hybrid parallel robot were investigated for industrial application [58, 59].

Serial-parallel robot is a new configuration investigated in order to increase the performance of PKM robots [60]. However, there is some research concerning the inverse kinematic and dynamic of a 2(RPS) hybrid parallel robot configuration [61].

2.4 Path Planning Review

To plan paths for parallel manipulators, the singularity configurations of the manipulator should be avoided. Kinematic singularities are particular poses of the end-effector where parallel robots lose their inherent infinite rigidity. J.-P. Merlet categorized singularities into two types of serial and parallel singularities [62]. It is widely believed that serial singularities are obtained on the boundary of the workspace, while parallel singularity presents when the

actuator forces on the legs cannot support the path planning approach of the hybrid parallel robot developed based on its inverse kinematic analysis. Inverse kinematic analysis gives the relation between position of joint and end-effector poses based on the physical structure of a robot. For each given pose of the end-effector, the inverse kinematic analysis calculates out the length of the actuators on each leg of the robotic mechanism.

Dasgupta and Mruthyunjaya [63] presented a criterion of singularity configurations for the Stewart platform manipulators. They also developed a singularity-free path planning method based on linear interpolation and conquer algorithm. A singularity-free path planning approach considering the kinetic and potential energy of parallel mechanisms for various types of parallel robots has been introduced by Shamik et al. [64] using Euler-Lagrange equations to solve the singularity-free path. Anjan Kumar Dash, I-Ming Chen et al. [65] described a singularity-free path-planning algorithm by grouping singularity points into various clusters. Currently, a number of researchers are investigating the issue of the singularity-free path planning problems for parallel robots, especially for the Stewart platform parallel manipulators [66].

The parallel robots offer high accuracy and stiffness as compared to serial robots, despite their complex kinematics and small workspace. However, high stiffness of parallel kinematic mechanisms is a crucial characteristic for applications needing strong mobility and high-speed motions. For such motions' controlling model, force and speed of each actuator has to be managed in order to get the desired profile motions of the end effector. In order to calculate

the actuator's stroke for a particular motion, the kinematic relations of the system need to be developed. Forward and inverse kinematics of different structures of PKMs have been studied [67-71]. The kinematics of parallel robots are the most important development for improving the workspace and dynamics. The required force and speed of each actuator for particular motions has been developed based on the dynamic model [72]. Parallel robots are used for applications needing high accuracy, such as surgery [73-75]. However using a neural network tool is another methodology in order to estimate gravity and friction force. In the following method, the inverse kinematic was not used while the velocity of the end effector is an important factor for path planning [76].

The control strategy of a hexapod structure has been investigated with different methods, such as fuzzy and vision-based [77, 78]. Even though there are advantages with parallel robots in terms of stiffness and accuracy, as compared to serial robots, control modelling of parallel robots is complex in practice. Therefore, high accurate controlling of actuators is a good strategy to identify the position of the end effector [79]. Position control strategy and the Generalized Elastic Path Control strategy are two methods applied on parallel robots based on force controlling [80]. In order to obtain the required force for a specific motion, a dynamics model of the system has to be developed. Different structures of parallel robots have been investigated to calculate the force and control model [81-83]. The hydraulic, electromotor actuators have been used in 6-DOF parallel robots in different research while the strategy of controlling is similar [84-87]. The inverse dynamic and controlling strategy of different modeled 3-DOF PKMs was developed [88, 89]. Different methodologies are applied to the

robot in order to enhance the efficiency of the system. Artificial intelligence methods such as fuzzy logic and neural networks are non-classic strategies for controlling the robots [90, 91]. Predicting the control function for a robot manipulator was one of the recent investigations to track the position of the end-effector [92, 93].

The singularity in workspace is the most important weakness of parallel mechanism kinematics. The proposed model is a 9-DOF hybrid parallel robot, being investigated to cover the singular points for particular path motions. This model contains 6-DOF and 3-DOF PKMs that are serially connecting to each other. In this investigation, the considered path for a robot manipulator is studied while initial and end positions are known. The path is calculated based on developed stiffness and the dynamic formulation developing for the end-effector.

Chapter 3

Inverse Kinematic and Workspace Analysis

3.1 Introduction

The paper addresses developing workspace and stiffness of parallel mechanism which includes nine linear actuators connecting three platforms. A new design of parallel robot is developed for pick and place application in the aerospace industry. Two important factors of parallel robots are stiffness and workspace. The proposed method calculates the position vector of each actuator in each pose by using the developed inverse kinematic of the system to obtain the amount and direction of force. The obtained results of stiffness and workspace are compared with hexapod and tripod models. The validity of performance and results are verified with FEA simulation as well as experimental data obtained by sensors.

3.2 Kinematic Mapping Motion

Generally, the position of point can be identified by a transformation matrix containing six independent quantities (linear and rotational motions in XYZ). In order to calculate the position of the end effecter in a particular motion the developed transformation matrix is used, as shown in Equation 3.1.a [94].

$$[T] = \begin{bmatrix} c\phi c\psi & -c\phi s\psi & s\phi & 0 \\ c\Theta s\psi + c\psi s\Theta s\phi & c\Theta c\psi - s\phi s\psi & -c\phi s\Theta & 0 \\ s\Theta s\psi - c\Theta c\psi s\phi & c\psi s\Theta + c\Theta s\phi s\psi & c\Theta c\phi & 0 \\ L & M & N & 1 \end{bmatrix} \quad (3.1.a)$$

$$L = s\psi((mc\Theta + ns\Theta) + c\psi(lc\phi - s\phi(nc\Theta - ms\Theta)) \quad (3.1.b)$$

$$M = c\psi(mc\Theta + ns\Theta) - s\psi(lc - s\phi(nc\Theta - ms\Theta)) \quad (3.1.c)$$

$$N = ls\phi + c\phi(nc\Theta - ms\Theta) \quad (3.1.d)$$

Where,θ,$\emptyset$,ψ are defined rotational components and l, m and n are linear motions in X, Y, Z direction respectively.

The system contains two moveable platforms as shown in Figure 3.1. The motion profiles that contains positions and orientations of the end-effector, is defined for the system.

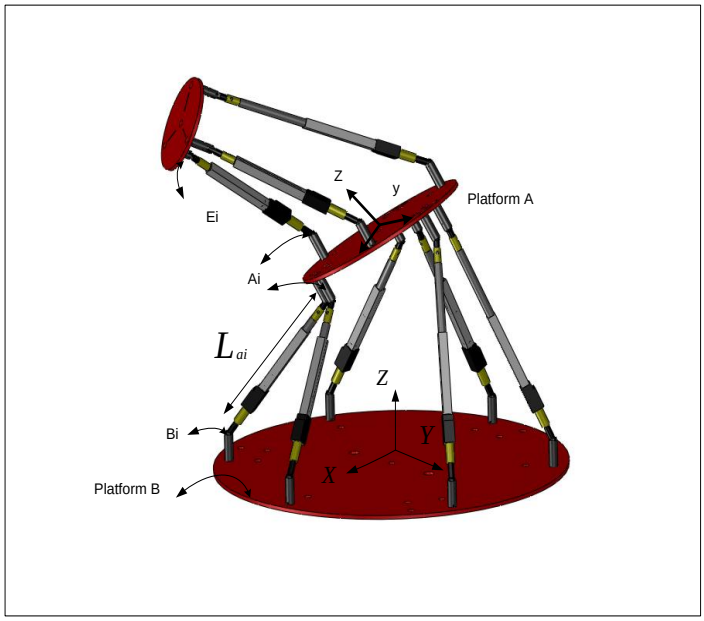

Figure 3-1: CAD Model and Kinematic Mapping

All positions of the platforms and joints are mapped based on the coordinate on the stationary platformO_{XYZ}, therefore the formulation of the centre point and joint position of platform A is obtainable by the motion of the hexapod while the three actuators of the tripod are not moving as follows:

$$[A_i] \times T_O^{A^{-1}} \times R_{\theta\emptyset\psi}^{O} \times T_O^A \times T_{lmn}^A = [A_{2i}]. \quad (3.2)$$

Where, $[A_i]$ is the initial centre position of the centre and all the joints on platform A, $T_O^{A^{-1}}$ is the inverse translation matrix returning centre point of platform A to the origin. $R_{\theta\emptyset\psi}^{O}$ is the rotational matrix with Euler angles, T_O^A is the translation matrix returning back point A to

initial, T_{lmn}^{A} is the translation motion required to reach to the desired position from the initial position and $[\mathrm{A_{2i}}]$ is the centre point and the joints' positions after motion.

Therefore, position of the end effector and joints on platform E by motions of all actuators is calculated in Equation 3.3.a and 3.3.b.

$$[E_i] \times {T_O^A}^{-1} \times R_{\theta\emptyset\psi}^{\mathrm{O}} \times T_O^A \times T_{lmn}^A = [E_{2i}] \tag{3.3.a}$$

$$[E_{2i}] \times {T_{lmn}^E}^{-1} \times {R_{\psi\emptyset\theta}^{\mathrm{O}}}^{-1} \times R_T^{\mathrm{O}} \times R_{\theta\emptyset\psi}^{\mathrm{O}} \times T_{lmn}^E \times T_{lmn}^F = [E_{Fi}] \tag{3.3.b}$$

Where, $[E_i]$ is the initial positions of the centre point and position of the joints on platform E, $[E_{2i}]$ is the position matrix of the end effector centre point and position of the joint after the motion of six actuators, ${T_{lmn}^E}^{-1}$ is the translation matrix returning the centre point of platform E to origin, ${R_{\psi\emptyset\theta}^{\mathrm{O}}}^{-1}$ is the rotational matrix returning platform E to normal orientation. Also R_T^{O} is the rotational matrix created by three actuators, T_{lmn}^E is the translation matrix returning platform E to its initial position. T_{lmn}^F is the translation matrix transforming platform E to the desired position and E_{Fi} is the final position of the end effector.

In Equation 3.3.a, the position of the platform E by the motion of six actuators of the hexapod and the motions of three of the other actuators is applied to determine the final positions of the end effector.

3.3 Workspace Analysis

Inverse kinematics identifies the positions of the platforms and the joints' position through any motion. However, applying the structural limitations of design identifies points existing in the workspace. The applied limitations are the length of strokes and the joints' range of motion. The position of the joints on the hexapod for a particular motion is obtained by Equation 3.2. Therefore, the stroke of each actuator is obtained by calculating the length of each actuator's position vector.

$$L_{Hi} = A_{2i} - B_i \qquad \text{For i= 1,...6} \qquad (3.4.a)$$

Where, L_{Hi} is the position vector system actuators connecting to platform A and B (i=1...6), B_i is the positions of the joints connecting on platform B.

However the positions of the joints attaching on platform E are calculated by Equation 3.3.b in order to find position vectors of three actuators as shown in Equation 3.4.b.

$$L_{Hi} = E_{2j} - A_{2i} \qquad \text{For j= 1, 2, 3 and i= 7, 8, 9} \qquad (3.4.b)$$

Where, L_{Hi} is the position vector of system connecting platform A and E (i=7...9), E_{2j} is the position of joints connecting to platform E, A_{i2} the position of joints connecting to the top of platform A (i=7..9).

The system contains eighteen joints that should be checked for workspace analysis. The angles between the actuators and joints demonstrate the motion of the joints. The angles of joints on platform B are calculated as follows:

$$\alpha_{Bi} = cos^{-1}\left(\frac{U_X.L_{Hi}}{|L_{Hi}|}\right) \qquad \text{For i=1,...,6} \qquad (3.5.a)$$

$$\beta_{Bi} = cos^{-1}\left(\frac{U_y.L_{Hi}}{|L_{Hi}|}\right) \qquad \text{For i=1,...,6.} \qquad (3.5.b)$$

Where, U_X and U_y are axes of the joints on platform B, L_{Hi} is the actuator position vector, α_{Bi} is the angle of the joint with its x-axis and β_{Bi} is the angle of the joint with its Y-axis.

The joint's axes on the platform A is moving with the motion provided for the system (Equation 3.2). The angles of the joint are calculated by Equation 3.6.a and 3.6.b:

$$\alpha_{Ai} = cos^{-1}\left(\frac{u_X.L_{Hi}}{|L_{Hi}|}\right) \qquad \text{For i=1,...,9} \qquad (3.6.a)$$

$$\beta_{Ai} = cos^{-1}\left(\frac{u_y.L_{Hi}}{|L_{Hi}|}\right) \qquad \text{For i=1,...,9.} \qquad (3.6.b)$$

Where, α_{Ai} and β_{Ai} are the joint's angles with their own X-axis and Y-axis respectively and u_X and u_y are axes of the joints after the motion. u_X and u_y are changed respect to U_X and U_y based on rotational motions that applied for the system. Therefore, the axis of revolute joints on platform E is obtained by replacing u_X in Equation 3.b. However the angles of revolute joints are obtained in Equation 3.7.

$$\alpha_{Ei} = cos^{-1}\left(\frac{u_{2X}.L_{Hi}}{|L_{Hi}|}\right) \qquad \text{For i = 1, 2, 3} \qquad (3.7)$$

Where, α_{Ei} (i=1, 2, 3) are the angles of the joints connecting to platform E after the particular motion and u_{2X} is the axis of the revolute joints in a particular pose and orientation.

The structural limitations are applied to the inputs of the desired motions. The workspace of the system is programmed with Cartesian and polar algorithms in MATLAB software packages. The initial positions are obtained by data from the CAD model. The developed program calculates the workspace of the hexapod and tripod as well as that of the hybrid system. The maximum strokes of all actuators are the same in the structure (100 mm). The boundary shapes of the tripod, hexapod and hybrid parallel robot are demonstrated in Figures 3.2, 3.3 and 3.4 respectively.

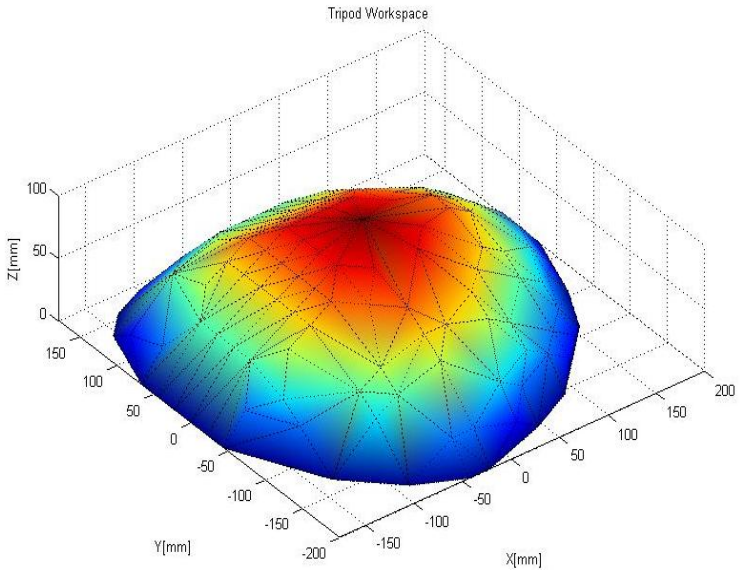

Figure 3-2: Workspace Results of Tripod

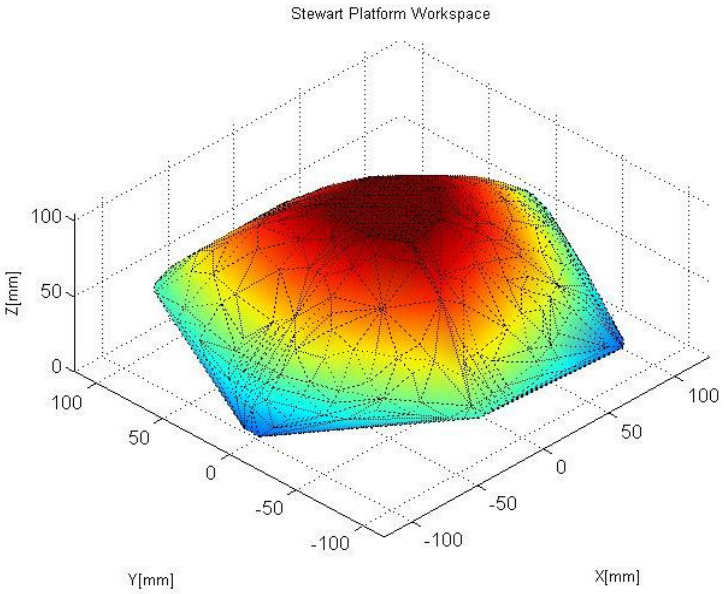

Figure 3-3: Workspace Results of Hexapod

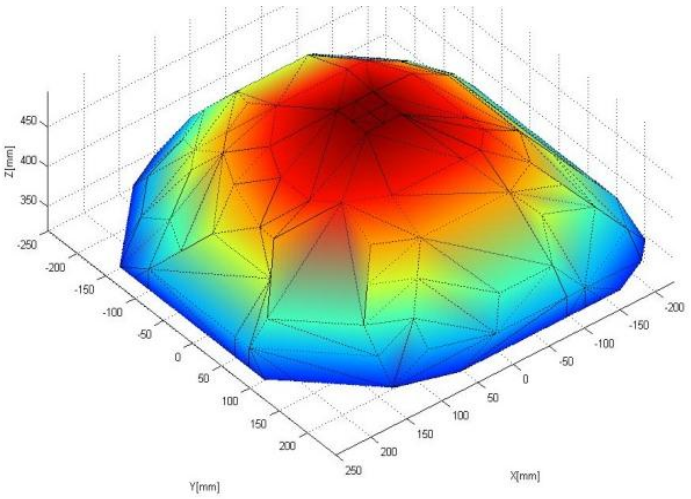

Figure 3-4: Workspace Results of Hybrid Parallel Robot

The obtained results are based on checking the points assumed to be in the workspace; the shape of the workspace is more accurate by increasing the resolution of the number.

3.4 Verification of Kinematic

The robot model was developed using codes based on 3D Visual Python (VPython), Line Collision, Mesh Model, distance and interpolation. The VPython provides 3D visual and graphing as Pencil-Line visualizations.

The workspace of the hybrid parallel robot is first obtained by a numerical method using the inverse kinematic mapping of the system. Then a 3D CAD model was developed in Python. The system is able to perform parametric sweep searches to find non-singular positions. Boolean logic is used to control the search flow and boundaries. Several cases have been simulated such as obstacle-avoidance and mesh-surface workspace. Interval analysis and data slicing were then used to optimize the search method. This method reduces the computational time by reducing search boundaries and focusing on the area of the designed path. The case studies demonstrate non-singularity points for any particular workspace. The obtained data for position and orientation of the moving plates from the simulation is then sent to a pre-verified CAD model for verification.

3.4.1 Parametric Sweep Modeling

Parametric sweep modelling or discretization is a search for workspace following a grid structure shaped as primitive geometric objects, such as square or hemisphere. The object dimensions and grid size are configurable. However, a control structure is required to optimize the search. These controls include the selection of grid type, grid size, region, filter, analysis and strategy. The search is bound for redundant data and involves repeated visits for a node. The obtained data from the numerical method is used to check for the limitation of stroke and angles of the actuators and joints in the robot. However, in this section the limitation in the workspace are obstacles and the surface mesh. Here, the condition for the obstacle can be described in Equation 3.8.

$$W_H = P_w - \cup Q_i \tag{3.8}$$

Where, W_H is the workspace of the hybrid system without obstacle, P_w is the workspace of the hybrid, and Q_i is obstacle space and mesh.

Furthermore, data slice is a method that reduces the searching time for specific motions, to find any particular plane that fits a particular path, as well as modifying the path if singularities are found.

3.4.2 Boolean Logic Search Control

The Boolean method is based on the logic controls of the search and validation strategy to determine singular and non-singular position and orientation workspace. Boolean logic is the control structure that defines the search parameters; search criteria and analysis (refer to Equation 3.10). Search parameters include upper and lower bound and parametric sweep shape. Search criteria include search technique and filter.

Table 1 gives test parameters for 'case 1'. Here, the end-effectors are directed to follow a path, while the system performs workspace analysis for platform A to determine its best path. The process completion time is resolution-dependent, where interval and slicing allows detailed analysis of the region of interest. The numerical method has been used for calibration of the kinematic points.

Table 1: Parametric sweep performance for Case 1

Type	Travel Limit (x, y axis)	Resolution	Time (seconds)
Python Test 1	40 cm	1 unit	34000
Python Test 2	40 cm	5 unit	1100
Python Test 3	40 cm + z – axis(2 slices)	5 unit	2000
Python Test 3	40 cm (x, y & z – axis)	5 unit	17000

Analysis is done on the dataset based on a general structure, constrained structure (by obstacle type and shape), interval analysis and data slicing analysis. The case studies presented here are based on literature search results for various typical and specific workspaces. Reference is made to Figure 3.1 in the following descriptions: Case 1 is a special-case for a hybrid robot system, where the search is for platform E's workspace when platform A is following a pre-defined 3D path. Case 1 optimizes platform E's travel while ensuring minimum trajectory changes during travel. Case 2 is a search for obstacle-free workspace when a set of primitive objects are placed within a known workspace. This obstacle is user-defined, where the dimension, position and accuracy can be configurable and can be used for obstacle-free path planning. Case 3 is an end effector's search for position on a 3D mesh surface. Interval analysis can add a higher resolution search on a specific path on the 3D mesh surface. Case 4 are optimized search strategies, where Boolean analysis is performed on selected information only, which is either a slice or a set.

3.4.2.1 Case 1: Boolean Search for Platform A's Path When Platform E's Path is Known

This experiment attempts to find the middle plate's workspace and path when the top travelling plate is positioned to travel along a given path, where the z-axis has a fixed value. The path parameters show a gradient change in all axes and are as displayed in Figure 2 as 2D array for Platform E. Figure 3.5 shows the collections of non-singular points, which is dictated by different colors to differentiate each region that represent each path segment.

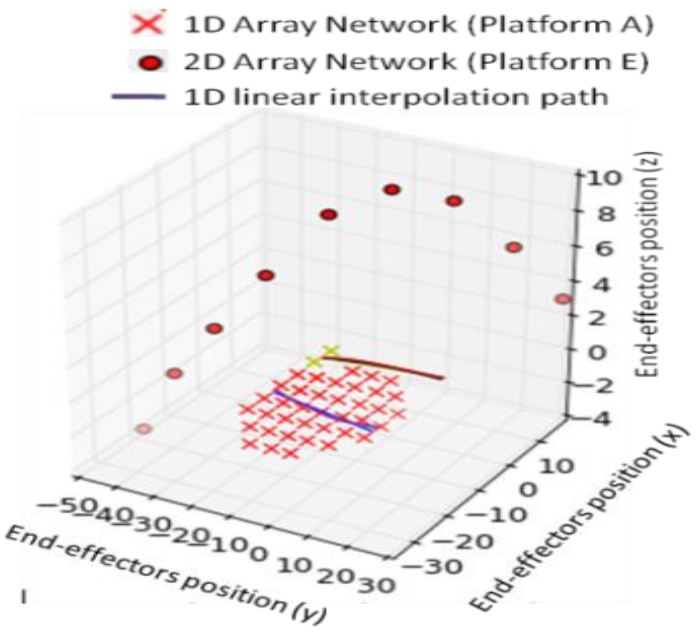

Figure 3-5: 1D Array Network

The collection of possible paths is interpolated to optimize the results. The simulation uses the shortest distance to platform A's centre-point, whose coordinates must be identical to those of the next node in the queue to form platform A's path. The 1D-array interpolation cannot solve the problem without additional values, whereas a 2D-array would help find the optimized path. The additional attribute to make the 2D-array is obtained from the stiffness factor, Grassmannian vector factor, and minimum distance to the centre-point of each corresponding node. The system uses n-D interpolation based on various strategies. An example presented involves weighted value processing based on Equations 3.11 and 3.12 for a random generated position. An example of n-D grid is presented as a trilinear interpolation method based on Equation 3.9.

$$pos[0] = \big((x-g),(y-g),(z-g)\big) \tag{3.9.a}$$

$$pos[1] = \big(x,(y-g),(z-g)\big) \tag{3.9.b}$$

$$pos[2] = \big((x-g),y,(z-g)\big) \tag{3.9.c}$$

$$pos[3] = \big((x-g),(y-g),z\big) \tag{3.9.d}$$

$$pos[4] = (x,(y-g),z) \tag{3.9.e}$$

$$pos[5] = \big((x-g),y,z\big) \tag{3.9.f}$$

$$pos[6] = \big(x,y,(z-g)\big) \tag{3.9.g}$$

$$pos[7] = (x,y,z) \tag{3.9.h}$$

Where pos [0-7] = trilinear interpolation matrices that produce weighted value and g is the resolution.

The weighted value is a collection of processes starting with the establishment of a grid, populating the grid with a strategy, then checking for singularities. The result is then processed for Grassman and other ranking criteria; for example, the nearest distance to the centre-point or a pre-defined path. This ranking criteria, grid and grid population method is extendible. The concept is presented here in Equations 3.10, 3.11 and 3.12:

$$angle_1 = \big(\underline{x}i_1 + \underline{y}j_1 + \underline{z}k_1\big) \tag{3.10.a}$$

$$angle_2 = \big(\underline{x}i_2 + \underline{y}j_2 + \underline{z}k_2\big) \tag{3.10.b}$$

Where angle 1, 2 = vector angle for leg between 2 poses,

$$p = \underline{x}i_1 + \underline{x}i_2 \tag{3.10.c}$$

$$q = \underline{y}j_1 + \underline{y}j_2 \tag{3.10.d}$$

$$r = \underline{z}k_1 + \underline{z}k_2 \tag{3.10.e}$$

$$|a, b, c, d| = \sqrt{p^2 + q^2 + r^2} \tag{3.10.f}$$

Where |a, b, c| = legs stroke or vector magnitude,

|d| = distance to the plate's centre, and $\underline{x}i_1$, $\underline{y}j_1$ *and* $\underline{z}k_1$ represent the start pose, while $\underline{x}i_2$, $\underline{y}j_2$ *and* $\underline{z}k_2$ represent the end pose.

$$angT[0-3, center] = \cos^{-1}(\bar{a}.\bar{b})/(|a|.|b|) \tag{3.10.g}$$

$$angH[0-6, center] = \cos^{-1}(\bar{a}.\bar{b})/(|a|.|b|) \tag{3.10.h}$$

Where AngT represents the tripod angle and AngH represents the hexapod angle,

$$f(pos, limit, error) = pos \wedge limit \rightarrow error \tag{3.10.i}$$

Where pos = end-effector's position x, y and z, limit is the search limit, and error is the stroke, angle and collision error.

$$\omega_a = \sum_{n=0}^{3,center}(\text{angT}[n] - d) > 0 \tag{3.11.a}$$

$$\omega_b = \sum_{n=0}^{6,center}(\text{angH}[n] - d) > 0 \tag{3.11.b}$$

$$\omega_c = \sum_{n=0}^{3,center}(|a[n], b[n], c[n]| - e) > 0 \quad (3.11.c)$$

$$\omega_d = \sum_{n=0}^{6,center}(|a[n], b[n], c[n]| - e) > 0 \quad (3.11.d)$$

$$\omega_e = \sum_{n=0}^{x}(|d[G_n]| \cap |d[G_{n+1}]| \neq 0) \quad (3.11.e)$$

Where ω_a = weighted value for tripod angle if f (ω_a)>0,

ω_b = weighted value for the hexapod angle if f (ω_b)>0,

ω_c = weighted value for the tripod stroke if f (ω_c)>0,

ω_d = weighted value for the hexapod stroke if f (ω_d)>0,

ω_e = weighted value for distance to the plate's centre and at least one data for each group, and G_n represents the slice workspace for each fixed value along the end-effector's path, and e and d are the threshold values.

$$angG[o_1, o_2] = \cos^{-1}(\bar{a}.\bar{b})/(|a|.|b|) \quad (3.12)$$

Where angG [o_1, o_2] = angle differences between various pair-wise comparison of o_1 and o_2, where they represent Grassmann pencil lines such as planar sides, planar planes and line vector sets.

Weighted f, ω_f for σ_n = angG [o_1, o_2] if they are coplanar or meet at infinity, given by the Grassmann rules.

The large sets of comparison-wise checks for a non-coplanar condition have to consider the non-redundant loop and Boolean validation method for all pairs σ_n. Boolean validation where $\sigma_0 \cap \sigma_1 \neq 0$ and $\sigma_n \in$ (comparable pair-wise set σ_c), and σ_c must produce Grassman errors. Grassman error rules include (a) lines for any o_1 and o_2 that meet at infinity, (b) lines for any o_1 and o_2 that have different angles equal to 0 or 180 degrees, and (c) a virtual axis is formed where any opposing force may produce instantaneous rotation resulting in unwanted degrees-of-freedom.

If total weighted, $\omega_{T,}$ for all pairs is found, then weighted sum is calculated to find non-singularities or singularity positions inside or outside the workspace during an application.
An interpolation test for the Python path is carried out by using the scatter distribution of test positions. This can be done, for example, through using 3 sets of 1D-interpolation or trilinear interpolation in order to populate the plot using a random generator (refer to Equation 3.9). Table 2 demonstrates NumPy random generator multivariate normal is tested here for various 3-D arrangements to demonstrate the system potential, and to establish a random-generated 3D grid for cases 2, 3 and 4

Table 2: Random generator for 3D interpolation

Random Generator Types	Time (seconds)	Grassmann Weighted Value ω_f
3-axis x 1-plane arrangement (case 2)	880	17280
3-axis x 4-plane arrangement (case 2)	4400	83008
Trilinear arrangement (case 2)	700	12684

3.4.2.2 Case 2: Boolean Method for Search Whilst Avoiding Obstacle

This case study demonstrates a method of using the Boolean operation to find non-singular positions outside the obstacles placed within the non-singular workspace of the robot system. Two spherical obstacles were placed at two different coordinates. The formulation for the collection of detectors shaped to form the spherical-shaped obstacles is based on standard sphere formula.

Figure 3-6 is an example case for obstacle avoidance or collision detection, where the avoidance of two obstacles placed within the work volume region is demonstrated. The obstacle (developed using Equation 3.8) can be described as a pick and place object, obstacle or working plane. Haptic interaction shall include force feedback interaction with the obstacle while the user navigates or collides with the obstacle.

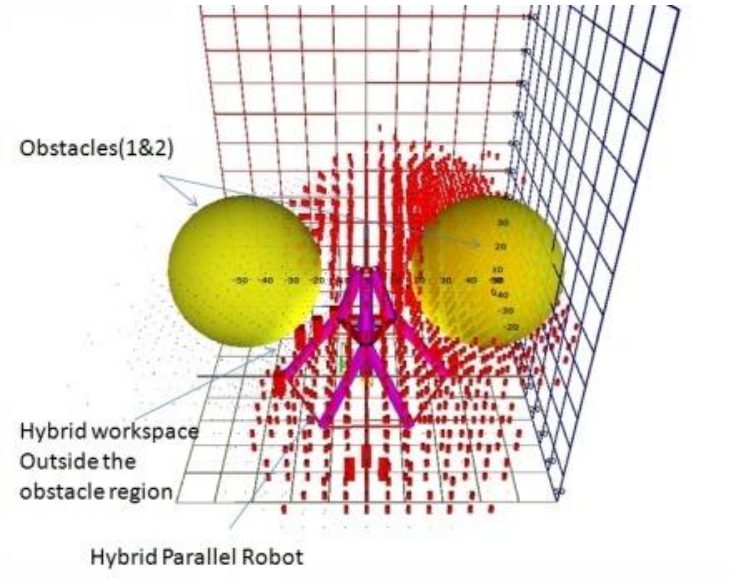

Figure 3-6: Work Volume Outside the Two Obstacles Volumetric Region

3.4.2.3 Case 3: Boolean Method for Search on a Surface Mesh

This is a study of platform E's path for a non-singular condition following a surface mesh placed within the robot workspace. The search objective is to find points on the mesh that have non-singular positions. The search for non-singular points on the mesh surface is generalized by Equation 3.8. Figure 3.7 shows the plot for non-singular points on the mesh. There is no limit to the number of meshes, locations and the shape variations placed in the workspace. A 1D array of the results of regression analysis produces lists of paths. The simulation then continues to perform a parametric sweep to find the best possible path on the mesh surface based on the slicing of sets of planes.

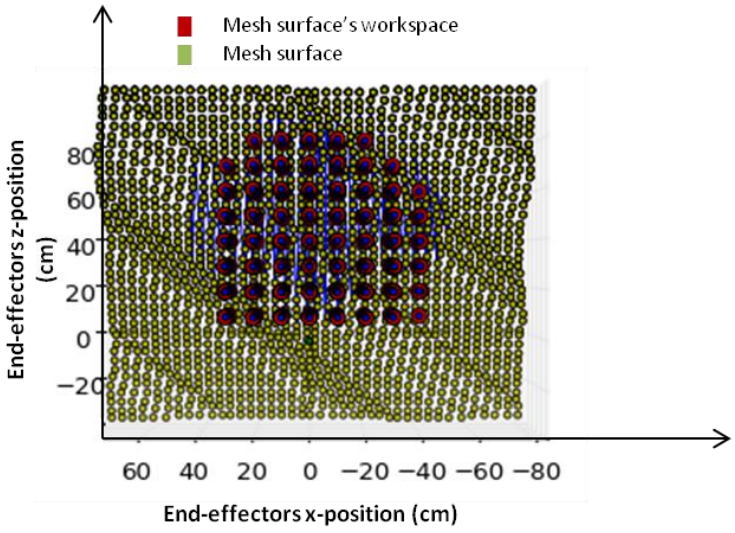

Figure 3-7: Boolean Method Search Avoiding Obstacles

3.4.2.4 Case 4: Boolean Method for Data Slicing Analysis

Slicing analysis operation is a data interpolation between points as shown in Figure 3.8. Here, a 'constant orientation slice' checks a path that goes past each slice of information. The interpolation between points along the path and the slices give extra information regarding the path trajectory. There is a collection of possible points that connect the two data slices at the given 'constant orientation workspace', as shown in Figure 3.9. This is a 2D curve spline interpolation working on 1D-array data.

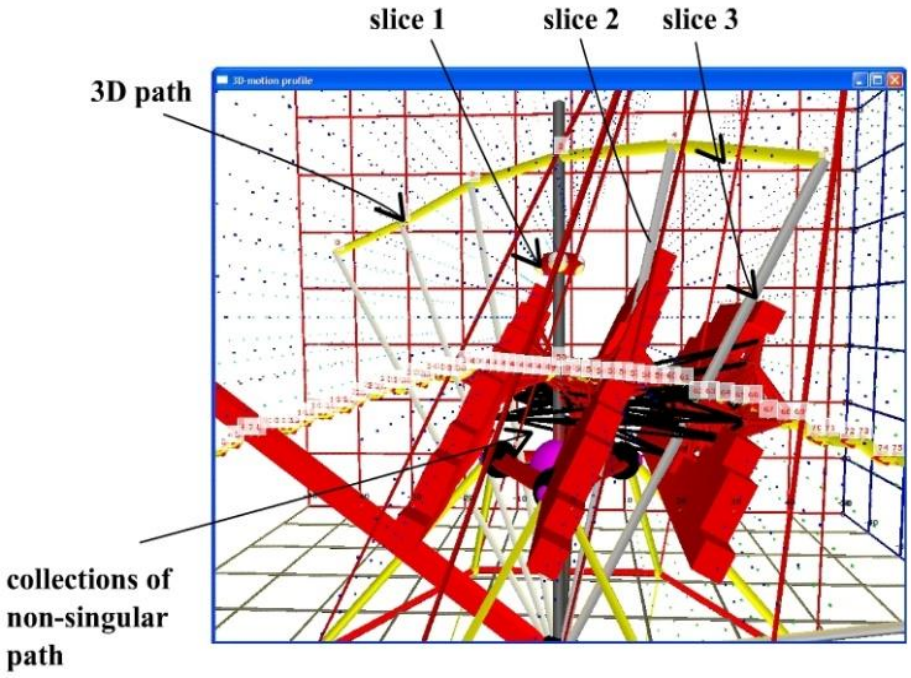

Figure 3-8: Interpolation between Slices

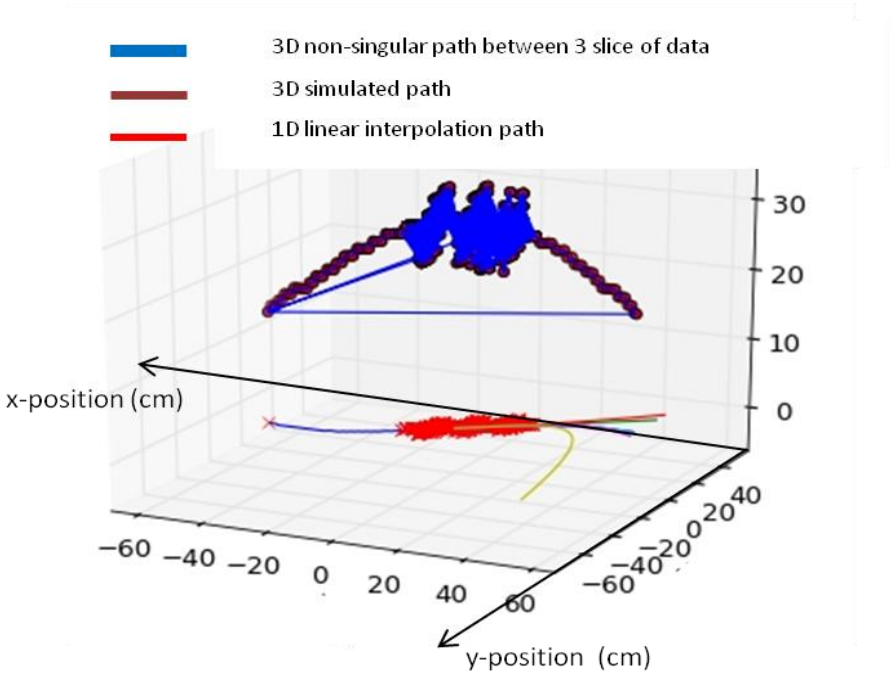

Figure 3-9: 1D Path between the 3 Data Slices

3.5 Results

The numerical method (Inverse Kinematic) is used to validate the accuracy of the proposed methodology through a demonstration of the robot end-effector's motion. Here, the position provided for the end-effector by the Python simulation is $P = (36 \quad 70 \quad 95 \quad 5 \quad 5 \quad 0)$. The stroke of the actuators is calculated in MATLAB based on the developed kinematic map of the mechanism. The obtained results of the end-effector's position by simulation and numerical methods are compared and shown in Figure 3.10. The figure shows a close match in X, Y, and Z directions between the results obtained by the proposed methodology and those obtained using the theoretically-based numerical method.

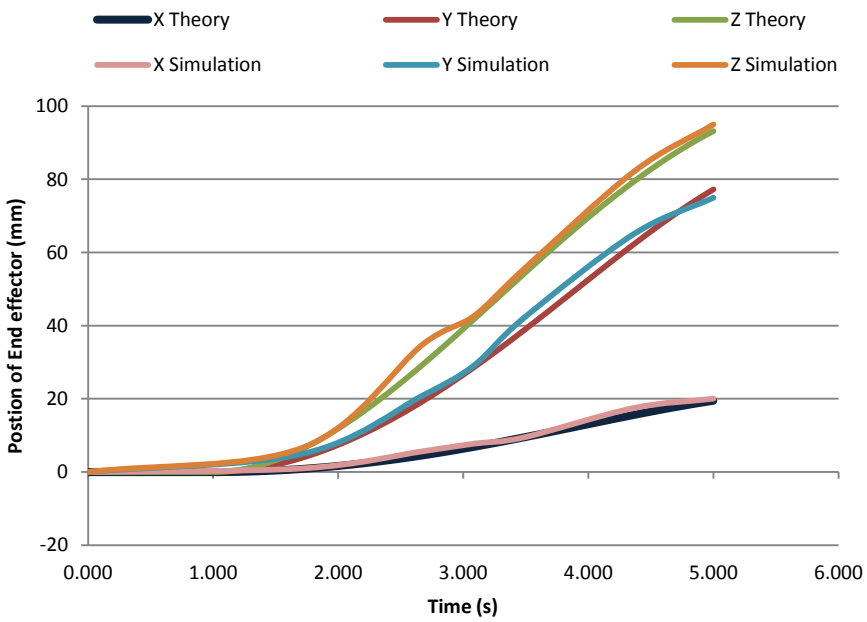

Figure 3-10: End Effector Tracking Position

This proposed methodology has the capability of performing various workspace searches, such as constant orientation and position workspace. The parametric workspace search performs well with obstacles like 3D objects and mesh surface where the search is for obstacle-free workspace and 3D surface interpolation.

The case studies show that the Python 3D simulation can search for non-singular or singular positions according to rules such as fixed position, fixed orientation, path planning, and obstacles within the workspace. The proposed methodology exhibits very good potential for rapid scenario tests and validations previously difficult to perform using existing parallel robot design methods.

3.6 Conclusion

This paper presents a new configuration of parallel robot with increased workspace for automated applications in the gripping of large aerospace components, such as those employed in an aircraft wing box. The developed stiffness formulation of the hybrid parallel robot is based on the calculation of vector direction of each actuator. Different configurations of the hybrid system were simulated using finite element analysis. The workspace formulation of the model is developed by defining the path motion profile of the tripod, which assists to determine the size of the actuators and the joints' angles. The obtained data are compared against the maximum actual size of the actuator and the maximum rotation angle of the joints,

respectively. The results show that the workspace of the new hybrid parallel robot has significantly increased compared with that of a hexapod.

A simulation system has been developed in order to provide and control singular and non-singular workspace searches using simple Boolean logic. Four case studies were considered to test the simulation system. The case studies were compared with conventional mathematical approaches including linear interpolation and linear regression. The results show that the simulation system has the capability of developing more accurate path planning for a hybrid parallel robot system. A theoretical inverse kinematic analysis model was developed and used in order to compare and validate the proposed simulation methodology through importing obtained data from the simulation into SOLIDWORKS and MATLAB software tools. The results show that the proposed simulation system offers a fast solution in designing new parallel robot configurations and geometries through local and global optimization of the search area.

Chapter 4

Dynamics Analysis

4.1 Introduction

This chapter proposes a methodology for developing dynamic formulations of a hybrid parallel robot containing nine actuators and two moving platforms. The dynamic formulation is developed by using Newton Euler and inverse kinematics in order to identify the best configurations based on stiffness and velocity of the system in that position. The control model of the proposed configuration is developed. The experimental results of actuator force are compared with theoretical and simulation.

4.2 Methodology

The dynamics of the mechanism composed of hexapod and tripod parallel manipulators assembled serially were investigated. As shown in Figure 11, this system consists of a lower platform (LPM), its mechanism type is 6-UPU, and an upper platform (UPM) with 3-RPU

structure. This arrangement is selected to increase the stiffness of the system and reduce the effect of the bending moment on the LPM during the positioning of the objects.

The lengths of actuators of the modeled configuration are calculated by inverse kinematics using a transformation matrix based on coordinate O (XYZ) defined on platform B (Figure 4.1) [94].

$$T = T_r \times \left(R_\theta \times R_\emptyset \times R_\varphi\right) \tag{4.1}$$

Therefore, the unite vector of each actuator is calculated in order to categorize the direction of the force applying to the systems. The formulation of linear force and moment is developed to find out the linear and angular velocities for platform A. The motion of Platform E is considered based on the coordinate system on platform A.

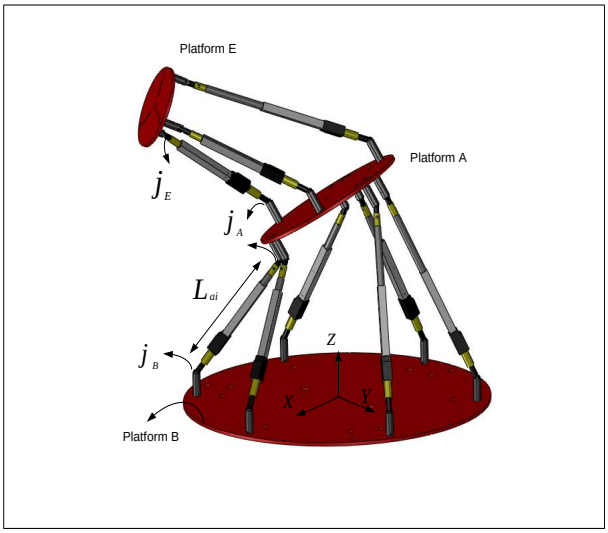

Figure 4-1: **Hybrid Parallel Robot System**

The crucial point in the following methodology is considering the different possibilities of motions for the LPM and RPM to reach, to move the end-effector to the desired position. Therefore, the position and orientation of the LPM and UPM are identified in Equations 4.2.a and 4.2.b.

$$P_{LPM} = u \times (P_f - P_i) \qquad 0 \leq u \leq 1 \tag{4.2.a}$$

$$P_{UPM} = P_f - P_{LPM} \tag{4.2.b}$$

Where, u is the coefficient for optimum motion,P_{LPM},$P_{UPM}$are the positions and orientation of platform A, E respectively and P_f, P_i are desired and initial position and orientation of end-effector respectively.

Changing the coefficient u allows the system to identify the possibilities to reach to the desired pose and orientation.

4.3 Dynamics formulation

The dynamic model of the parallel robot platform is driven by Newton's second law and the Euler's equation of motion expressed in Equations 4.3.a and 4.3.b.

$$\sum_{i=1}^{9} \vec{F_i} - m_E\, \vec{g} - F_f = m \frac{d^2}{dt^2}(r) \tag{4.3.a}$$

$$\sum_{i=1}^{9} \vec{M}_i = \dot{H} + \omega_{xyz} \times \vec{H} \qquad (4.3.b)$$

In which, $\vec{F}_i$ and $\vec{M}_i$ are applied force and moment exerting on the end effector, respectively. m_E is the platform's mass, $\vec{H}$ is angular moment ,ω_{xyz} is the angular velocity of platform E and F_f is friction force.

The first step is defining values and directions of force exerted by the actuators by using the Equation 4.4.

$$F_i = f_i \times \frac{L_{Hi}}{||L_{Hi}||} \qquad i \in \{1 \dots 9\} \qquad (4.4)$$

Where, F_i is force vector applied in the system and f_i is scalar force vale exerted by the actuators. The value is based on actuator properties and length of stroke.

The moment applied on the moving platform is developed by the Euler-Newton formulation in order to determine angular velocity of the platforms in Equation 4.6 [95].

$$\sum M_{xyz} = \sum_{i=1}^{6} F_i \times r_{\frac{O}{Ai}} \qquad (4.5)$$

$$\sum_{i=1}^{6} F_i \times r_{\frac{O}{Ai}} = \begin{bmatrix} -I((\dot{\varphi})^2 sin\theta cos\theta) + I_z \dot{\varphi} sin\theta \left(\dot{\varphi} cos\theta + \dot{\psi}\right) \\ -I\left(2\dot{\varphi}\dot{\theta} cos\theta\right) - I_z \dot{\theta}\left(\dot{\varphi} cos\theta + \dot{\psi}\right) \\ I_z\left(\dot{\varphi}\dot{\theta} sin\theta\right) \end{bmatrix} \qquad (4.6)$$

Where, M_{ai} is moment of inertia created by the actuators on platform E and $\dot{\theta}_T$, $\dot{\varphi}_T$, $\dot{\psi}_T$ are the angular velocity according to XYZ coordinates.

The relative velocity of platform E is obtained by using a work and energy equation developed for the system.

$$\sum_{i=1}^{3} \vec{F_i} \times D_i = {}^1/_2\, m_E {V_{E/A}}^2 + {}^1/_2\, \mathrm{I}\omega_{\mathrm{E}}{}^2 \tag{4.7}$$

Where, $\vec{F_i}$ is the force vector of the actuators connecting to platform E, m_E is mass of platform E, I is moment of inertia matrix and ω_E is angular velocity vector of the platform.

From the vector base equation the relative velocity of platform E is calculated. The position of platform E related to platform A is calculated as:

$$r_{E/A} = E_o \times {T_{lmn}^{E}}^{-1} \times R_{\theta\emptyset\psi}^{\mathrm{O}} \times R_T^{\mathrm{O}} \times T_{lmn}^{E} \times T_{lmn}^{F} - A_o \times {T_O^A}^{-1} \times R_{\theta\emptyset\psi}^{\mathrm{O}} \times T_O^A \tag{4.8}$$

Where, $r_{E/A}$ is the relative position of the platforms, T_{lmn}^{E}, $R_{\psi\emptyset\theta}^{\mathrm{O}}$ are translation and rotational motion matrix of platform A respectively, R_T^{O} and $T_{lmn}^{F}$are the linear and rotation matrix of platform E motions. E_o and A_o are the centre point of platforms A and E respectively.

The acceleration formulation of platform E is developed in Equation 4.9, where the angular acceleration is neglected.

$$a_E = \frac{d}{dt} V_A + \omega_{XYZ} \times \left(\omega_{XYZ} \times r_{E/A}\right) + 2\omega_{XYZ} \times V_{E/A} + \frac{d}{dt} V_{E/A} \tag{4.9}$$

Where, ω_{XYZ} is the angular velocity of platform A, $r_{E/A}$ and $V_{E/A}$ are relative position and velocity of platform E with respect to A.

Therefore, the amount of displacement of the joints in this instance is calculated in order to identify the new position vector of the actuators.

4.4 Optimization Motion

The methodology described in previous sections is developed by Equations 4.2.a and 4.2.b to find the optimum configuration in order to reach the desired position. In this study, time of the motion is priority. The developed program checked all the possibilities for considered motions and selected the one based on priority. The data is saved in the file to reduce the time of processing. The considered motion in Table 3 is examined for the results.

The formulation is expanded in order to determine the applied force on six other actuators. By subtitling the obtained value of F_{Ti} in Equation 4.10, three linear equations can be developed. As the stiffness is calculated in a static position, other three linear equations can be obtained by developing a moment of inertia equation regarding to point o_{XYZ}.

$$\sum_{i=1}^{3} L_{Ti} \times F_{Ti} + \overrightarrow{M_T g} = \sum_{i=1}^{6} L_{Hi} \times F_{Hi} \tag{4.10}$$

$$\sum_{i=1}^{6} L_{Hi} \times F_{Hi} \times (A_i - o_{XY}) = 0 \tag{4.11}$$

Where, M_T is the weight of all components on top of platform A, moreover L_{Hi} and F_{Hi} are direction and applied force of the actuators respectively.

The axial displacement of each actuator is obtained by considering axial stiffness that involves with material properties (Equation 4.12).

$$\varepsilon_i = \frac{F_{Hi}}{K_i} \qquad For\ i = 1 \dots 9 \tag{4.12}$$

Where, ε_i is axial displacement of an actuator and F_{Hi} is amount of the force applied to an actuator.

The potential energy of the actuators due to external force applied is equal to energy of external force on the platform E as is developed in Equation 4.13. Therefore, the displacement of the whole system is obtained in Equation 4.14.

$$PE = \sum_{i=1}^{9} \frac{1}{2} K_i {\varepsilon_i}^2 \tag{4.13}$$

$$f \times \Delta U = \sum_{i=1}^{9} \frac{1}{2} K_{Axi} {\varepsilon_i}^2 \tag{4.14}$$

$$\mathrm{K_{HP}} = \frac{\mathrm{f}}{\Delta \mathrm{U}} \tag{4.15}$$

Where, ΔU is total deformation of the system due to external force on the platform E, and K_{HP} is the axial stiffness of the robot. However, the optimizing method is applied on the system for two identified motions which are demonstrated in Table 3.

Table 3: Applied motions to hybrid parallel robot

Study	factor	X(mm)	Y(mm)	Z(mm)	θ^o	φ^o	ψ^o
Case 1		-60	70	100	10	10	10
Case 2		70	80	85	15	15	10

The results in Figures 4.2 and 4.3 demonstrate velocity and stiffness changing for possible configurations of case 1 and 2 respectively.

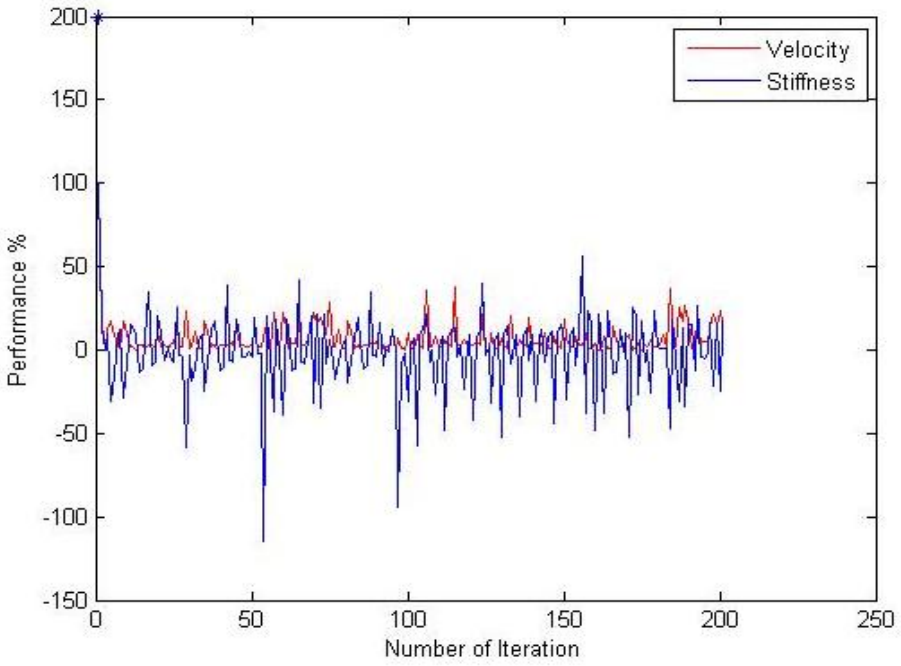

Figure 4-2: Enhancing the system performance case 1

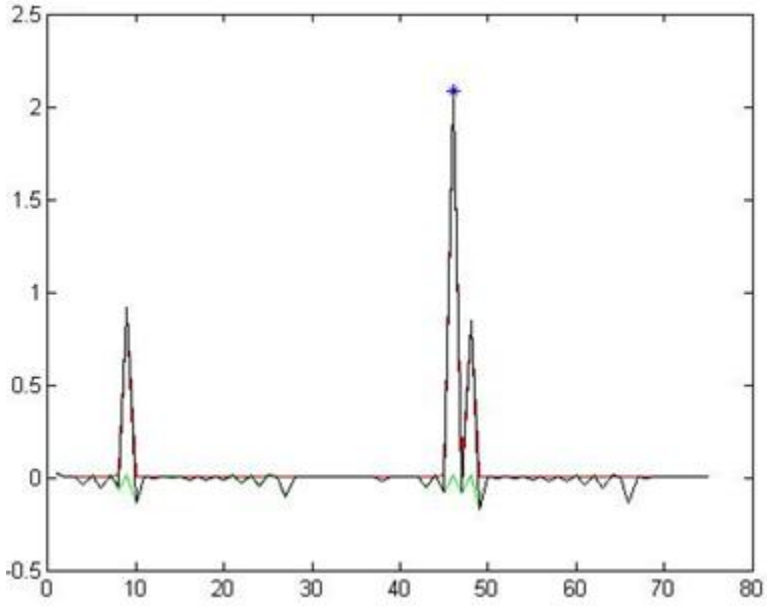

Figure 4-3: Enhancing the system performance case 2

As the results demonstrate, the program calculates stiffness and velocity of the system for each possible configuration. The optimum configuration is obtained based on higher speed and stiffness. For the cases 1and 2 the data obtained for hexapod and tripod is shown in Table 4.

Table 4 : Optimum Motions

	parameter	l (mm)	m(mm)	n(mm)	Θ (rad)	Ø (rad)	ψ (rad)
Case1	Hexapod	-20	40	50	0.058	0.058	0.058
	Tripod	-40	30	50	0.058	0.058	0
Case2	Hexapod	35	45	45	0.058	0.058	0.058
	Tripod	35	35	40	0.058	0.058	0

The obtained results are stored in a file in order to reduce the process time for the same motions. The flexibility of the program assists the consideration of other parameters such as accuracy to the system. The priority of the data could be changed for different applications in the program to find different path motions, higher priority of speed or stiffness.

4.5 Control Strategy

There are two methods for controlling the robots: 1.The input is the path motion of the end-effector, 2. Second position and pose of end-effector. Jigging the application positioning is an important factor for controlling the system. Input data goes through the inverse kinematics' formulation in order to calculate the size of each actuator. The size of the actuator is sent to a micro controller that sends a signal to related servomotors. The benefit of servo motors is the close loop system that modifies the error of motion by itself. The inverse kinematic formulation is programmed in MATLAB.

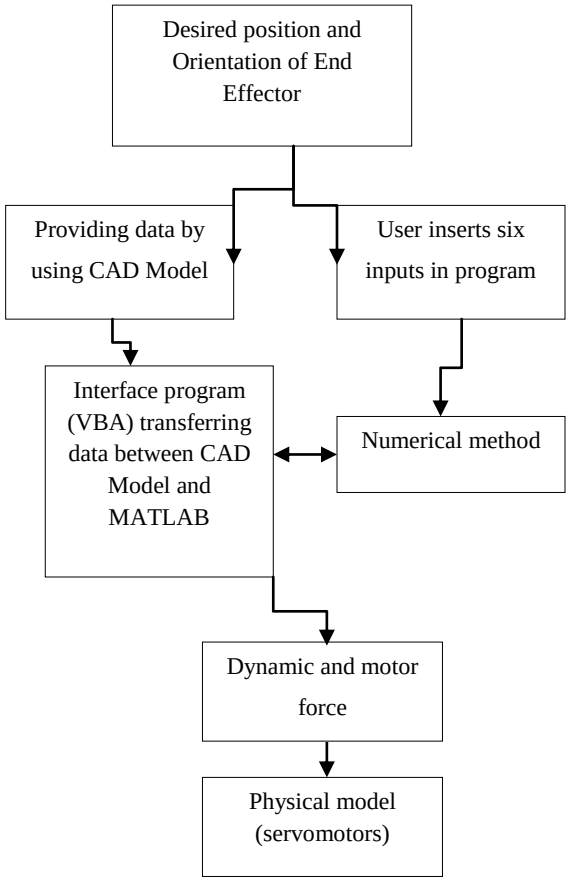

Figure 4-4: Functional schematic of Control Model

The crucial factor of the control model is to enhance the positioning of the tripod Three degrees of freedom robots could move in space with three translations and three rotations motion, while three of them are not controllable. The structure of the tripod is UPR, therefore, one translation motion in Z direction and two rotational motions around X and Y are controllable. The other parameters have to be calculated based on the structural limitation of the model. The amount of translation in x and y are obtained by Equations 4.16.a and 4.16.b respectively.

$$l_T = -(n_T + d_{\underline{\underline{E}}}) \times \sin(\varnothing_T) \times cos(\Theta_T) \quad (4.16.a)$$

$$m_T = (n_T + d_{\underline{\underline{E}}}) \times sin(\Theta_T) \quad (4.16.b)$$

Where, l_T and m_T are translation motions of the tripod in X and Y directions respectively. n_T is allocated translation motion in z direction. Moreover, Θ_T and $\varnothing_T$ are rotational motions around X and Y axes. $d_{\underline{\underline{E}}}$ is initial distance between platforms A and E.

4.6 Results and Discussion

The dynamics formulations of the hybrid parallel robot were applied in developed Matlab program in order to analysis the theoretical behavior of the system. The frictions force between the components is not considered for obtained results in this section. The calculated actuators' forces for the considered motions in Table 4 are demonstrated in Figures 4.5 and 4.6. The forces are changing based on actuators' stroke as well as created moment through the motions. The obtained results of velocity and acceleration profiles of end-effector are demonstrated in Figure 4.7 and 4.8 respectively.

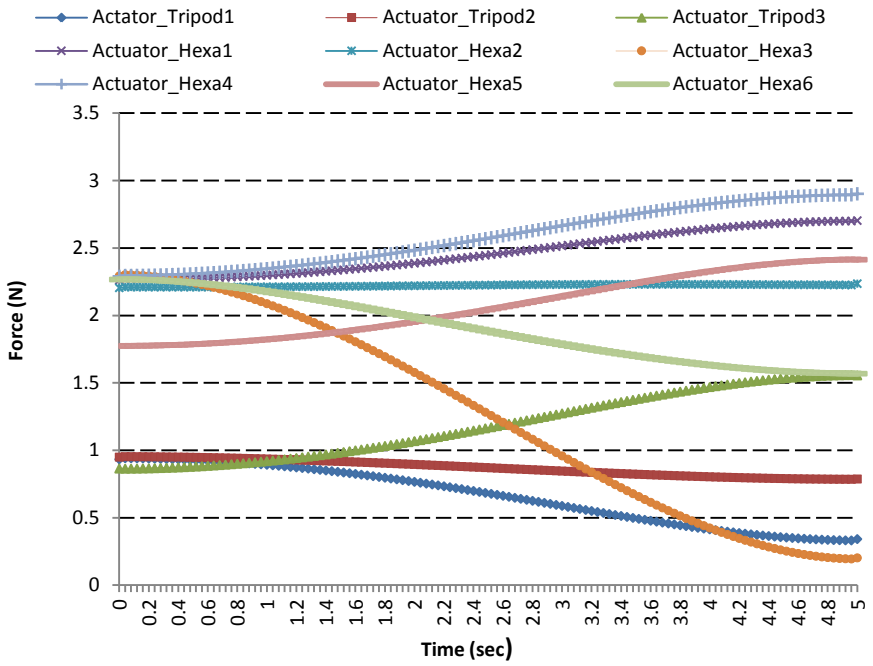

Figure 4-5: Ideal Force of Actuators through the Motion Case 1

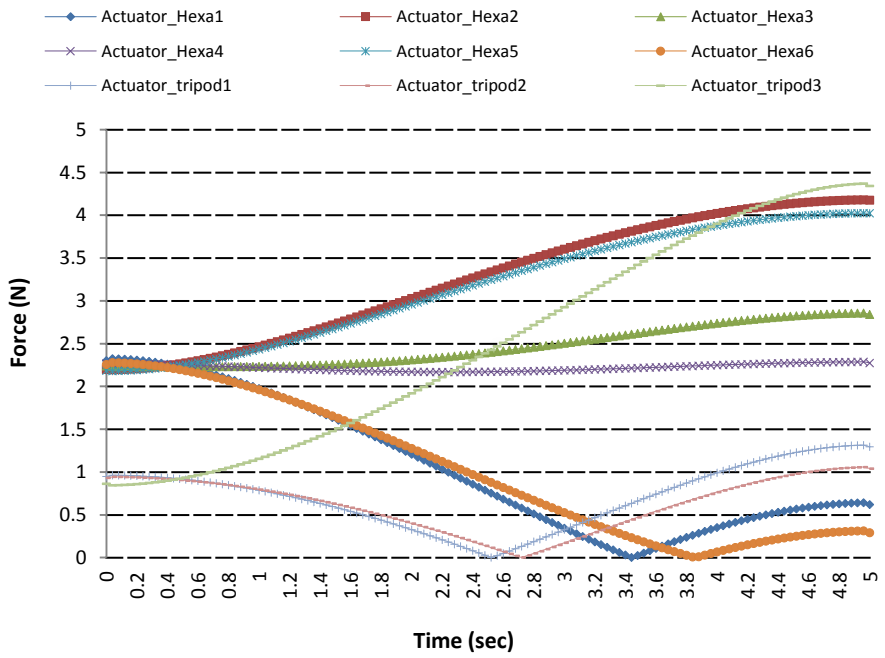

Figure 4-6: Ideal Force of Actuator through the Motion Case 2

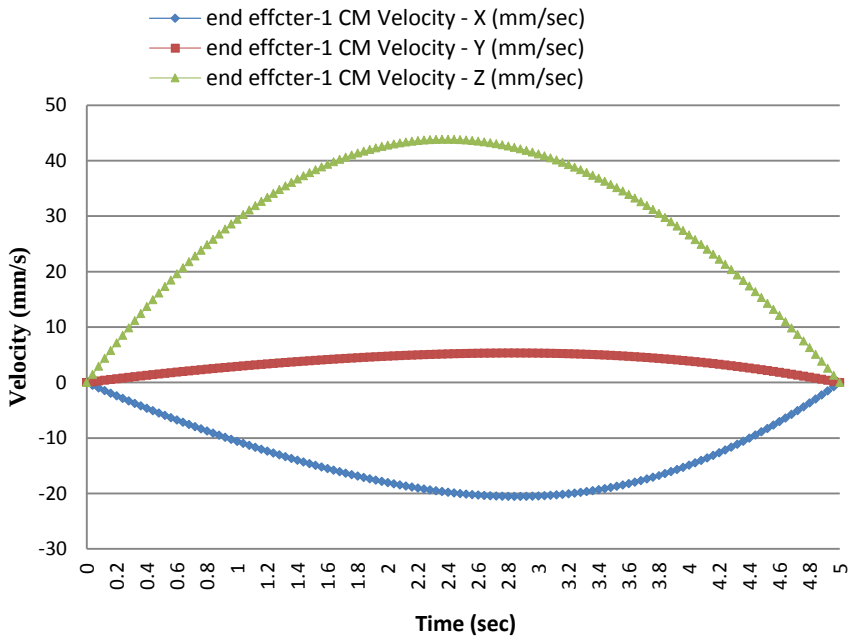

Figure 4-7: Velocity Profile of Platform E Case 1

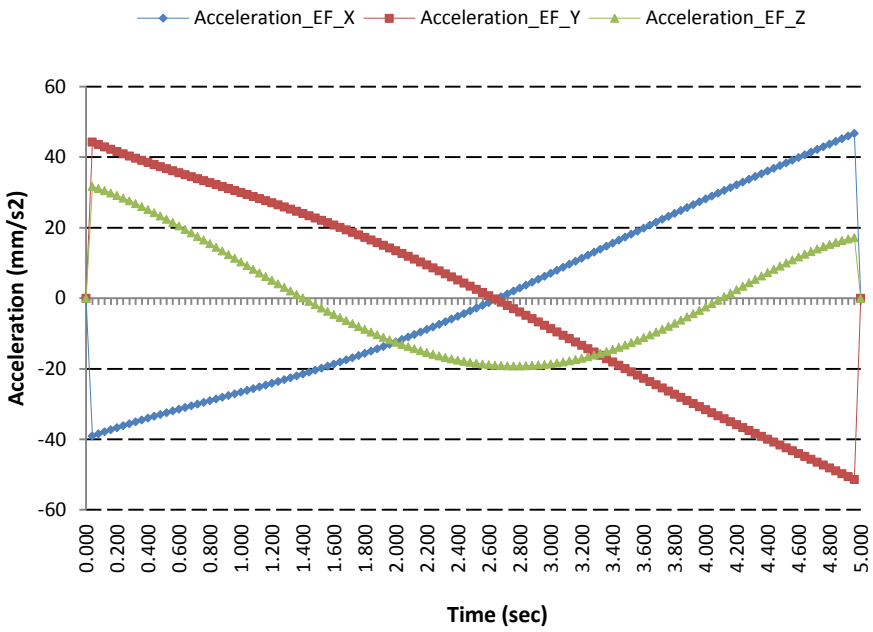

Figure 4-8: Acceleration Results of End-Effector for Case 1

As it is demonstrated in Figures 4.5 and 4.6, the required forces for tripod's actuators is less than those of the hexapod due to weight of the components on the actuators. The required force for the actuator_Hexa3 in Figure 4.5 is dramatically reduced due to direction of end-effector rotation and effect of moment.

The difference between minimum and maximum applied force on the actuators in case 2 (refer to Figure 4.6) are more than case1due to orientation of end-effector.

4.7 Conclusion

This chapter presented the dynamic formulation of a new configuration of a hybrid parallel robot by determining the actuators' vectors through motion in real time by expanding the associated transformation matrix. This method provides a more accurate solution for the positioning of the end-effector. The angular velocity and applied actuators' force calculated by using Euler-Newton methods. The 3D model of the system has been linked to a MATLAB simulation in order to develop the robot's control system. The obtained results of forces show the required force for a particular motion. The calculated velocity and stiffness of the end-effector are used to find the optimum motion for the system. The control strategy is developed for the system to power the actuators for considered motion. The CAD model that will explain in next chapter assist to validate the dynamics formulations as well as control strategy.

Chapter 5

Robot Modeling and stiffness Analysis

5.1 Introduction

In this chapter, the CAD model of the hybrid parallel robot is designed with SOLIDWORKS software package by considering the joints' limitation and actuators' strokes. A fully defined CAD model is used to simulate the stiffness of the system based on the applied force on the system. The theoretical model of stiffness is developed for the proposed model. The experimental results validate the theoretical calculation of applied force on the actuators in different positions through the workspace of the system.

Due to the high accuracy and stiffness required for motions, six or more degrees of freedom are necessary. There are some well known structures which have been investigated such 6-DOF Stewart platform and 3-DOF parallel robot (tripod). The hexapod (6-DOF) has high mobility force due to its numbers of actuators and structural model; on the other hand, singularities in the workspace cause a collapsing system through the performance. The added

tripod assists to increase the work volume as well as support the singularities while a particular end effector position is necessary.

The hexapod is the base of the system due to the large bending moment applied to the middle platform. The structure contains nine linear actuators connecting one stationary and two moveable platforms. Fifteen universal joints and three revolute joints connect the actuators to the platform.

5.2 Designing Hybrid Parallel Robot

The reconfigurable model for the proposed hybrid parallel robot is designed based on a considered application of the system. In this section the necessary issues needing to be considered are discussed.

Based on products in the market the actuators are designed in a SOLIDWORKS software package. The performance and characteristics of the designed components are explained in this section.

The modified design of the parallel robot contains three platforms in its structure. The diameters of the platforms are obtained based on the length of the actuators used in the system. The extra holes help to change the configuration of the structure as well as assisting in

passing the wires to reach the controller. The lower, middle and upper platforms of the system are demonstrated in figures 1, 2 and 3 respectively. The diameter of the lower platform (LP), middle platform (MP) and upper platform (UP) are 50 cm, 25 cm and 12.5 cm respectively. The thickness of all platforms is 5 mm. The aluminium alloy is selected as the material for the platforms due to its high strength and very low weight, which is very important for reducing the static force on the actuators.

The design of the actuator is similar to a design which can already be purchased. The actuator provides linear motion by using a servo motor to provide power.

Universal joints are used for a 6-DOF parallel robot in order to connect the actuators to the platforms. Their high efficiency in motion, easily adjustable design and their availability in a variety of size and model, are the main reasons for selecting this design.

This small mechanical design assists the attachment of the actuators to the joints. The diameter of the outer circle is 10 mm which exactly fits inside the universal joints. The other side is attached to the actuator. The figure demonstrates the designed road clevis.

The components in the software connect to each other with an appropriate mate and condition. The result is fully defined assembly that is ready to be simulated in FEA and motion analysis (Figure 5.1).

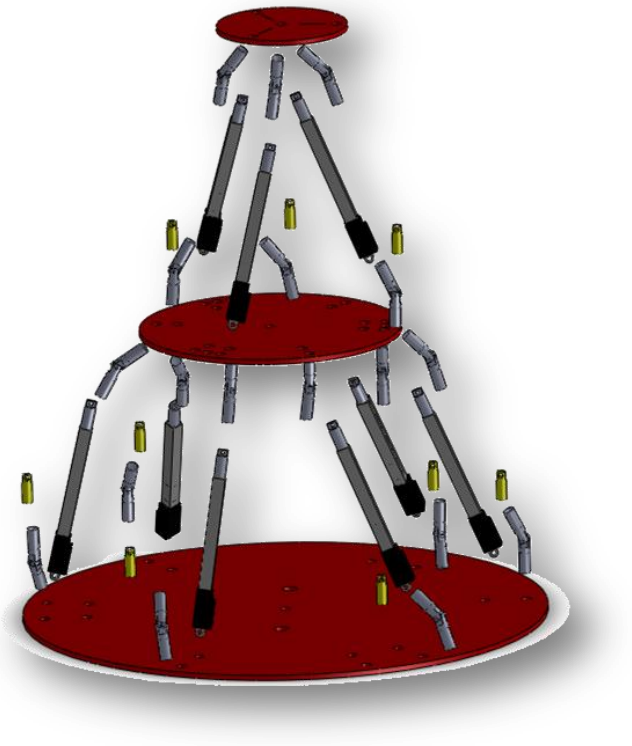

Figure 5-1: Components of Hybrid Parallel Robot in Assembly

5.3 Stiffness Calculation

The stiffness calculation is dependent on determining the force vector on the actuators which is found with inverse kinematics. The potential energy of the system is determined by considering the axial deformation of each actuator. Therefore, the total displacement of the system is developed by an equilibrium equation of work and energy. However, linear stiffness of the system could be calculated by Equation 5.1.a and 5.1.b.

$$K_l = \sum_{i=1}^{9} {}^{f}/_{S_i} \qquad (5.1.a)$$

$$K_i = \frac{A \times E}{|L_{Hi}|} \qquad \text{For } i = 1, \dots, 9 \qquad (5.1.b)$$

Where, K_l is linear stiffness and f is the external force applied on the end effector. Moreover, S_i and $|L_{Hi}|$ are axial stiffness and length of all actuators respectively, moreover E is module of elasticity and A is the effective area onto which force is applied.

In order to find angular stiffness, the force applied on each actuator is calculated by equation 5.2.a. However, the axial stiffness of each actuator is calculated as previously (chapter 4) in Equations 4.10 and 4.11. The amount of deformation of each actuator is obtained to find the amount of angular displacement based on the kinematic equation.

$$K_\theta = {}^{M}/_{\Delta\theta} \qquad (5.2.a)$$

$$M = \sum_{i=1}^{9} F_i \times D_i \qquad (5.2.b)$$

Where, K_θ is rotational stiffness and M is external moment exerting to the system. Moreover D_i is the position vector of the platform centre point and joints, F_i is the force vector created by each actuator.

The derived formulation of stiffness is developed to calculate the total stiffness of the system by considering the axial stiffness of each actuator due to the external force in each position.

Direction of applied external force is changed through motion and different positions. The force direction is calculated by a transformation matrix developed for the end effector by considering the initial direction while the system is in a normal position, as shown in Equation 5.3.

$$[U_{EZ}] = [U_Z] \times R_T^O \times R_{\theta\emptyset\psi}^O \tag{5.3}$$

Where, $[U_{EZ}]$ is direction of force after motion and $[U_Z]$ is initial direction that is (0, 0, 1).

Therefore, the vector of the external force in a different position is obtained by considering the amount of exerted force that is shown by f in Equation 5.4.

$$\vec{F} = f \times [U_{EZ}] \tag{5.4}$$

Previously the position vectors of the actuators have been calculated by using inverse kinematics, therefore, based on the equilibrium of force theory, the applied force on each actuator can be obtained. There are three equations for X, Y and Z direction to calculate the amount of force on each actuator. The equation based on the vector is shown in Equation 5.5.

$$\sum_{i=1}^{3} L_{Ti} \times F_{Ti} = F \tag{5.5}$$

Where, L_{Ti} and F_{Ti} are direction and applied force of tripod actuators respectively.

The formulation is expanded in order to determine the applied force on six other actuators. By subtitling the obtained value of F_{Ti} in equation 5.5, three linear equations can be developed. As the stiffness is calculated in a static position, three other linear equations can be obtained by developing the moment of inertia equation regarding to point o_{XY}.

$$\sum_{i=1}^{3} L_{Ti} \times F_{Ti} + M_T g = \sum_{i=1}^{6} L_{Hi} \times F_{Hi} \tag{5.6}$$

$$\sum_{i=1}^{6} L_{Hi} \times F_{Hi} \times (A_i - o_{XY}) = 0 \tag{5.7}$$

Where, M_T is the weight of all components on top of platform A, moreover L_{Hi} and F_{Hi} are direction and applied force of the actuators respectively.

The axial displacement of each actuator is obtained by considering axial stiffness that is involved with the material properties (Equation 5.8).

$$\varepsilon_i = \frac{Fa_i}{K_i} \qquad \text{For } i = 1 \dots 9 \tag{5.8}$$

Where, ε_i is axial displacement of actuator and Fa_i is amount of the force applied to an actuator.

The potential energy of the actuators due to the external force applied is equal to the energy of the external force on platform E, as is developed in Equation 5.9. Therefore, the displacement of the whole system is obtained in Equation 5.10. Therefore, stiffness of the system is calculated in Equation 5.11.

$$PE = \sum_{i=1}^{9} \frac{1}{2} K_i {\varepsilon_i}^2 \tag{5.9}$$

$$f \times \Delta U = \sum_{i=1}^{9} \frac{1}{2} K_{Axi} {\varepsilon_i}^2 \tag{5.10}$$

$$K_{HP} = \frac{f}{\Delta U} \tag{5.11}$$

Where, ΔU is total deformation of system due to external force on platform E, and K_{HP} is the axial stiffness of the robot.

The following method is utilized to specify just one number for the stiffness; that makes the comparison easier for different configurations in the same particular position. However the stiffness of the system in Z=50cm shown in the Figure 5.2.

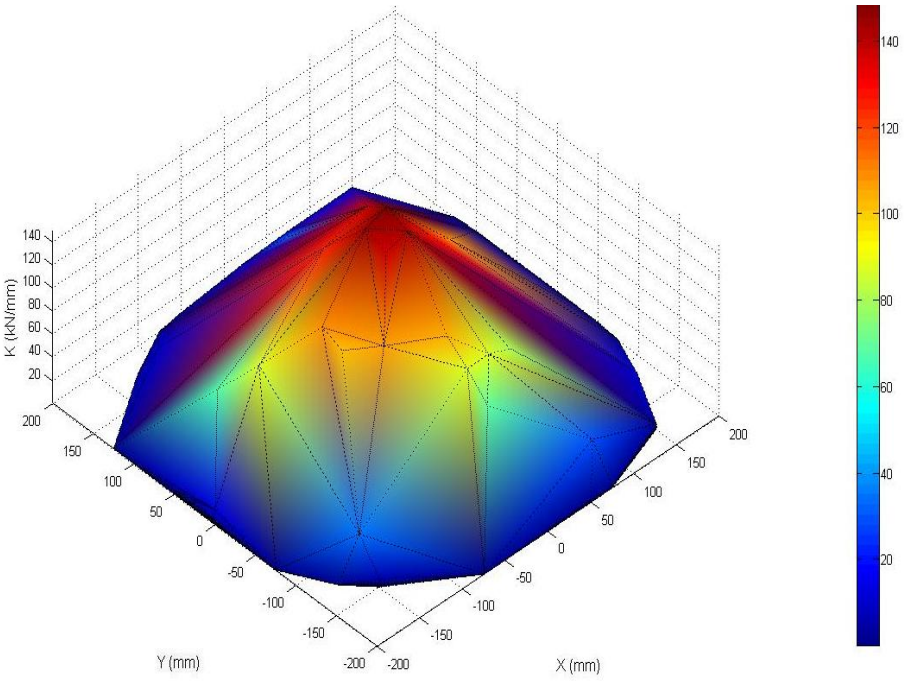

Figure 5-2: Stiffness Distribution in Z=50

According to obtained stiffness results of the system, shown in Figure 5.2, the total stiffness of the system is reduced while end effector moves in X and Y directions due to bending moment on the system.

The matrix base development of hybrid parallel robot's stiffness is demonstrated in Appendix A.

5.4 FEA Analysis and Case Studies

In this section, displacement of the hybrid parallel robot due to external force is simulated by software in order to validate the theoretical method. Stiffness of the hybrid system is simulated in different positions and orientation. The stiffness of the tripod and hexapod are investigated in different positions in order to compare with those of the hybrid system.

Besides the material properties of the actuator and joints, the physical structure and position and orientation of the end effector are considered for the simulation software. The developed software calculates the size of the actuators by inverse kinematic mapping and sends it to the designed CAD model in the software to apply FEA on the system. The boundary conditions of the simulation and size of parameters are demonstrated in Table 5. While in Table 6 the end effector's position and the length of the actuator in the simulation test is identified. The FEA analysis and theoretical results for the considered translation motions are demonstrated in Table.6. The obtained data of the simulation demonstrate the range of stiffness in a static position. It is planned that the body and joints are fixed to investigate the effect of trajectory on the system. The FEA of the system are investigated in a primary position and boundary position, demonstrated in Figures 5.3 and 5.4 respectively. The obtained results of theory and simulation are compared in Table 7.

Table 5: Size of Components of Assembled CAD Model

Parameters	Quantity	Parameters	Quantity
D_B mm	500	F (N)	100
D_A mm	250	Li (mm)	226
D_E mm	125		

Table 6: Lengths of Actuators and End-effector position

Parameters	Quantity	parameter	Quantity
L1,L2,L3	100, 90, 20 (mm)	X	160mm
L4,L5,L6	20,50, 50 (mm)	Y	212mm
L7,L8,L9	100, 0, 0 (mm)	Z	-7mm

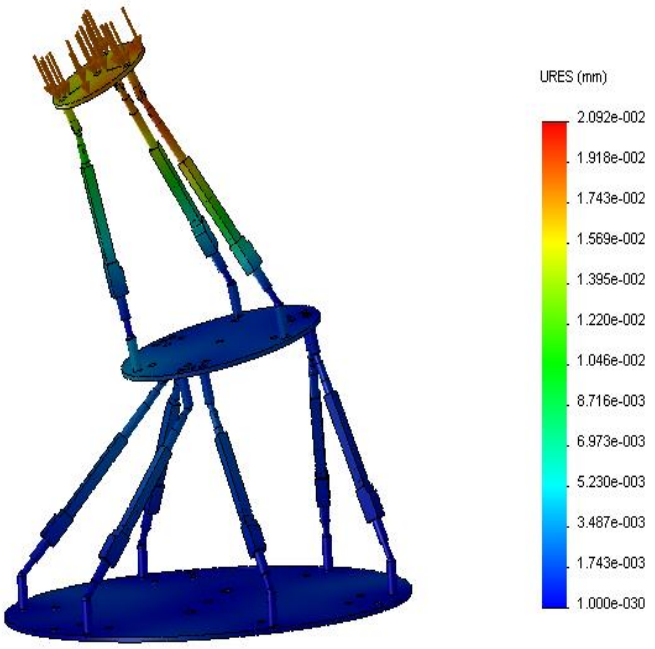

Figure 5-3: FEA Results on Hybrid Parallel Robot

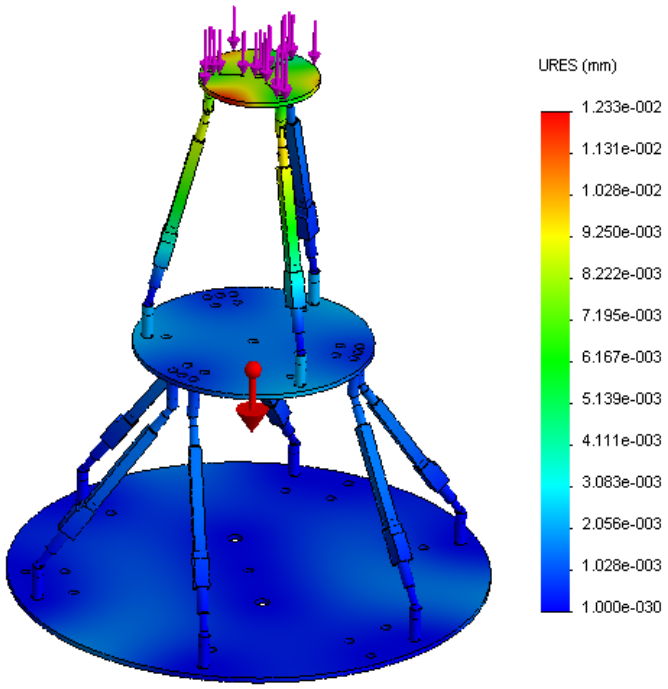

Figure 5-4: FEA Results of System in Initial Position

Table 7: Results of Translation Motion Effect on Stiffness in Theory and Simulation

	Simulation		**Theoretical**	
Motion (l, m, n, θ, ø, φ)	***Deformation (mm)***	***Stiffness (N/mm)***	***Deformation (mm)***	***Stiffness (N/mm)***
(0,0,1,0,0,0)	0.01233	8110.300081	0.010693	9351.912466
(6,7,10,0,0,0)	0.01678	5959.475566	0.014888	10113.26861
(50,50,50,0,0,0)	0.01917	5216.48409	0.016194	6175.2192
(60,60,50,0,0,0)	0.01972	5070.993915	0.018792	5321.5219
(0,0,100,0,0,0)	0.01835	5449.591281	0.011586	5321.5219
(70,60,50,0,0,0)	0.02043	4894.762604	0.020656	4841.1298
(60,70,100,0,0,0)	0.02077	4814.636495	0.0215	4841.1298
(70,80,80,0,0,0)	0.02622	3813.228113	0.02678	3734.3439
(80,70,100,5,0,0)	0.0376	2659.57	0.0355	2818.72
(60,70,100,5,5,5)	0.0148	6756	0.0151	6622.51
(80,70,100,10,5,10)	0.0492	2032.59	0.04062	2206.5057
(50,50,55,10,10,10)	0.05422	1844.33	0.0501	1996.21
(-70,100,35,15,15,10)	0.02092	4770.18	0.021595	4630.7

The finite element analysis results obtained by the software compared different configurations of parallel robot, including the six and three degrees of freedom mechanisms. The figures demonstrated the stiffness comparisons of models in the same positions. More results of FEA for the hybrid, hexapod and the tripod are depicted in Appendix B.

5.5 Dynamic Stiffness

In order to find more accurate modelling for stiffness, the stiffness of the system was investigated through the motion. In the following section the motor force and external force and moment are considered to find the result. However, the defined motions are inputs of the kinematic program. In order to find the length of the actuator and stiffness of the system the results of the theory and simulation are compared for different motions which are provided in Table.6.

As the results demonstrated in Figure 5.5, the maximum deformation in the considered motions reduced due to the exerted force by the actuators. In order to calculate stiffness of the manipulator through the motions, the dynamic of each actuator is calculated based on work and energy formulation.

$$T = \frac{1}{2} \times m \times v^T \times v + \frac{1}{2} \times I \times \omega^T \times \omega \tag{5.12}$$

Where, $v = [\dot{x} \quad \dot{y} \quad \dot{z}]$ and $\omega = [\dot{\theta} \quad \dot{\emptyset} \quad \dot{\varphi}]$; m and I are mass and moment of inertia respectively.

$$F \times L^T - T - mgz = K_i \Delta L \tag{5.13}$$

Where, $F = [F_x \quad F_y \quad F_z]$ and $L = [l_x \quad l_y \quad l_z]$; m and K_i are the mass and axial stiffness of an actuator.

However, the velocity vector of each actuator could be determined by the inverse kinematic formulation and stroke of the actuators that is related to the actuator properties.

The promoters D and $\Delta\Theta$ in the graphs is calculated by equation 5.14.a and 5.14.b respectively.

$$D_i = \sqrt{{l_i}^2 + {m_i}^2 + {n_i}^2} \qquad i \in \{1, 2 \dots 8\} \tag{5.14.a}$$

$$\Delta\Theta = \sqrt{{\theta_i}^2 + {\emptyset_i}^2 + {\varphi_i}^2} \qquad i \in \{1, 2 \dots 5\} \tag{5.14.b}$$

In which, l_i, m_i and n_i are allocated linear motions to the system in X,Y and Z respectively. Moreover, θ_i, $\emptyset_i$ and φ_i are the rotational motions around x, y and z respectively for the considered motions.

The motions were demonstrated in Table 6 are applied to CAD models to determine the stiffness of the system. The stiffness of the system is illustrated while linear and rotational motions are applied in Figures 5.5 and 5.6 respectively.

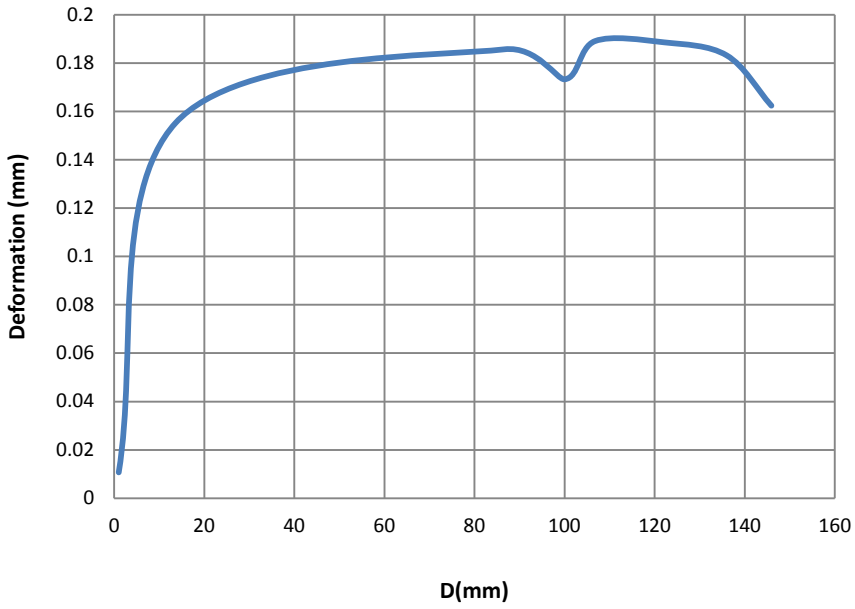

Figure 5-5: Deformation for Translational Motion

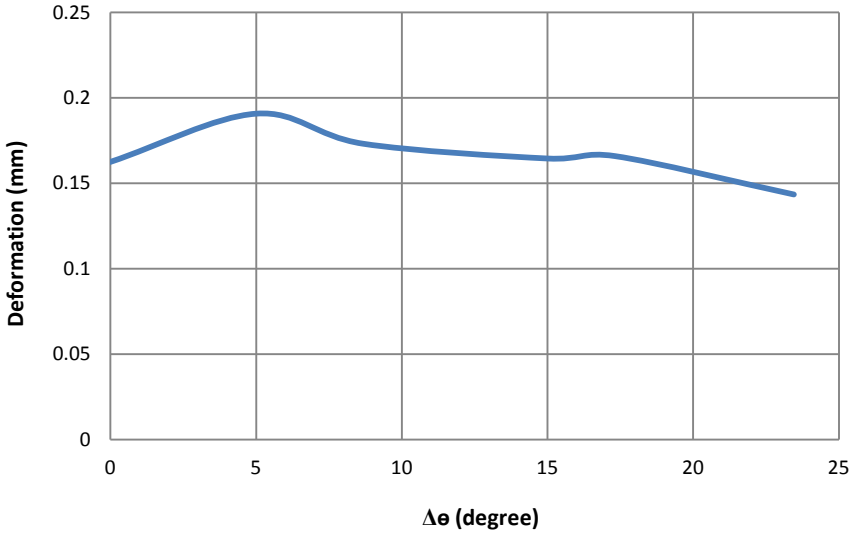

Figure 5-6: Deformation of Rotational Motions

The stiffness of the system is reduced while size of the motion is increased. As shown in Figure 5.5, the stiffness of system is increased while total motion is 100 mm because whole the motion is just in Z-axis, therefore the exerted bending moment is reduced.

The angular deformation of the system (Figure 5.6) is slightly increased through the increase of angular motion. However most of the angular motions are created by the hexapod while the weakest part for applied moment is the tripod.

5.6 Dynamic Simulation

The desired position and orientation are the input of the software to simulate motion of the system. The friction of the actuators and joints is considered in this study while the only external force applying on the system is the weight of the system. The applied motions are demonstrated in Table 8.

Table 8: Applied motions to hybrid parallel robot

Study	factor	X (mm)	Y(mm)	Z(mm)	θ^o	φ^o	ψ^o
Case 1		60	70	100	10	10	10
Case 2		70	80	85	15	15	10

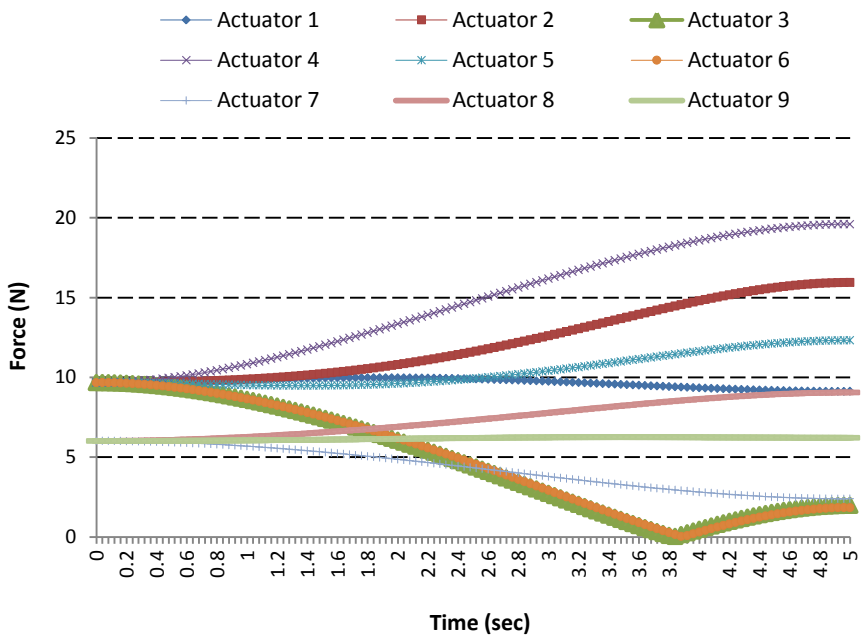

Figure 5-7: Force of actuator through the motion Case 1

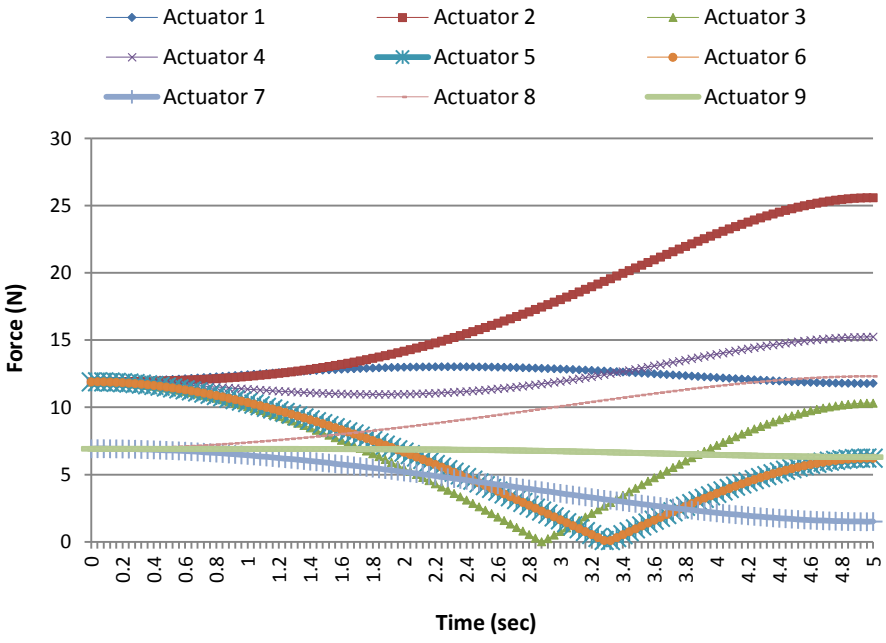

Figure 5-8: Force of actuator through the motion Case 2

The desired motions are applied to a kinematic program (Matlab) in order to find the length of the actuators for particular motions. The calculated lengths are transferred to the interface program (VBA) in order to modify the motors developed in the assembled CAD model in Solidworks (Appendix D). The CAD software calculates the motor power based on the force applied and stroke size of each actuator. Based on the obtained results by the developed intelligent motion system, the best possible configuration to reach to the assigned position and orientation is identified based on the maximum velocity and payload of the system. Theoretical results of the velocity profile of the end effector relating to the coordinate on the fixed platform (platform B) are compared with simulation for two considered cases.

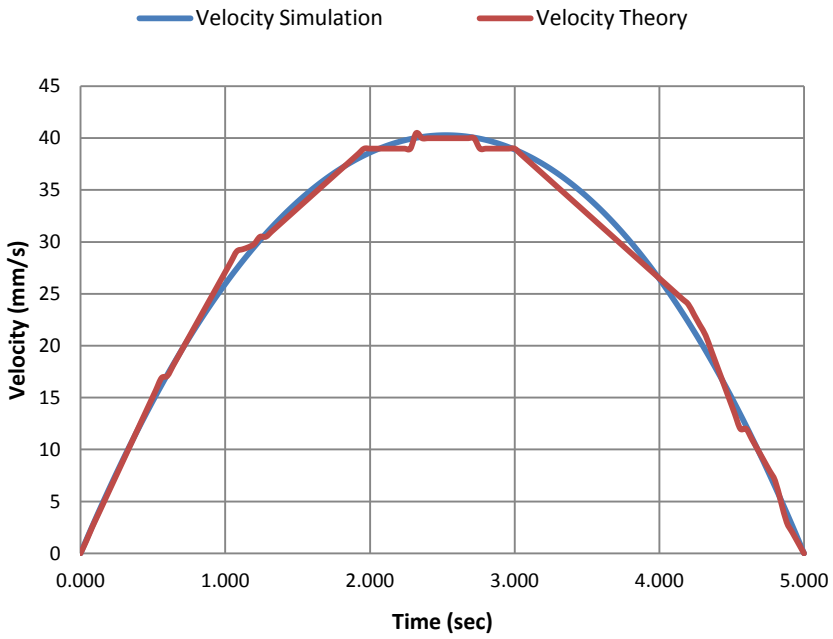

Figure 5-9: Velocity Profile Case 2

The contact between components assists to calculate friction force through the motions. The obtained results from simulation demonstrate the required force (Figures 5.7 and 5.8) for mentioned motions in table 7. The maximum force in case one is 18 N while it is 25 N in case 2. The applied motion in case two positioned the end-effector close to boundary of workspace while the actuator one in the hexapod had the lowest stroke. Therefore the weight of the structure is tolerated by that actuator.

5.7 Control Simulation Results

The obtained data is imported to the developed inverse kinematics of the hybrid parallel robot in order to find the position of the end effector.

The accuracy and controlling system of the hybrid parallel robot is experimented in eight cases. The results of error in the controlling model for linear motions are demonstrated in the figures below. For each case the length of the actuators is imported to simulation software to find the position of the end effector from a forward kinematic method.

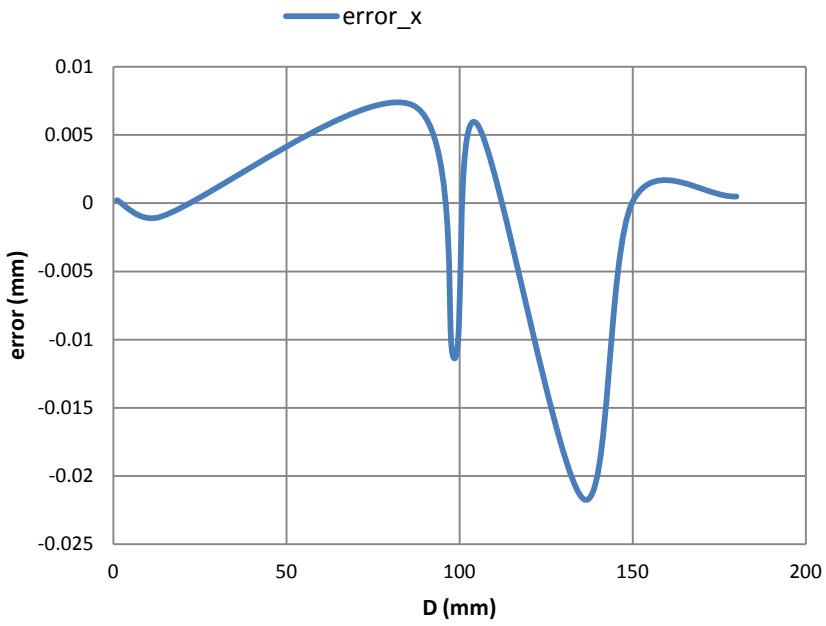

Figure 5-10: Position Error of End Effector in X-axis

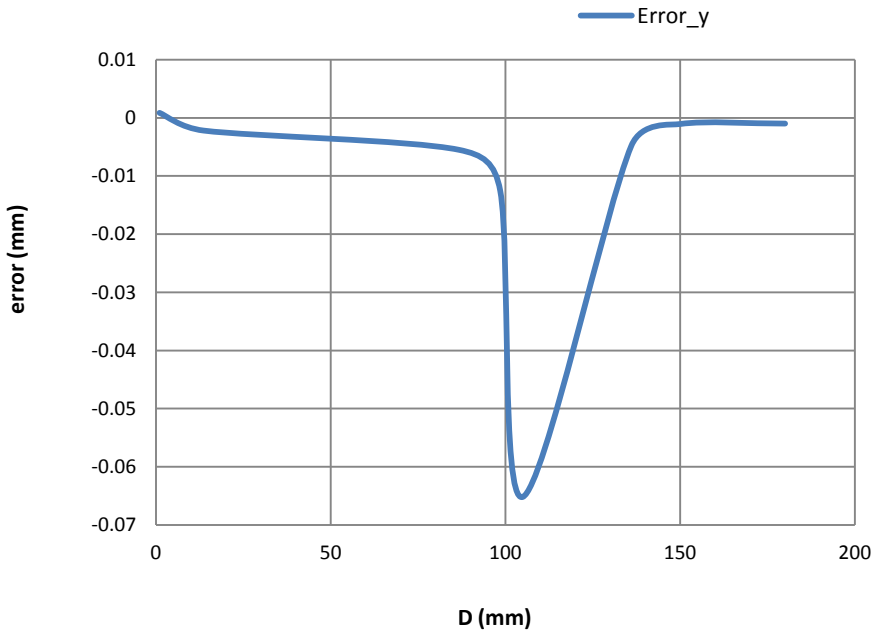

Figure 5-11: Position Error of End effector in Y-axis

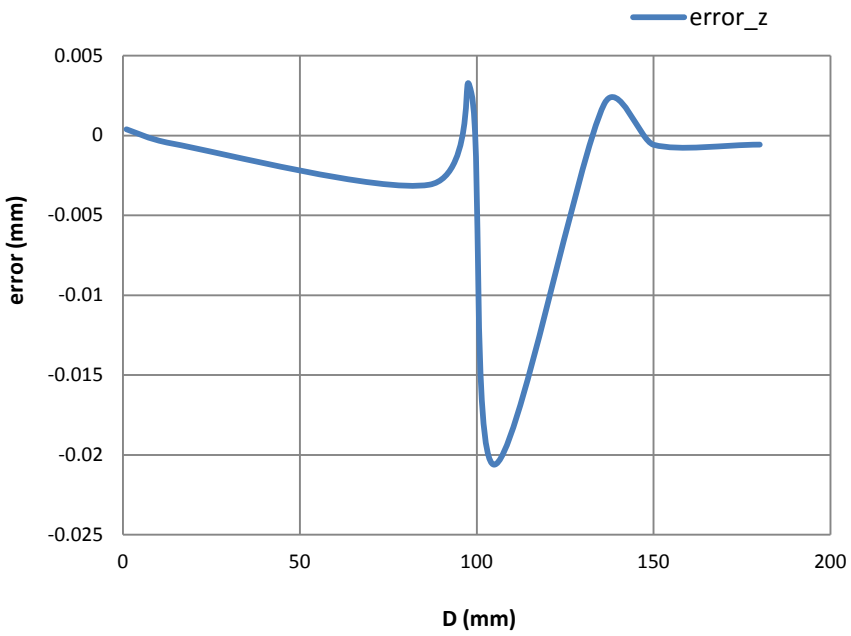

Figure 5-12: Position Error of End effector in Z-axis

As Figures 5.10, 5.11 and 5.12 illustrated the accuracy of theoretical and simulation results, the maximum errors are 0.023mm, 0.06mm and 0.02mm in x, y and z directions respectively. The errors in considered linear motions could be ignored for rehabilitation application.

5.8 Conclusion

This chapter presented a new configuration of parallel robot with increased workspace. The developed stiffness formulation of the hybrid parallel robot is based on calculation of vector

direction of each actuator. Different configurations of the hybrid system were simulated using finite element analysis. The workspace formulation of the model is developed by defining the path motion profile of the tripod, which assists to determine the size of the actuators and the joints' angles. The obtained data are compared against the maximum actual size of the actuator and the maximum rotation angle of the joints, respectively. The results show that the workspace of the new hybrid parallel robot has significantly increased compared with that of a hexapod. The dynamics of the system is simulated for two considered motions to determine the forces required for each actuator. The accuracy of control strategy validated the developed control strategy and kinematics formulations of the system. The experimentations on the physical model are needed to validate the simulation and theory of developed formulations.

Chapter 6

Physical Prototype Building

6.1 Introduction

This chapter addresses the process of building a physical model of a hybrid parallel robot based on a designed CAD model. Static and dynamic experiences are applied on the physical model and the obtained results are compared with simulation and theory. The static experiments and dynamic experiments involve the stiffness and dynamic theory and simulation respectively.

6.2 Physical Model Components

The components of the physical model are selected based on their performance and price and are explained in this section.

The linear actuator is selected for the structure due to the joints' model and high accuracy in motion. Actuators produce energy with a servomotor. The gears convert the rotational motion of the motor to linear motion. The potentiometer inside the system makes the close-loop control providing high accurate motion.

The universal joint is selected based on the connection size of the actuator. Therefore, the size of the inner diameter of the joint should not be less than 1cm.

This component is manufactured based on a design in CAD software. This component is manufactured by a machining group in the University of Birmingham.

The discussed joints are connected to platforms by using an M10 bolt. The fully assembled system is demonstrated in a figure below here.

The SCC-32 is a servo controller with the capability to connect to a computer by a serial port. The controller works with 6V and has 32 channels for connecting. The program of the serial port is developed by MATLAB.

6.3 Static Experimentation and Results

The designed experimentation plans to determine the force exerted to the actuators in different poses with nine force sensors connecting to the system, as is shown in Figure 6.1. Deformation of the system is investigated for the eight different cases comparing the theoretical model and simulation.

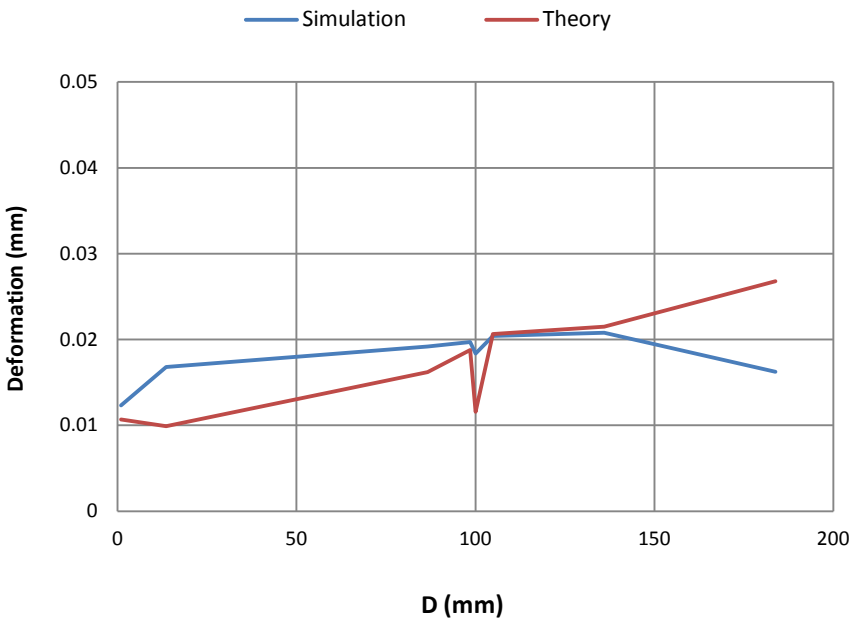

Figure 6-1: Results of Deformation for Theoretical and Simulation Methods

The identified desired points are inputs of the experiment. The length of the actuators is sent to the microcontroller which makes the robot move; the data of the force is considered while the system reaches stability. Applied force to each actuator through to each case of motion is

demonstrated in Figures 6.3 and 6.4. The selected points all are positively related to the coordinate system on the lower platform, which makes the different lengths of actuators and force. The physical model and experimentation conditions are demonstrated Figure 6.2. The force sensors are calibrated before placing for experimentation. The calibration methodology and results are illustrated in Appendix C.

The force sensor model is FlexiForce, which has suitable characteristics for the considered static and dynamic experimentations. Linearity error of the sensor is 3% while the repeatability of the sensor is 2.5% of full scale. The response time of the sensor is 5 microseconds. this is an important factor for dynamic experimentation. The force range of the sensor is between 0 and 440N.

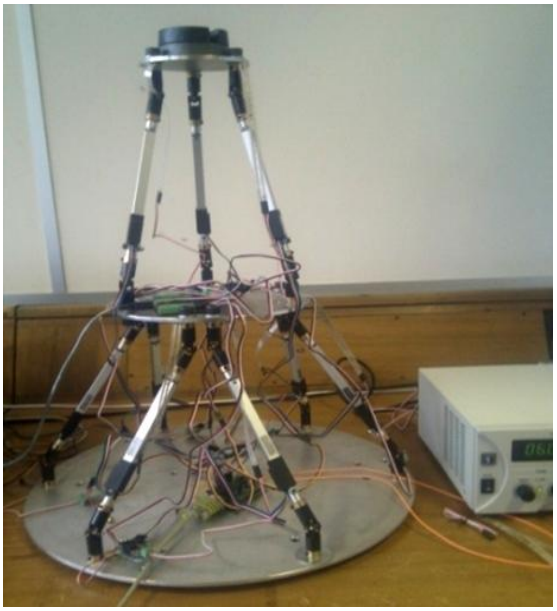

Figure 6-2: Prototype and Experimentation Model

The results were obtained while an external force (100 N) was applied to the system on platform E.

The parameter D in the graphs is previously defined in chapter five (Equation 5.14.a). The same motion in Table 6 is selected for static experimentations.

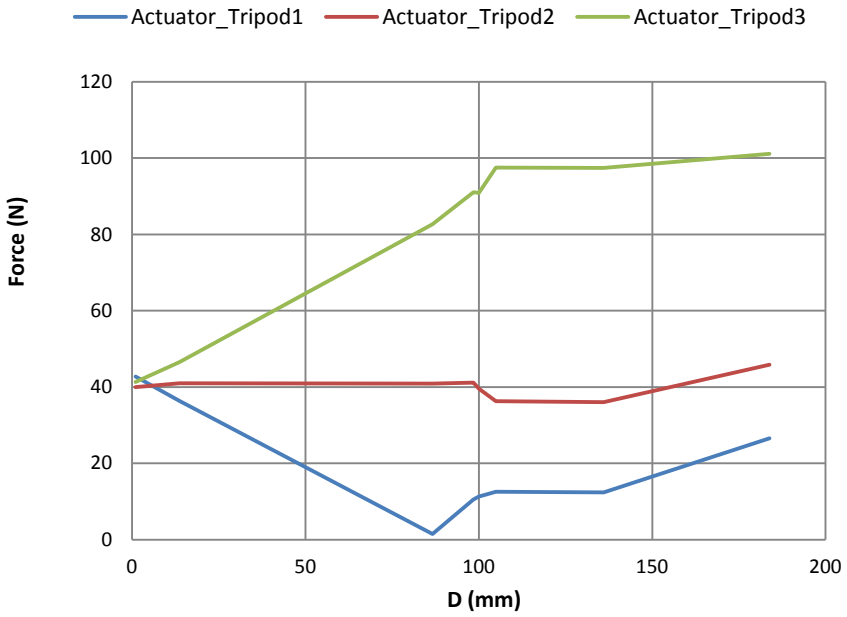

Figure 6-3: Force on Actuators of Tripod

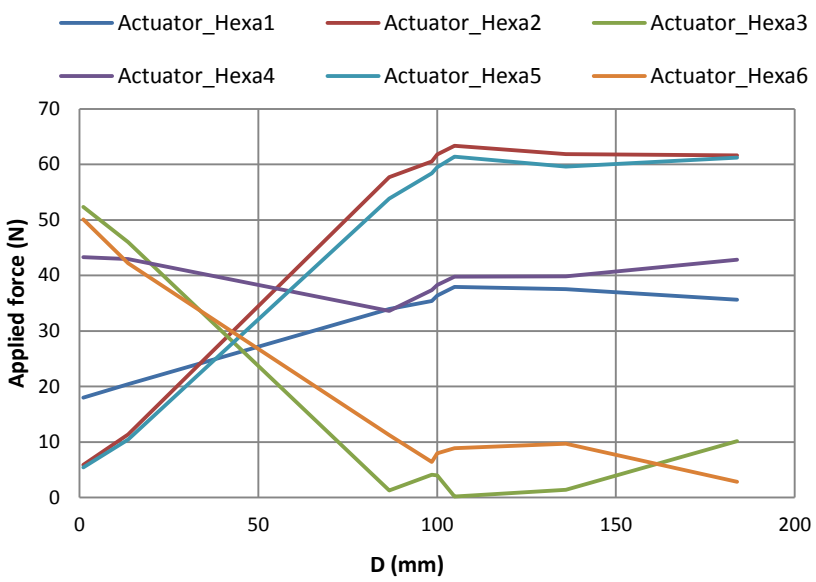

Figure 6-4: Applied Force on Actuators on Hexapod

The applied forces on the actuators by changing the stroke size of two actuators in the hexapod structure are compared in Figure 6.5. While applied force on the actuators in theory and experiments are compared in Figure 6.6.

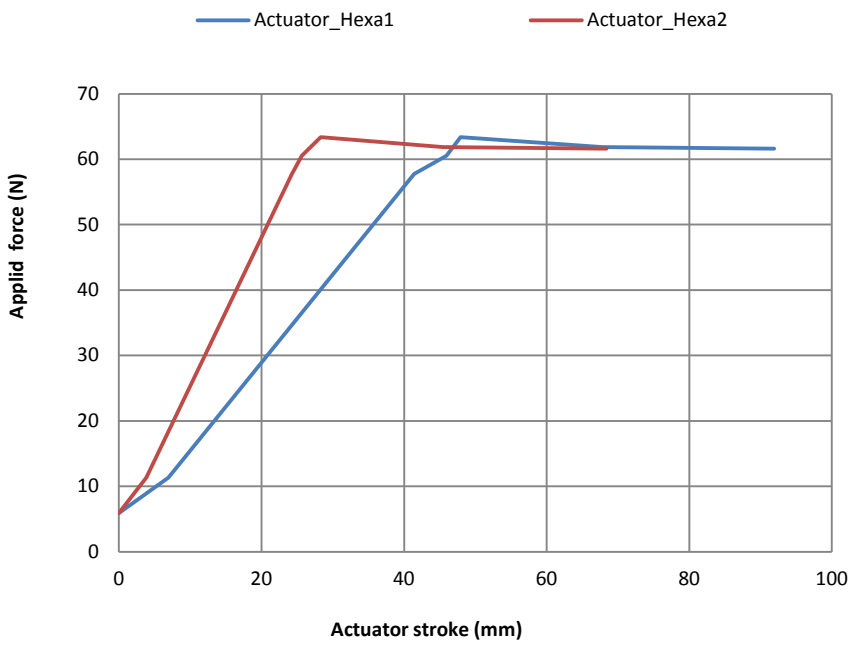

Figure 6-5: Force on the Actuators based on the Size of Stroke

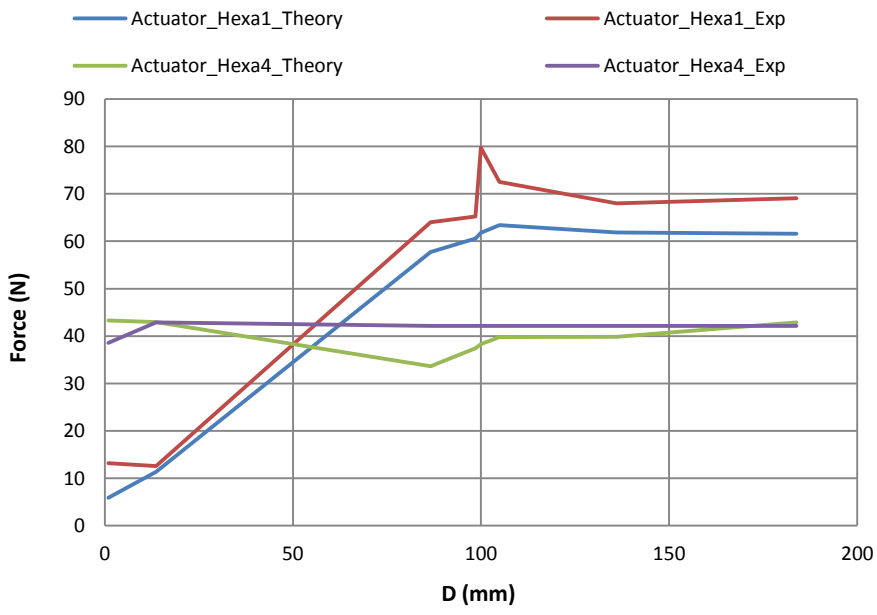

Figure 6-6: Comparison of Theoretical and Experimental Results

The considered experimental for the system verified the theoretical value force on the actuators through translation motion, which is shown in the Figure 6.6. The trends of force in theory and experiment results are the validation for theory. The difference in value could be calculation of friction and also the error in the sensors.

6.4 Dynamic Experimentation and Results

In the first step the results of the actuator force were obtained by the force sensor on the system while the robot was in different positions. In this study, the obtained force results from the sensor are compared with the simulation results.

In this experiment the force applied on the actuators through identified motions (Table.7) is determined by using force sensors placed between the joints and actuators shown in Figures 6.7 and 6.8 for case 1. The experimentation rig and sensors are demonstrated in Figure 6.9.The results of the experiment are compared with simulation in Figures 6.11, 6.12 and 6.13.

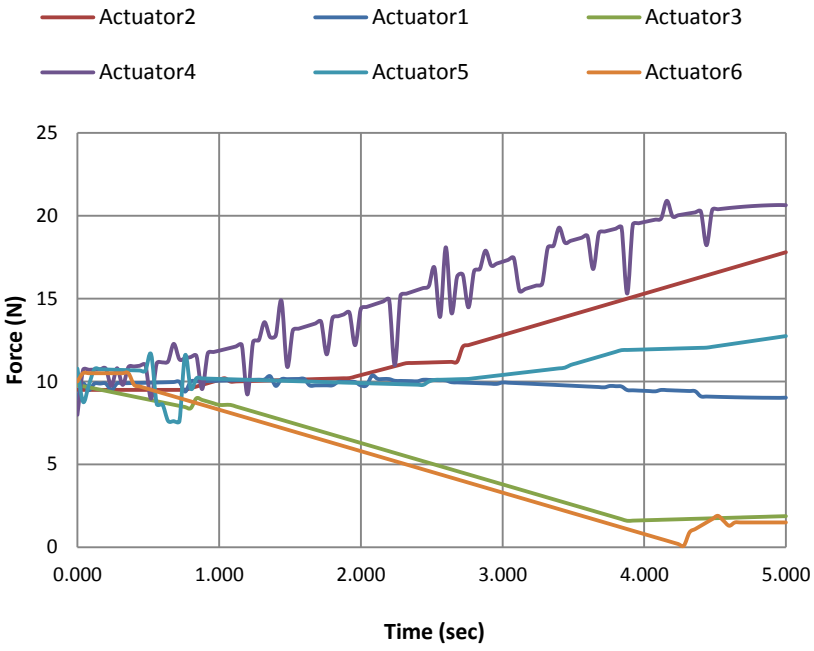

Figure 6-7: Motor Force for Experimental Result Case 1

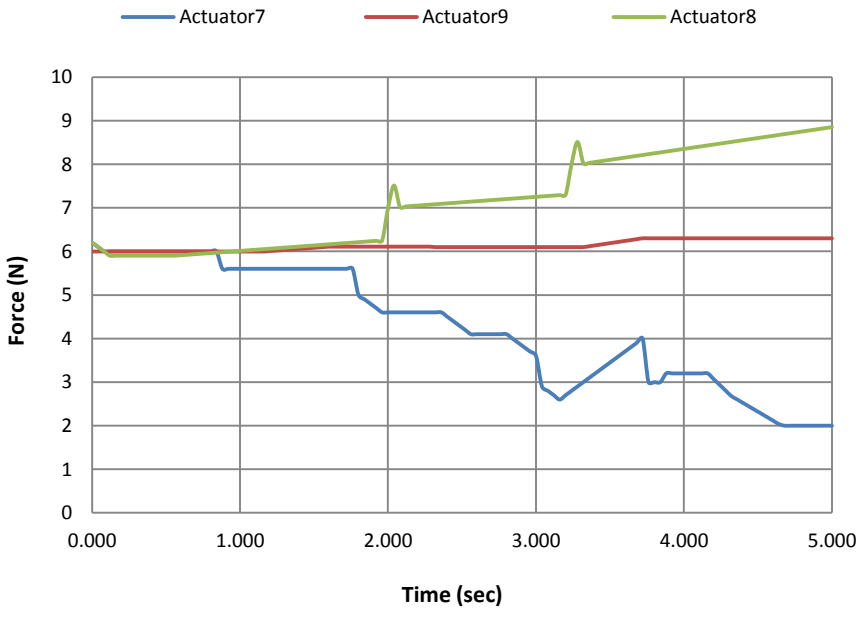

Figure 6-8: Experimental Results of Actuator Force of Case1

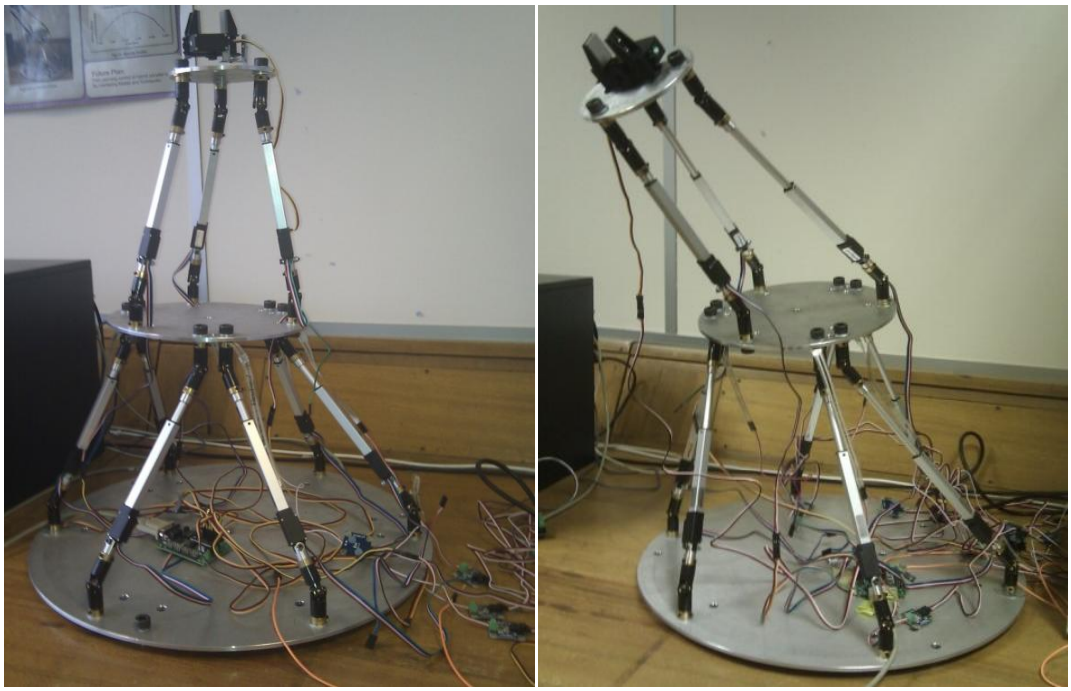

Figure 6-9: Prototyped Hybrid Parallel Robot for Dynamic Test

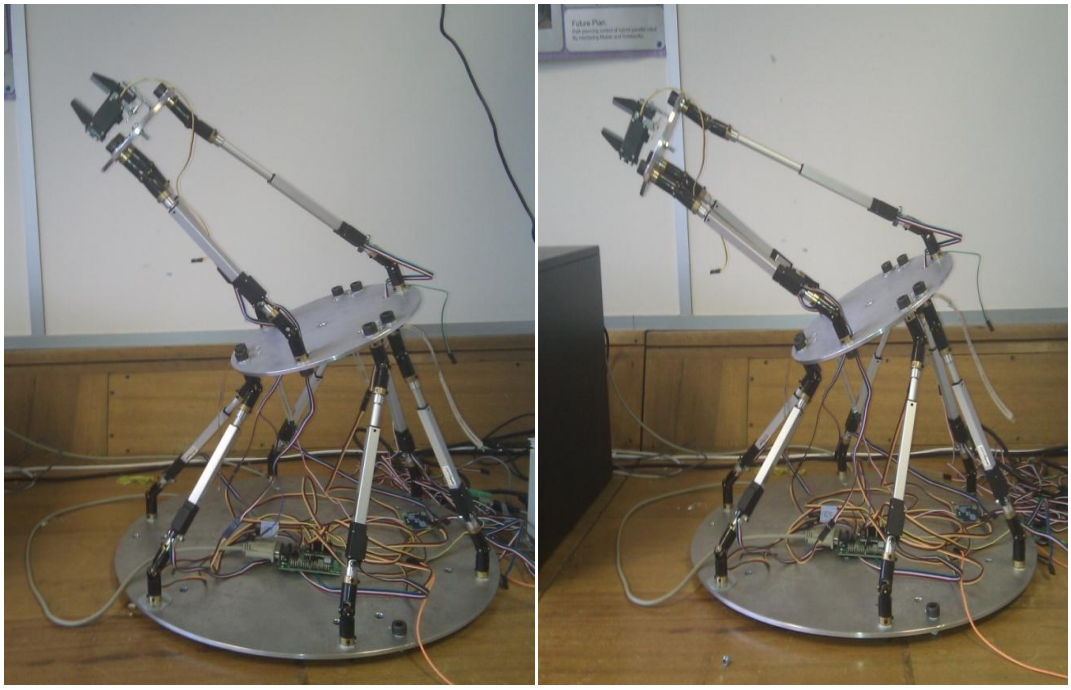

Figure 6-10: Prototyped Hybrid Parallel Robot for Dynamic Test

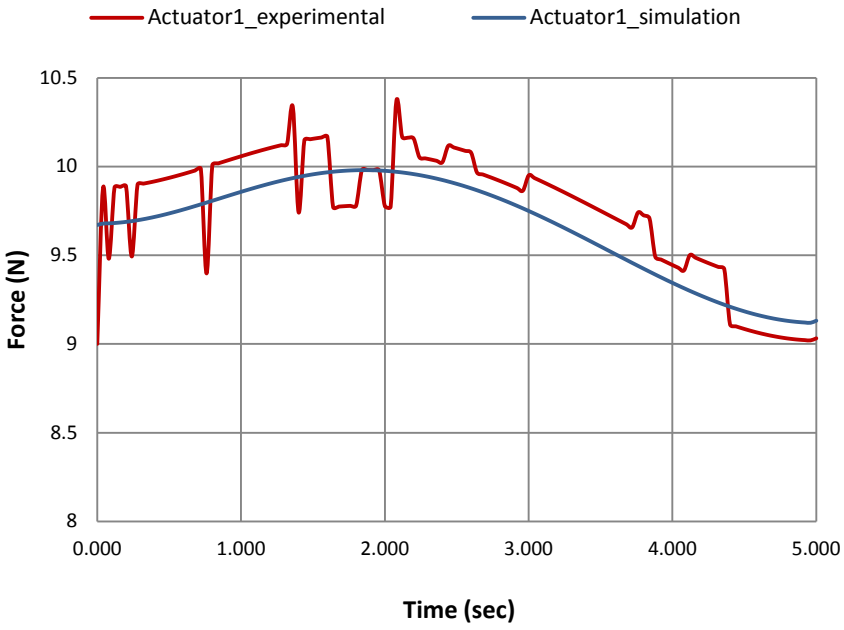

Figure 6-11: Force Comparison on the Actuator in Case 1

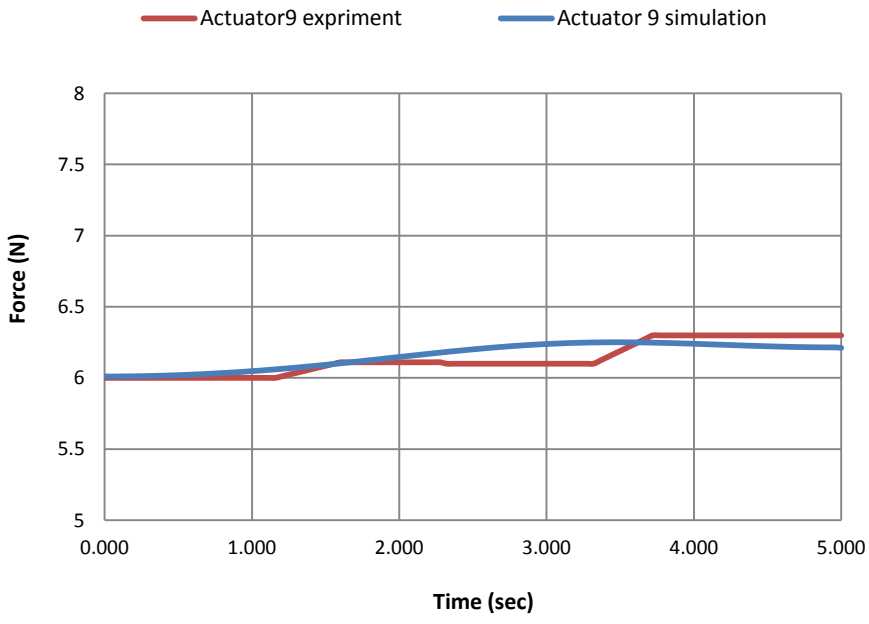

Figure 6-12: Force Comparison on the Actuator in Case 1

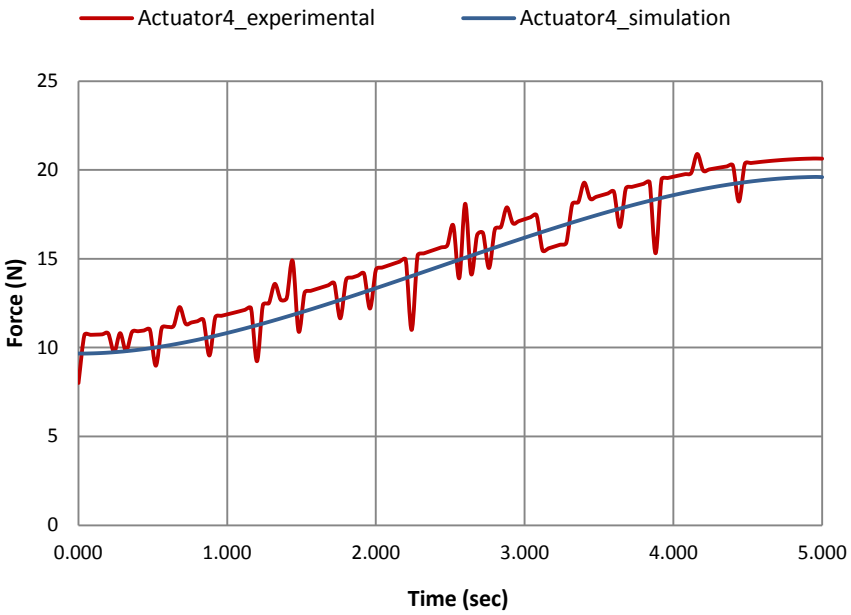

Figure 6-13: Force Comparison on the Actuator in Case 1

As the comparison figures of experimental and simulation results illustrated, the simulation results are completely validated. However the experimental results have fluctuation from the begging to end of the motion due to quality of the force sensors for dynamic tests. Filtering the received data (Developed program in Matlab) are applied for the second case to modify the experimental results for comparison.

The experimental results for case two are demonstrated in Figures 6.14 and 6.15. The simulation and experimental results are compared in Figure 6.16.

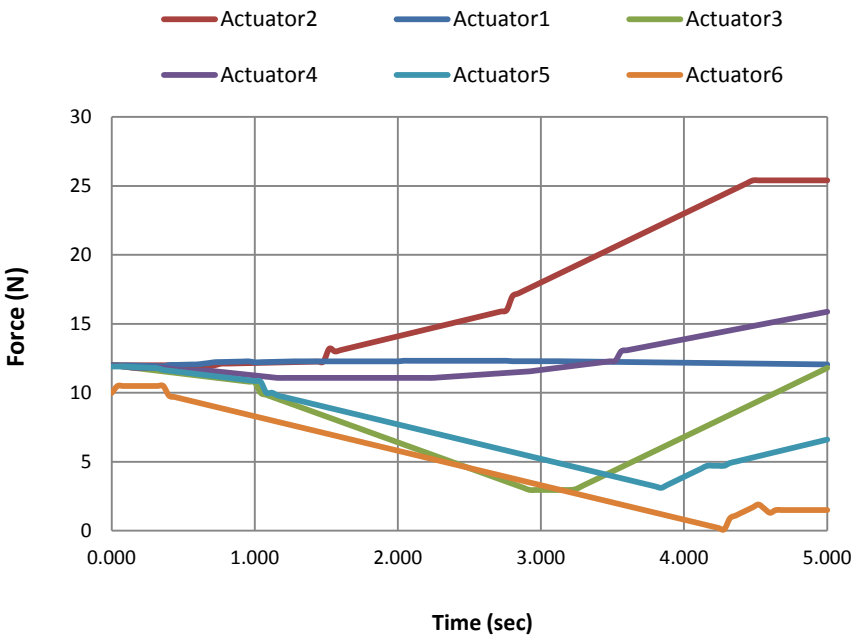

Figure 6-14: Experimental Results of Actuator Force Case 2

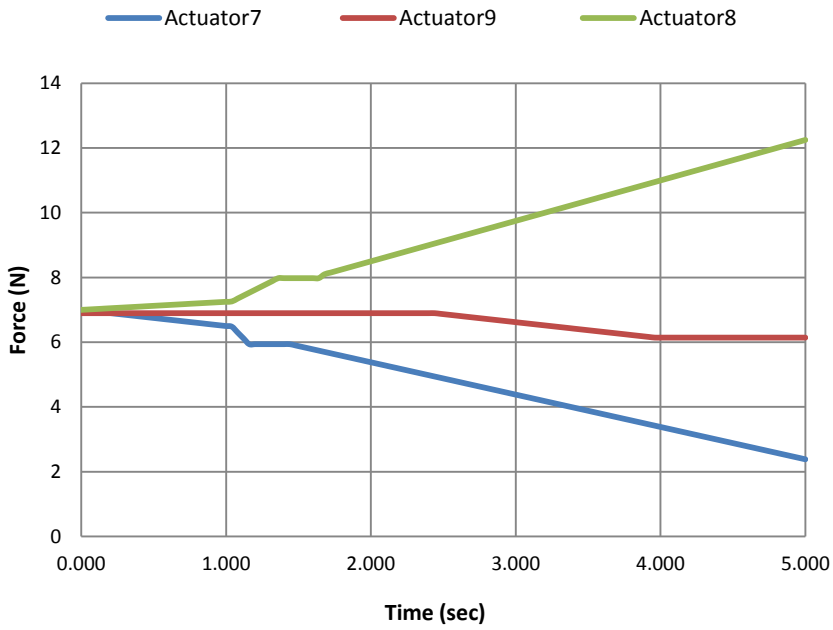

Figure 6-15: Experimental Results of Actuator Force Case 1

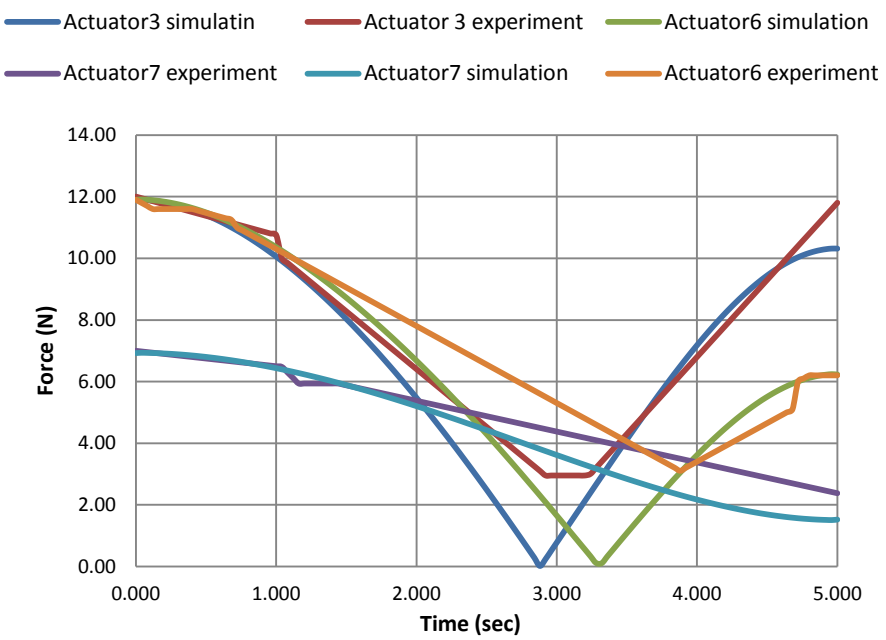

Figure 6-16: Comparison of Experimental and Simulation Result Case2

The results of experimentation of dynamics are obtained by using the force sensor through second motion while the beginning and ending points were identified. As the Figures 6.13 and 6.14 are demonstrated, the applied force on the actuators changed according to size of strokes and velocity of the actuators. The comparison of the simulation and experimental results are demonstrated in 6.15 validate the simulation results. However, there are several factors affecting the obtained data from the force sensors such as the pressure between the components while the bolt fixed on the washer, the weight of the components, the positioning of the force sensors between the components. The required actuator force reduced through the motion due to influence of the friction at the beginning of the motion. The increase of the force in the second part of the motion is due to affect of the weight in some of the actuators.

The actuator-3 has different force path rather than others that is due to stroke size that is less than the others.

The obtained results from experiments were successfully validated the simulation results. However the offset between the trend of experimental and simulation results could be due to sensor error and effect of the weight through the motions.

6.6 Conclusion

In this chapter, the description of the physical model of the hybrid parallel robot is given. The prototype is built in order to validate static and dynamic simulation and theory results. The components of the assembly were introduced. The static and dynamic experiments were designed for the system. The obtained results from the static experiments determined the applied force on the actuators while the end-effector moved to different positions. The comparison figures illustrated validate the simulation and theory results. The difference between results could be due to accuracy of force sensors that were used for experiments. The dynamics experimentation results were compared with the results of simulation. The comparison figures validate the obtained results in simulation and theory. The dynamics tests were successfully were applied on the system while the force sensors capturing the applied force on each actuator. The theories and the methodologies of stiffness and dynamics were validated that verify the proposed hybrid parallel robot configuration.

Chapter 7

Path Planning and Control Strategy

7.1 Introduction

This chapter presents a singularity-free path planning approach for a hybrid parallel robot as well as tracking the end-effector's position. The best configuration of the robot for reaching to the desired position would be decided according to the developed stiffness and inverse dynamic of the system. The developed network allows consideration of all the possibilities and takes into account the velocity and stiffness of the motion profile. Methodology is developed to avoid the singularity configurations of the hybrid parallel robot in this chapter. Nominal polynomial paths are used for the motion of the end-effector and the strokes of each actuator are calculated by using developed inverse kinematics. A MATLAB program has been developed to generate the designed paths, and several poses have been tested in a CAD model of the hybrid parallel robot to validate the feasibility of the path planning approach.

The positions of the joints attaching to the platforms are calculated by using a transformation matrix while initial positions of joints are fully defined. The developed kinematic of the

system is used to find the end-effector's positions and position vectors of the actuators through the motion [96]

7.2 Singularity Analysis

In general, the singularities happen, while some of the vector force of the actuators in particular poses and orientations of the end-effector are zero. Singularities in the workspace can be calculated by identifying the force transfer matrix of the structure. A typical consequence caused by the singularities of parallel robots is collapsing of the parallel structure.

The proposed hybrid structure is composed of nine actuators that are connecting two moving and one fixed platform. Inverse kinematics calculate the position vector of actuators that are not related to each other. The unit vector of each actuator demonstrates the direction of the force created by the actuators.

In Cartesian space (global frame), the pose X of the end-effector is determined by the position variables ($x \quad y \quad z$) and orientation variables ($\alpha \quad \beta \quad \gamma$), which can be expressed in equation 7.1.

$$X = [x \quad y \quad z \quad \alpha \quad \beta \quad \gamma]^{T} \tag{7.1}$$

The exerted force on the top platform hexapod (platform A) is developed in equation 7.2.

$$F_{in}(X) = [\, F_1 \quad F_2 \quad F_3 \quad F_4 \quad F_5 \quad F_6 \,]^T \tag{7.2}$$

Where, F_{in} is the force matrix of the hexapod created by the actuators on platform A and F_i actuator force.

In order to calculate the vector force, the unit vector of the actuators is obtained.

$$S_i = \frac{L_{Hi}}{\|L_{Hi}\|} \qquad i \in \{1 \dots 6\} \tag{7.3. a}$$

$$F = \sum_{i=1}^{6} s_i F_i \tag{7.3.b}$$

The created moment on the platform A due to linear forces of the actuators is obtained by equation 7.4.

$$M = \sum_{i=1}^{6} (A_i \times s_i) F_i \tag{7.4}$$

The results of the actuators' force for each motion could be defined in a matrix that is expressed in equation 7.5.

$$F_{out}(X) = [F \quad M]^T \tag{7.5}$$

The relations of the input and output load of the hexapod parallel manipulator can be given by

$$F_{out}(X) = H(X) \cdot F_{in}(X) \tag{7.6}$$

The matrix $H(X)$ is a 6×6 force transformation matrix which indicates how the output load is related to the input forces.

The force transformation matrix of the hybrid parallel robot is obtained as:

$$H(X) = \begin{bmatrix} \overset{s_1}{A_1 \times s_1} & \overset{s_2}{A_2 \times s_2} & \overset{s_3}{A_3 \times s_3} & \overset{s_4}{A_4 \times s_4} & \overset{s_5}{A_5 \times s_5} & \overset{s_6}{A_6 \times s_6} \end{bmatrix} \quad (7.7)$$

The force transformation matrix H represents the relations between the input forces F_{in} and the output forces F_{out}. When H(X) is singular, the kinematics equation will be degenerated and some loads (forces and/or moments) on the upper platform cannot be supported by the actuator forces. As a result, the end-effector gains some extra degrees of freedom and becomes uncontrollable.

Therefore, the criterion of the singularity configuration of the hexapod platform is equivalent to the singularity of the force transformation matrix. Therefore, the criterion of the singularity configuration of the hexapod parallel manipulator is given as:

$$\det(\mathrm{H}(\mathrm{X})) = 0. \quad (7.8)$$

Where, det is a command defined to calculate the determinant of a matrix in MATLAB.

The boundary singularity configuration is determined by the boundary conditions of the hybrid parallel robot; the boundary conditions are determined by the length limitations of the nine actuated legs.

The boundary condition of the hybrid robot can be expressed as

$$L_{min} \leq L_i \leq L_{max} \quad (i = 1\ to\ 9\ ) \tag{7.9}$$

Where, $L_{min} = 226.11\ mm$ and $L_{max} = 326.11\ mm$.

Thus, the criterion of the singularity configurations of the parallel robot consisted of the criterions of serial and parallel singularities. The singularity-free condition of the hybrid parallel robot can be expressed as:

$$\det(H(X)) \neq 0, \text{ and } L_{min} \leq L_i \leq L_{max} \quad (i = 1\ to\ 9) \tag{7.10}$$

7.3 Singularity-free Path Planning Approach

In this section different methodologies are developed in order to support the singularities as well as enhancing the performance of the system. The optimized methods are applied on developed polynomial path for end-effector.

7.3.1 Initial Polynomial Paths for End-effector

The path planning approach for the hybrid parallel robot starts with defining an initial nominal path to connect two given poses of the end-effector in the workspace. Initially, a straight line is used as the nominal path, however, when the end-effector moves along the considered path, large accelerations presented along the path, especially at the start and end poses.

This problem is solved by using a polynomial path as the nominal path; as a polynomial path is smooth, and the acceleration of the path can be taken in consideration by using high degree polynomial equations. A detailed description for generating polynomial paths is introduced [51].

In this section, a polynomial path will be formulated to connect a start pose P_0 and an end pose P_1 without considering the singularity and boundary conditions. The path is formulated as a function of a parameter $u\,(0 \leq u \leq 1)$ with the understanding that it can be parameterized with respect to time t. The function of the nominal path can be expressed as:

$$P(u) = a_0 + a_1 u + a_2 u^2 + a_3 u^3 + \cdots + a_n u^n \ (0 \leq u \leq 1) \qquad (7.11)$$

Where, $P(0) = X_0$ and $P(1) = P_1$.

Where, the parameter n represents the number of degrees of the polynomial equation which is determined by numbers of constraints. In order to finish the tasks faultlessly, the end-effector needs to move without velocity and acceleration when approaching the target poses P_0 and P_1. Thus, a rest to rest path with zero acceleration at the start and end pose is considered in this path planning approach, i.e. the first, second and third derivative of the polynomial path at both initial and final poses must equal to zero. Those constraints are given by

$$P(0) = P_0 \quad \dot{P}(0) = 0 \quad \ddot{P}(0) = 0 \quad \dddot{P}(0) = 0$$

$$P(1) = P_1 \quad \dot{P}(1) = \ddot{P}(1) = 0 \quad \dddot{P}(1) = 0 \tag{7.12}$$

To meet these eight conditions, a seven degree polynomial path is used, which can be expressed as:

$$\mathrm{P}(u) = a_0 + a_1 u + a_2 u^2 + a_3 u^3 + a_4 u^4 + a_5 u^5 + a_6 u^6 + a_7 u^7 \quad (0 \leq u \leq 1) \tag{7.13}$$

Substituting Equation (7.12) into Equation (7.11), gives the seven coefficients $a_0\ a_1, \ldots\ a_7$ of the polynomial path, and the initial nominal path of the path planning approach given by equation (7.13).

7.3.2 Serial Optimization Method

After a nominal polynomial path connecting the initial pose P_0 and final pose P_1 has been obtained, the path shall be optimized to avoid the singularity configurations of the end-effector. In this section, an optimization method is developed for the hybrid parallel robot.

According to the kinematic analysis of the hybrid parallel robot, the poses of the end-effector along the nominal path are determined by the equation shown below:

$$P(u) = P_H(u) + P_T(u) \tag{7.14}$$

$P_H(u)$ and $P_T(u)$ are the poses of the central points of the upper platform of the hexapod and tripod respectively. The values of position and orientation variables of $P_H(u)$ and $P_T(u)$ are based on the global coordinate system.

By defining a proportional factor Δ for the equation (7.11), the poses of the hexapod and tripod manipulator can be obtained with respect to the poses of the end-effector, which is expressed as:

$$P_H(u) = \Delta P(u),$$
$$P_T(u) = (1 - \Delta)P(u) \tag{7.15}$$

A default value was given to the proportional factor Δ, given as:

$$\Delta = \Delta_0 \tag{7.16}$$

Thus, initially, the path of the upper platforms of the hexapod and tripod manipulator can be expressed as:

$$\mathrm{P}_H(u) = \Delta_0 P(u),$$

$$\mathrm{P}_T(u) = (1 - \Delta_0) P(u). \tag{7.17}$$

While the end-effector moves along the nominal polynomial path, the poses of the end-effector will be checked with the singularity-free condition of the parallel robot; the condition has been obtained in Equation (7.13). When a specific pose is determined to be singular, an optimization method is developed to adjust the poses of both the hexapod and tripod parallel manipulator. This method is called the "Serial Optimization Method" in the remaining contexts of this section.

This "Serial Optimization Method" is designed to solve the problem of singularity by adjusting the proportional factor Δ of the hybrid parallel manipulator. Therefore, the pose of the hexapod $\mathrm{P}_H(u)$ and the pose of the tripod $\mathrm{P}(u)$ will be adjusted to support the singularity of the hybrid robot. Meanwhile, the end-effector will always stay at the same pose $P(u)$, and the nominal path for the end-effector will not be changed during this method. Thus, the smoothness and continuity of the seven degree polynomial path remains in the final singularity-free path. This is also a practical advantage of the hybrid parallel robot over the general type of parallel manipulators.

7.3.3 Detour Optimization Method

When the "Serial Optimization Method" fails to find a singularity-free path, then the pose of the end-effector has to be changed. In this kind of situation, another optimization method named the "Detour Optimization Method" will be applied to generate a singularity-free path. During this optimization method, a non-singular pose is found for the end-effector. The pose X_{via} will replace the initial singular pose on the nominal polynomial path. Therefore, this optimization method is designed to obtain a singularity-free path by optimizing the nominal path locally, and the final path will detour the singular poses presented on the nominal polynomial path.

While the end-effector moves along the nominal polynomial path, the poses of the end-effector will be checked with the singularity-free condition of the parallel robot, when a singular pose $X_{singular}$ presents on the nominal path, a via point X_{via} will be obtained by applying a loop algorithm. During the procedure of the loop, intermediate poses will be determined to replace the singular pose on the nominal path, and the intermediate poses are given by optimizing the position variables (x, y and z) of the singular pose. The singular pose found on the nominal polynomial path is expressed as:

$$p_{singular} = P(u) = [x_u \quad y_u \quad z_u \quad \alpha_u \quad \beta_u \quad \gamma_u]^T \tag{7.18}$$

Intermediate poses will be found by changing the coordinate value of the singular pose starting from x, y and z respectively. Finally, a non-singular via pose is found, which is expressed as:

$$P_{via} = [x_{via} \quad y_{via} \quad z_{via} \quad \alpha_u \quad \beta_u \quad \gamma_u]^T \tag{7.19}$$

The output of this detour optimization method is:

$$\mathrm{P}(u) = \mathrm{P}_{via} \tag{7.20}$$

Thus, after the method is finished, the singularity pose on the nominal path is replaced by a non-singular via pose. The nominal polynomial path has been locally optimized and becomes a singularity-free path for the end-effector. During the process of the method, a parameter ∂ is utilized to ensure that the via poses do not locate too far away from the singular pose on the nominal polynomial path. This parameter is designed to guarantee the smoothness of the final non-singularity path.

7.3.4 Time Determing Method

After the final singularity-free path $P(u)$ has been obtained, the path is formulated in terms of parameter u $(0 \leq u \leq 1)$. However, the movement of the end-effector should be controlled

by time t, and a time determing method is introduced in this section. This method is designed to determine a shortest moving time for the hybrid parallel robot along the singularity-free path.

The method is developed by finding a linear relation between parameter u and time t, the relation can be expressed as:

$$t = \varepsilon u + 1 \tag{7.21}$$

The maximum speed of the linear actuators utilized in the hybrid prallel robot is $12\ \mathrm{m/s}$, and the coefficient ε is chosen to ensure that the maximum velocity of the nine actuator legs is less than the speed limitation. The velocity of the nine actuators is calculated in the inverse kinematic analysis of the parallel robot [97].

Time t starts from $t = 1\mathrm{s}$ (when $u = 0$), and the first second remains for the parallel robot to adjust itself to the initial pose desired P_0.

7.4 Results and Discussion

A MATLAB program has been developed to implement the singularity-free path planning approach. The operation process of the MATLAB program is explained in Figure 7.1. The MATLAB program was developed in order to generate a singularity-free path based on the

original polynomial path, which has been described in this section. In addition, the MATLAB code for the inverse kinematic analysis of the hybrid parallel robot was developed.

The step interval τ in the MATLAB program is determined to be 0.01, so the nominal polynomial path is divided into 100 segments, and each of them will be checked for the singularity-free condition.

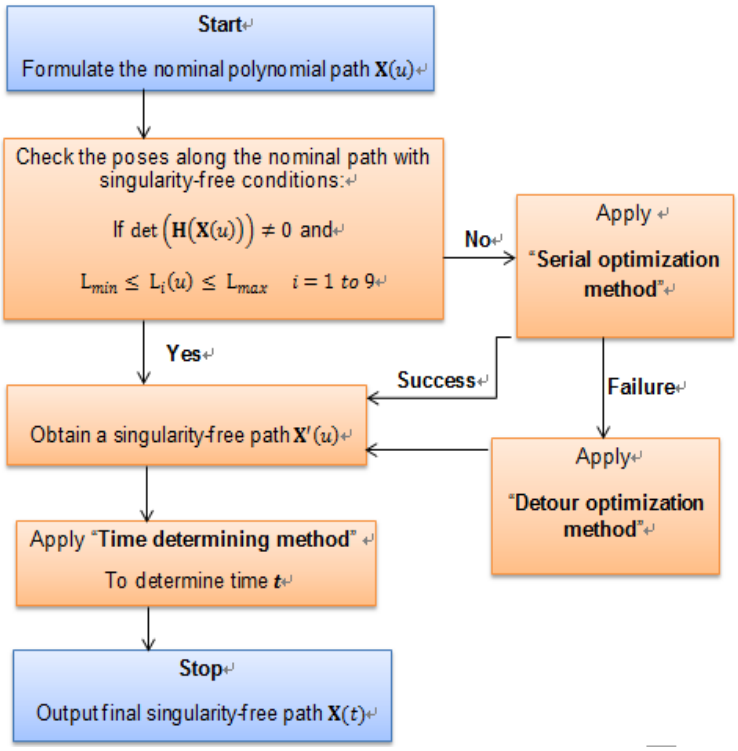

Figure 7-1: Flowchart of the MATLAB Program

After testing the MATLAB program with various trajectories, the best value of the default proportional factor is determined to be 0.5. Therefore, motion of the end-effector, is divided exactly similar between hexapod and tripod platform respectively. It can be expressed as:

$$\mathrm{P}_H(u) = 0.5P(u), \quad \mathrm{P}_T(u) = 0.5P(u) \tag{7.22}$$

The MATLAB program has been tested to generate a singularity-free path with various poses in the workspace, and one of them is shown below.

The planed path for the end-effector of the hybrid parallel robot starts from a start pose P_0 to a final pose P_1

$$\mathrm{P}_0 = [10 \quad 10 \quad 10 \quad 0 \quad 0 \quad 0]^T,$$
$$P_1 = [100 \quad 80 \quad 110 \quad 0.15 \quad 0.25 \quad 0]^T \tag{7.23}$$

The result of the determinant of the transformation matrix $\mathrm{H(X)}$ is given in Figure 47. It is shown the maximum value of the points on the graph is less than zero. Therefore, the criterion of parallel singularity given in Equation (7.10) has been met which shows there is no parallel singularity on the designed final path.

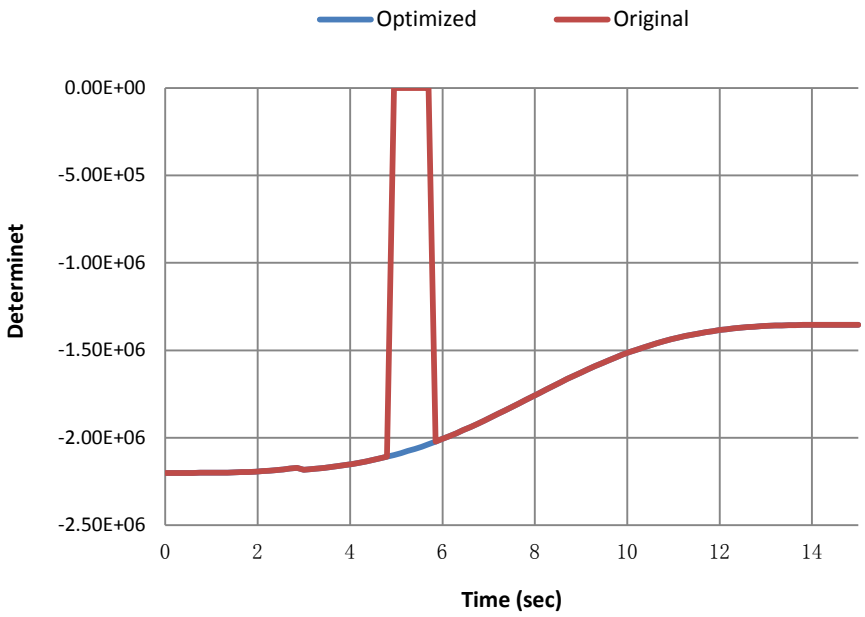

Figure 7-2: Singularity of the Original and Optimized Path

A path connecting these two poses has been generated by the path planning MATLAB program, which is shown in Figure 7.2.

After the singularity-free path is obtained from the MATLAB program, the CAD model of the hybrid parallel robot is utilized to validate the planned path. Using the motion analysis tool in SOLIDWORKS software, the path of the end-effector of the CAD model is determined by defining the displacement of the actuator on each leg. There are some poses in the workspace of the parallel robot where no singularity-free path exists. These situations represent when a pose found by the "Detour Optimization Method" goes beyond the boundary of the working

volume. However, these situations have been reduced effectively by the unique structure of the hybrid parallel robot. As two parallel manipulators (Hexapod and Tripod) have been integrated together in the hybrid parallel robot, one manipulator can remedy the structure limitation of the other. The results of middle platform motion in theory and simulation are compared in Figures 7.3, 7.4 and 7.5.

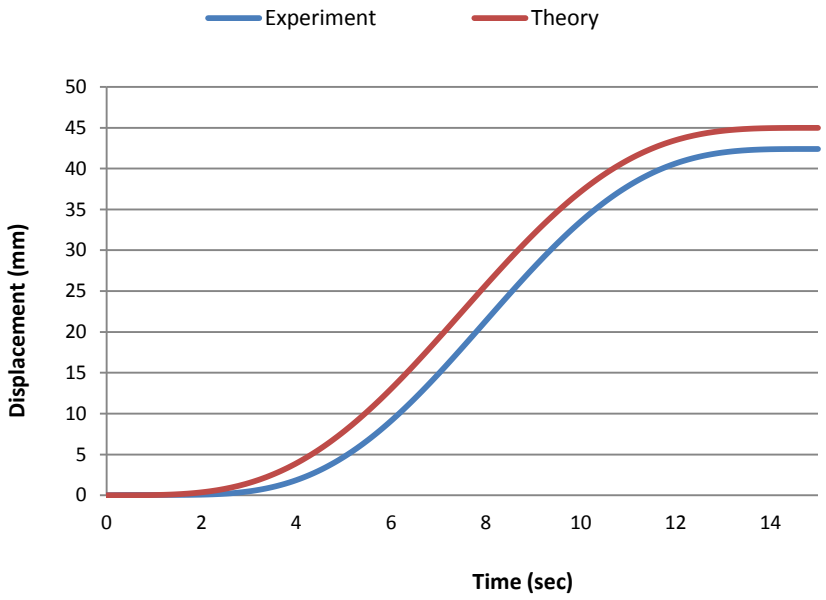

Figure 7-3: Motion of Platform A in X-Axis

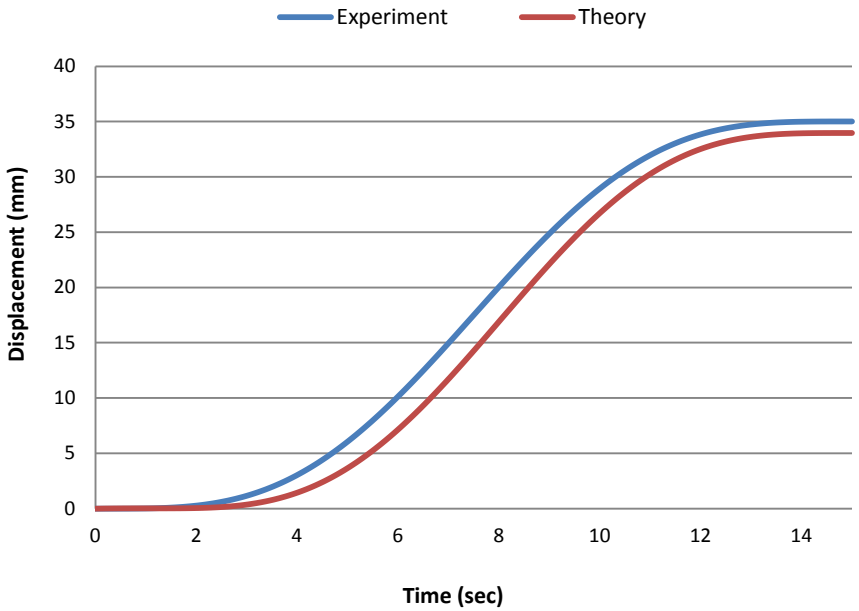

Figure 7-4: Motion of Platform A in Y-Axis

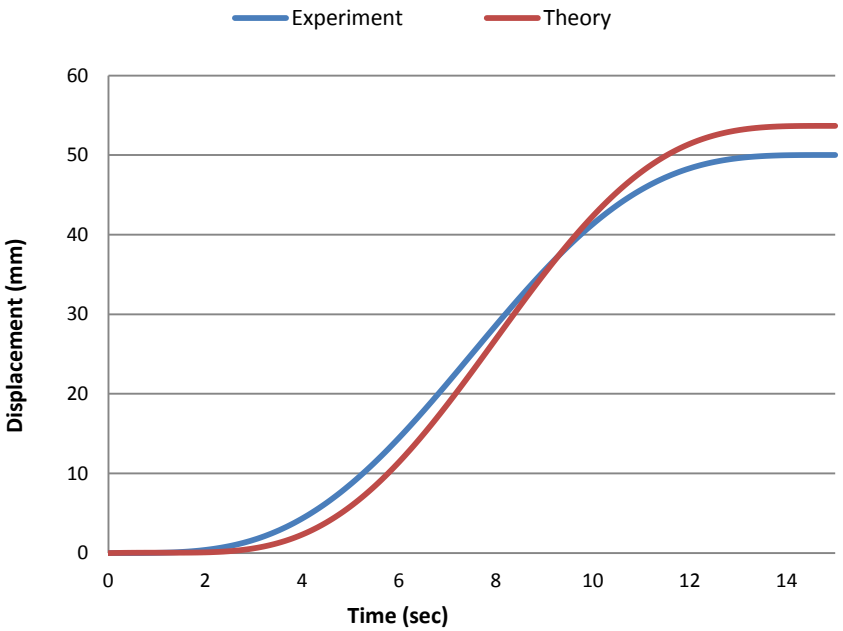

Figure 7-5: Motion of Platform A in Z-Axis

The limitations of this path planning approach are lack of prediction of the non-existence of a singularity-free path. The maximum errors for the motion of platform A were 2mm, 1mm and 1.5 mm in x, y and z respectively.

The results of the applied optimization method for a hybrid parallel robot are compared with simulation data in Figures 7.6, 7.7 and 7.8.

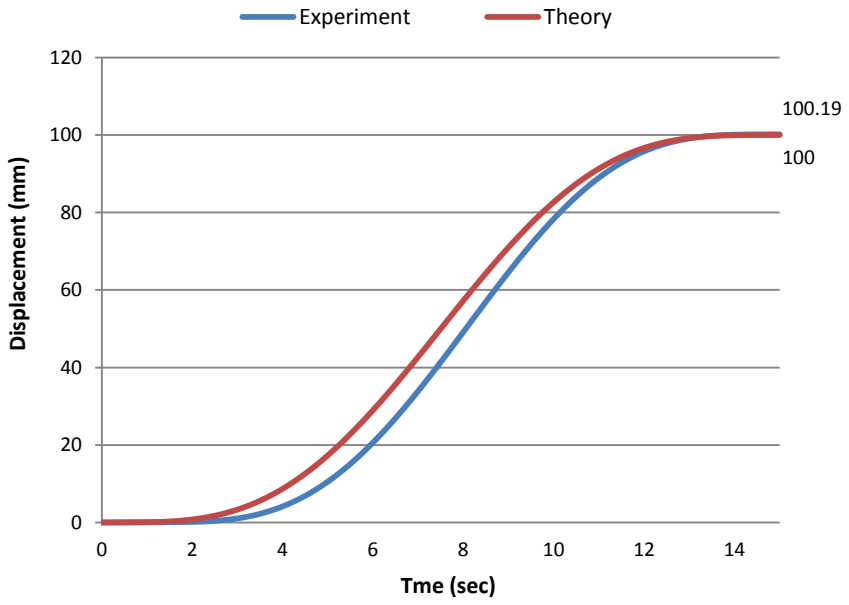

Figure 7-6: Motion of Platform E in X-Axis

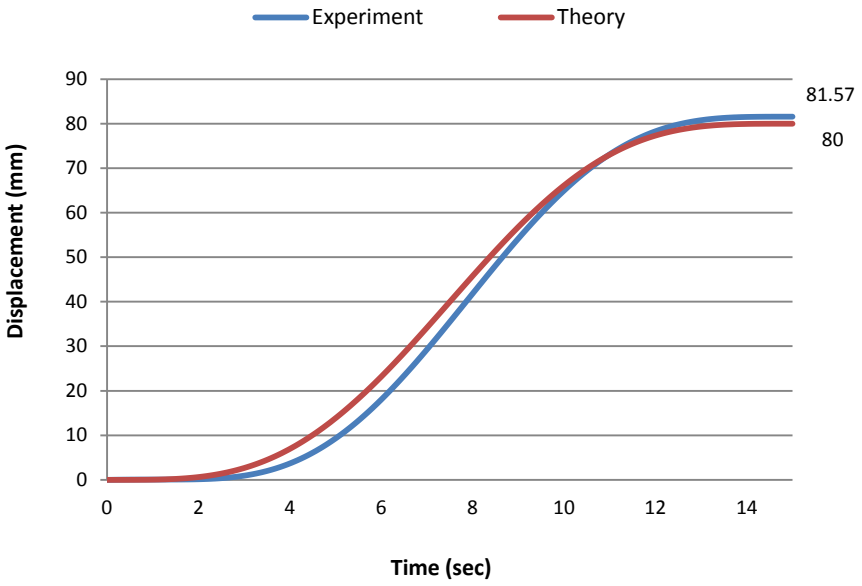

Figure 7-7: Motion of Platform E in Y-Axis

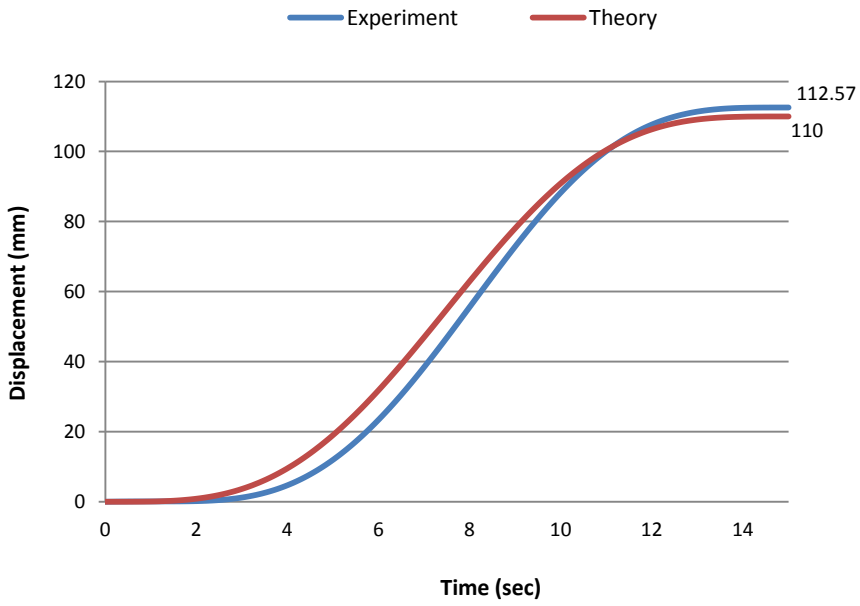

Figure 7-8: Motion of Platform E in Z-Axis

The obtained results from the simulation successfully validated the developed theory for hybrid parallel robot. The maximum error for end-effector 0.19 mm, 1.57 mm and 2 mm in x, y and z respectively.

7.5 Optimum Methodology

The developed methodology assists to define the path for the motion of the platforms while the beginning and end positions are known. The stiffness and velocity of the end-effector between the points have been calculated in order to select the priority for different applications. In the following section the inverse kinematic and inverse dynamic of the hybrid parallel are used.

7.5.1 Bezier Curve

The developed Bezier curve is used to assist the parallel robot's motions for point to point control strategy. The convex shape of Bezier curve guides the end-effectors in a motion in order to ensure the all actuators equally reach to considered stroke in each pass. In this section the Bezier path applied to end-effector motions. The theory and simulation results are compared. In the first steps, a surface patch defined by using The Bezier curve. The force of the each actuator in order to follow the defined curves is simulated. The general formulation

of the Bezier curves is defined in Equation 7.24.a and 7.24.b. The Developed Bezier curve formulation has four control points.

$$P(u,v) = \big(x(u,v), y(u,v)\big) = \sum_{i,j=0}^{3} B_i(u)\, B_j(v) P_{ij}\ . \tag{7.24.a}$$

$$B_i(u) = \binom{3}{i} u^i (1-u)^{3-i} \tag{7.24.b}$$

Where, $P(u,v)$ is defined surface patch and x and y are the parameters are defining surface. In addition $B_i(u)$ is cubic Bernstein polynomial. Moreover, the control points and orientation can be arranged to develop new surface meshes. The proposed concept is useful for the parallel robot's searching (parametric sweep) methodology to calculate the work volume [98, 99].

The methodology describes the control points and subdivides to create the surface mash between the beginning and end pints. The bilinear blended Coon patch formulation (Equation 7.25) is used to enhance the efficiency of the end-effector's motion. The developed patch connected the points of the path planning using the curve instead of the lines [100].

$$x(u,v) =$$

$$(1-u)\times(0,v) + ux(1,v) + (1-v)\times(u,0) + vx(u,1) -$$

$$[1-u \quad u]\begin{bmatrix} x(0,0) & x(0,1) \\ x(1,0) & x(1,1) \end{bmatrix}\begin{bmatrix} 1-v \\ v \end{bmatrix} \tag{7.25}$$

Where, the boundary conditions of curve are as listed: $x(u,0)$, $x(u,1)$, $x(0,v)$ and $x(1,v)$ [101, 102].

Figure 7.9 demonstrates the applied path on the robot's end-effector. The applied curve is used to developed the path in robot's workspace. The sweeping search method is used to find the singular points existing in the path. The developed path for the end-effector will be compared by obtained results from the simulation software in next section.

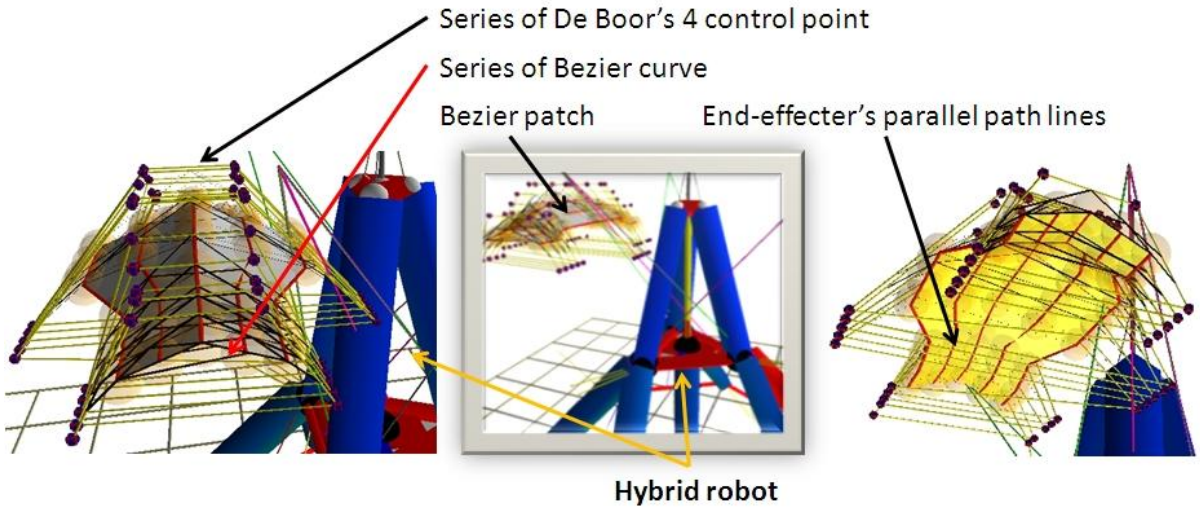

Figure 7-9: The Developed Bezier Curve for End-effectors

The case study is developed to test the develop methodology on hybrid parallel robot (Figure 7.9). In following investigation, the position and orientation is selected for end-effector to reach. The Bezier curve is assisting the end-effector in order to guide it to end position. The developed Bezier curve are programmed in Matlab software. The obtained results are depicted in Figure 7.10.

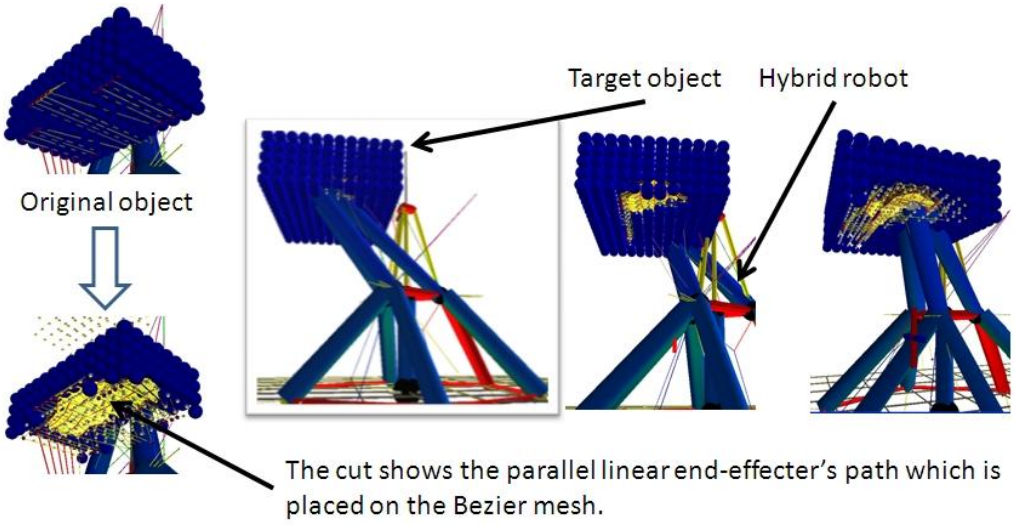

Figure 7-10: Machining Application for Hybrid Parallel Robot Using the Bezier Curve

The obtained data of the Bezier curve was applied to the hybrid parallel robot. The position of the end–effector's changes is calculated by inverse kinematic formulation that is developed for the system, the actuators' stroke are obtained and used for the simulation of the motion with software.

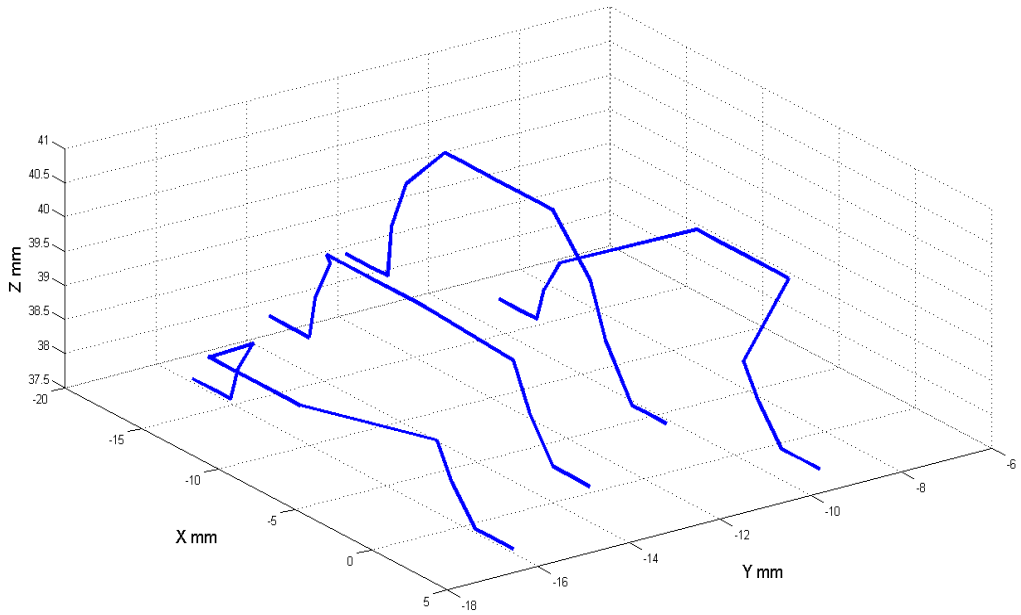

Figure 7-11: The Bezier Patch Data

The developed Bezier curves were demonstrated in Figure 7.11, are used as end-effector motion. In next section the theory and simulation results are compared.

7.5.2 Simulation Results

The size of the strokes for all the calculated paths is applied to the CAD model to determine the required force for the actuators through the motion. In this study, friction between the components is not considered. The only external force is the applying weight of the system.

The Figures 7.12, 7.13, 7.14 and 7.15 demonstrate the force analysis of the actuators for the applied Bezier curves.

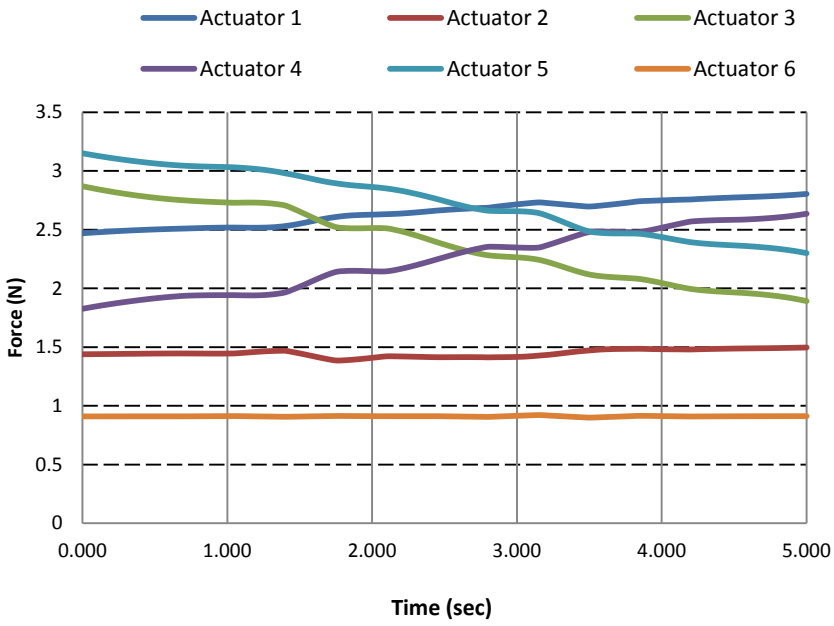

Figure 7-12: Applied Force on the Hexapod's Actuators through the Motion Path1

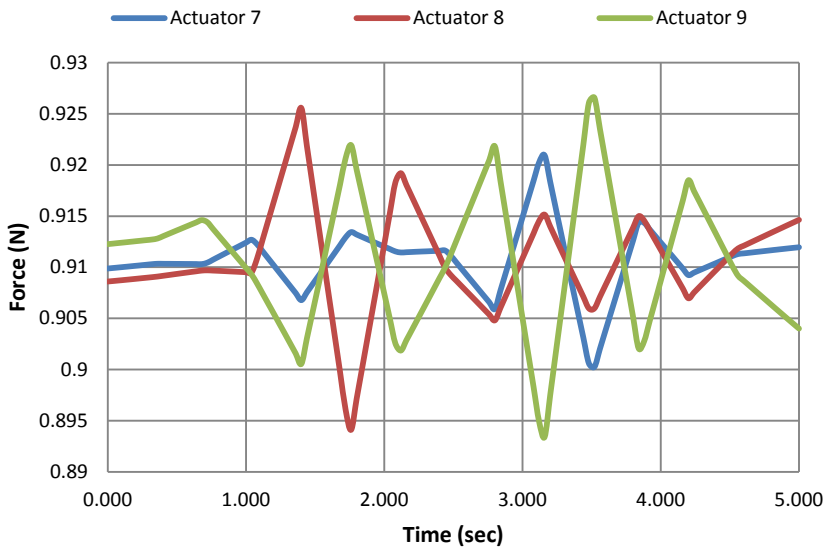

Figure 7-13: Applied Force on the Tripod's Actuators through Motion Path1

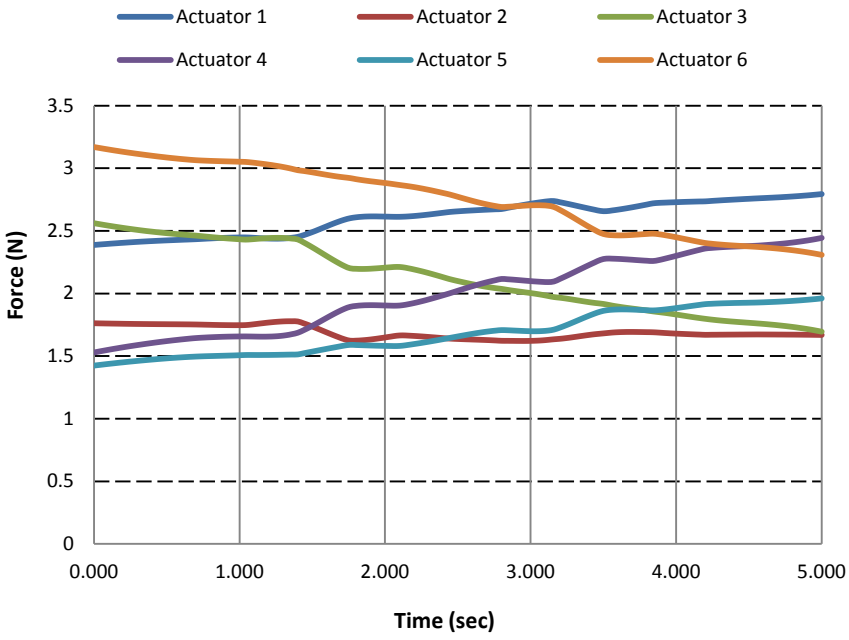

Figure 7-14: Applied Force on the Hexapod's Actuators Path 2

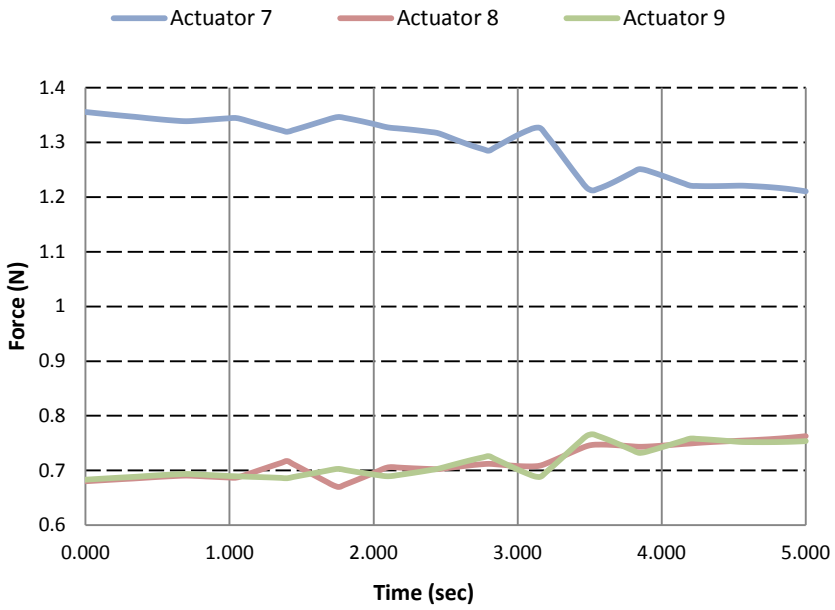

Figure 7-15: Applied Force on the Tripod's Actuators path 2

The obtained forces for actuators in order to follow the developed Bezier curve are demonstrated for two middle paths. In order to follow the paths the stroke size of actuators were changed in short time, therefore the obtained results had fluctuation. The external force on the end-effetor was not considered in this study. Therefore the weights of components have the maximum effect on the obtained results. The second path have larger amount of the angular motion rather than path one.

7.5.3 Results of the Optimum Method

The position of the end-effector is simulated for applied motions by using the SOLIDWORKS software. The Stroke sizes of actuators are imported data to simulation. The obtained results of simulation and developed theory are compared in Figures 7.16 and 7.17.

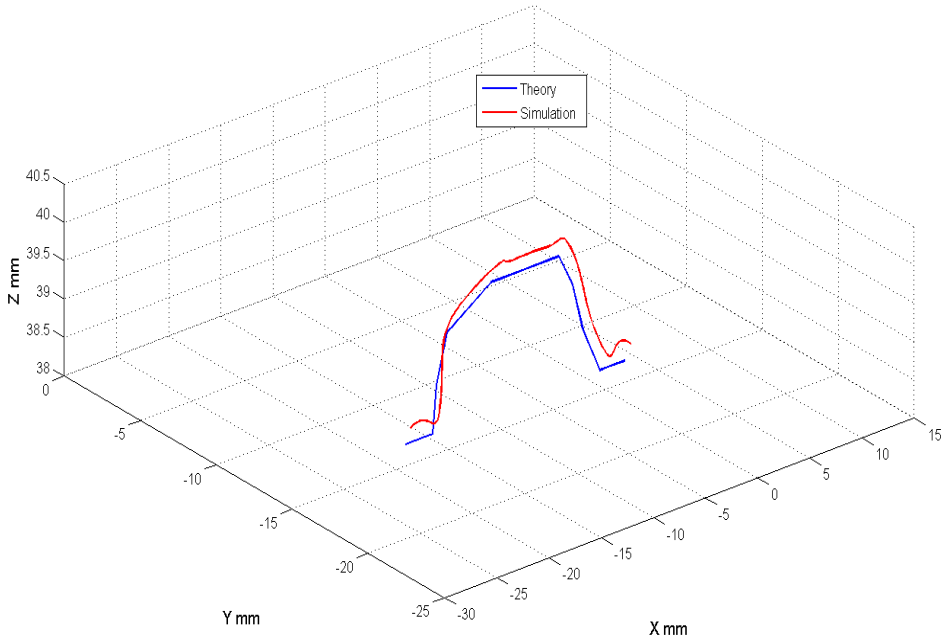

Figure 7-16: Theoretical and Simulation Results Comparison of Path 1

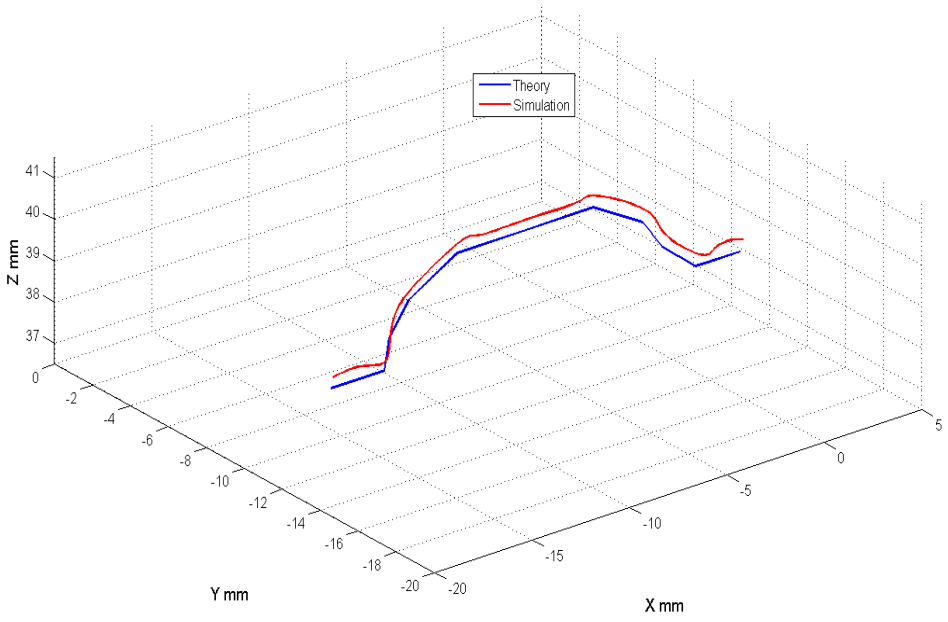

Figure 7-17: Theoretical and Simulation Results Comparison of Path 2

The Bezier curves successfully applied to the path planning of the end-effector. The obtained results illustrated maximum 1mm error is in the results of theory and simulation that is not effect on the application such as rehabilitation.

7.6 Conclusion

A singularity-free path plan has been developed for the end-effector of the hybrid parallel robot. The path is calculated based on a nominal polynomial path with zero acceleration at the start and end poses. The nominal path has been optimized to avoid singularity configurations

of the end-effector. Through the testing of several examples, the path planning approach is proven to be reliable to obtain a singularity-free path for various cases. A limitation of this path planning approach is lack of prediction of the non-existence of a singularity-free path for the end-effector.

In this chapter, the developed Bezier curve is applied to the hybrid parallel robot in order to enhance the motion efficiency of the robot while the beginning and ends of the motion are identified. The dynamic model of the hybrid parallel is developed in order to find the motor force needed for particular motions. The obtained simulation results of the end-effector's position are compared with a theoretical approach in order to demonstrate the validity of the developed system.

Chapter 8

Path Planning for Rehabilitation Application

8.1 Introduction

This chapter addresses the path planning of a hybrid parallel robot for ankle rehabilitation. The 6-UPU-3-UPR parallel robot is developed to simulate ankle motions for the rehabilitation of post-stroke patients with an affected ankle. The inverse kinematic of the hybrid parallel robot is developed in order to track the end-effector's position through Matlab software. The calculated stroke size of each actuator is imported to apply the forward kinematic for determining the position of the end-effector. The experimental and simulation values of the hexapod are compared with those of the hybrid structure through a number of exercise motion paths. The results reveal that, in general, the simulation values follow well the experimental values, although with different degrees of variation for each of the structures considered.

8.2 Methodology

The inverse kinematic of a hexapod is developed for 6-UPU structure in order to calculate the position of the end-effector and actuator stroke, while the path motion of the foot segment is applied. The singularity of the hexapod is calculated by using the actuator position vector.

High accuracy path motions for the rehabilitation application are needed while singular points in 6-DOF parallel robots cause deviation from the desired path. Therefore, in this chapter a new configuration of the hybrid parallel robot is introduced in order to increase the work volume and the position of the singular points. A 3-DOF parallel robot attached on top of the hexapod allows the end-effector to assume the desired position through a number of ankle exercise motions. The tripod is controllable for translational motion in Z direction and d rotational motions around X and Y axes. The developed inverse kinematic modeling for the hybrid parallel robot creates the required path for the identified ankle motions. Motion signature is defined as a skeletal model with joint characteristics and ranges including lower limb segments displacement information and kinematics with force distribution. To determine the path motion for the ankle rehabilitation, the motion signature of the able-bodied, identified by gait analysis and 3D gait data, were collected using Vicon system and processed by the Vicon Nexus (version 1.7.1) software.

8.2.1 Analysis of Experiment Data

A series of experimentations were performed in the gait laboratory at the West Midlands Rehabilitation Centre (WMRC). Thirty healthy male and female testers with a mean age of 25.34 ±6.32 years, mean height of 162.34 ±31.22 cm, and mean body mass of 70.34 ±4.47 participated in this experiment. The gait laboratory was equipped with 12 infrared cameras (six MX T40 cameras and six MX3+ cameras) with a sampling frequency of 100 Hz recorded

the 3D spatial location of each marker as the subject walked. A digital camera was located along the walkway to record the movements of the testers in coronal plane and another camera was located on the side of the walkway to record the movements in sagittal plane.
A Kistler force plate at a sampling rate of 1000Hz was embedded in the middle of the walkway which was leveled with the floor surface.

Before placing the markers on the lower limb segments, a number of anthropometric measurements were evaluated and recorded as required for processing the samples in Vicon software (plug-in gait lower body model). The 3D gait data were collected and processed using a Vicon system and Vicon Nexus (version 1.7.1) software, respectively. After reconstructing the limb segments by Vicon software, the gait events were marked by using the video of trials. To define different activities for ankle rehabilitation, different patterns have been defined based on path motions of the left foot segment from the first foot strike to the second foot strike in a gait cycle. The mean value for trajectories and rotations were calculated. Then, the path motion for the foot segment was defined based on the positions of the three markers, namely, Toe (which is placed on the second metatarsal head), LCAL (which was placed on the lateral aspect of the calcaneus , at the same distance from the most posterior point as STAL) which is shown in Figure 8.1.

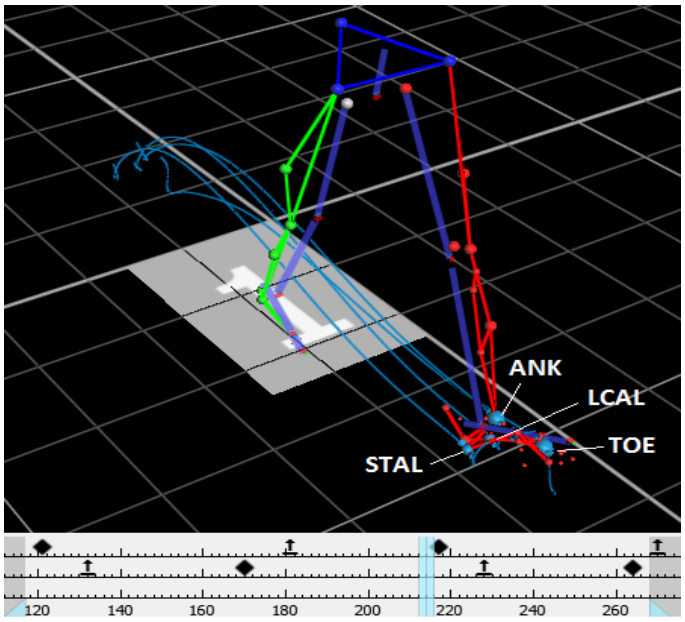

Figure 8-1: Vicon Software Simulation

The perpendicular normal vector of the plane that is created by these three markers was calculated based on Equations 8.1.a and 1.b:

$$n = (P_3 - P_2) \times (P_1 - P_2) \tag{8.1.a}$$

$$[L \quad M \quad N] = \frac{P_1 + P_2 + P_3}{3} \tag{8.1.b}$$

Where $P_1 P_2$ and P_3 are corresponding three mentioned markers respectively. The values of L, M and N are the total translational motion in X, Y and Z axes respectively.

Based on the translation of the calculated normal vector and angular rotation of the ankle (which is obtained directly by Vicon), a path motion for the end-effector of the robot has been

defined. Due to stroke limitation of the actuators, the obtained path motion was divided into three smaller parts and thus, three different rehabilitation activities have been defined, which are the entire required ankle rotations included in these three different activities.

Positions of joints attached to the platforms are calculated by using a transformation matrix, while the initial positions of the joints are fully defined. Figure 3.1 shows the hybrid parallel robot consisting of two moving platforms.

The position vectors of the hexapod could be developed by equation.2.

$$L_{Hi} = A_i \times T_B^A - B_i \qquad i \in \{1 \dots 6\} \tag{8.2}$$

Where, L_{Hi} is the position vector of each actuator connected to platforms B and A, T_B^A is the transformation matrix for the platform A, A_i is the initial position of the joint on platform A and B_i is the position of the joints on platform B.

The transformation matrix platform E (End-effector) is related to platform B as given in equation 8.3:

$$T_B^E = T_A^E \times T_B^A \tag{8.3}$$

Where,T_B^E is the transformation matrix of platform E related to B, T_A^E is the transformation matrix of platform E to B and T_B^A is the transformation matrix of platform A to B.

Therefore the length of each actuator is calculated by equation 8.4.

$$L_{Ti} = E_j \times T_B^E - A_j \times T_B^A \quad j \in \{1 \dots 3\} \tag{8.4}$$

Where, L_{Ti} is the position vector of each actuator connecting platform A and E, E_j is the initial joint position on platform E and A_j is the joint positions on top of platform A.

8.2.2 Singularity and Limitation

In this section the limitation and singularities of the hybrid parallel robot are calculated for the identified motions.

Fifteen universal joints and three pin joints are used in the hybrid system. Therefore, the angles between joint and actuators are determined for the hexapod from equations 8.5.a and 8.5.b:

$$\alpha_{Bi} = cos^{-1}\left(\frac{U_X.L_{Hi}}{|L_{Hi}|}\right) \quad i \in \{1 \dots 6\} \tag{8.5.a}$$

$$\beta_{Bi} = cos^{-1}\left(\frac{U_y.L_{Hi}}{|L_{Hi}|}\right) i \in \{1 \dots 6\} \tag{8.5.b}$$

Where, U_X and U_y are axes of the joints on platform B, L_{Hi} is the actuator position vector, α_{Bi} is the angle of the joint with its x-axis, and β_{Bi} is the angle of the joints with its Y-axis.

The joints' axes on platform A are moving with the motion provided for the system. The joints' angles are calculated by Equation 8.5.c an 8.5.d:

$$\alpha_{Ai} = cos^{-1}\left(\frac{u_X.L_{Hj}}{|L_{Hj}|}\right) \quad i \in \{1 \dots 6\} \tag{8.5.c}$$

$$\beta_{Ai} = cos^{-1}\left(\frac{u_y.L_{Hi}}{|L_{Hi}|}\right) \quad i \in \{1 \dots 6\} \tag{8.5.d}$$

Where, u_X and u_y are the axes of the joints after the motion of platform A, which can be obtained by equations 8.6.a and 8.6.b:

$$u_X = U_X \times T_B^A \tag{8.6.a}$$

$$u_y = U_y \times T_B^A \tag{8.6.b}$$

Moreover, α_{Ai} and β_{Ai} are the joints' angles with their own X-axis and Y-axis respectively.

However, the angles of revolute joints are obtained using equation 8.7.a, while the parameters u_{2X},u_{2y} are obtained through equations 8.7.c and 8.7.d respectively. The axis in Y direction of the joint should be zero.

$$\alpha_{Ej} = cos^{-1}\left(\frac{u_{2X}.L_{Ti}}{|L_{Tj}|}\right) \quad j \in \{1 \dots 3\} \tag{8.7.a}$$

$$u_{2y}.L_{Ti} = 0 \quad j \in \{1 \dots 3\} \tag{8.7.b}$$

$$u_{2X} = U_X \times T_A^E \times T_B^A \tag{8.7.c}$$

$$u_{2y} = U_X \times T_A^E \times T_B^A \tag{8.7.d}$$

Where, α_{Ej} (j=1, 2, 3) are the angles of the joints connecting to platform E after a particular motion, and u_{2X} is the xis of the revolute joints in a particular pose and orientation.

The singularities of the hexapod need to be considered as follows:

$$H = \begin{bmatrix} S_1 & \dots & S_6 \\ S_1 \times q_1 & \dots & S_6 \times q_6 \end{bmatrix} \tag{8.8}$$

Where H is the kinematic relation of the hexapod structure. Moreover, S_i and q_i are determined in equations 10.a and 10.b respectively.

$$S_i = \frac{L_{Hi}}{\|L_{Hi}\|} i \in \{1 \dots 6\} \tag{8.9.a}$$

$$q_i = O_B A_i - O_B O_A i \in \{1 \dots 6\} \tag{8.9.b}$$

Where, S_i is the unit vector of each actuator attached to platforms A and B. Moreover, O_B is the centre of platform B, O_A is the centre of platform A, and A_i is the position of the joints on platform A (this value could be calculated for each motion.)

The obtained data of the considered path is the total movement for the end-effector. This needs to be developed in order to determine the motions for the tripod and hexapod. The attached tripod has 3 DOF: one translational and two rotational motions in Z and around X, Y respectively. The others are not controllable. Hence,

$$l_T = -(n_T + d_{\frac{E}{A}}) \times \sin(\varnothing_T) \times cos(\Theta_T) \tag{8.10.a}$$

$$m_T = (n_T + d_{\frac{E}{A}}) \times sin(\Theta_T) \tag{8.10.b}$$

Where, l_T and m_T are translation motions of the tripod in X and Y directions respectively, n_T is the translational motion in z direction. Moreover, Θ_T and ϕ_T are rotational motions around X and Y axes, and $d_{\frac{E}{A}}$ is the initial distance between platforms A and E.

Therefore, changing the input data based on the capability of the hybrid system can assist in reaching the desired position while the hexapod is not in singularity. Thus,

$$N = n_T + n_H \tag{8.11.a}$$

$$\Theta = \Theta_T + \Theta_H \tag{8.11.b}$$

$$\phi = \phi_T + \phi_H \tag{8.11.c}$$

Where, N, Θ,ϕ are the total translational and rotational motions for the end-effector in Z, X and Y axes respectively. Furthermore, n_T,Θ_T and ϕ_T are the tripod motions, n_H,Θ_H andϕ_H are the motions of the hexapod.

The condition test theory is developed to find non-singular position and orientation for end-effector using Grassman methodology and workspace limitation such as joints' angles and stoke of actuators. The first step is to identify the structural limitation by using the developed inverse kinematics. The position vectors of the actuators are the crucial factors to find the error in the system. The developed program then check the singular points using Grassman.

Kinematics development uses the end-effectors position and orientation which are required to be confirmed. The kinematics and geometry limitations are explained in Equation 8.12.
Where, $angle\ 1,2$ = Vector angle of each actuator between pose A and B.

$$angle_n = x_n i + y_n j + z_n k \qquad n \in \{1,2\} \tag{8.12.a}$$

$$p = x_1 i + x_2 i \tag{8.12.b}$$

$$q = y_1 j + y_2 j \tag{8.12.c}$$

$$r = z_1 k + z_2 k \tag{8.12.d}$$

$$\left|S_j\right| = \sqrt{p^2 + q^2 + r^2} j \in \{1 \dots 3\} \tag{8.12.e}$$

Where, $pose1 = (x_{1,} y_1, z_1)$ and $pose2 = (x_{2,} y_2, z_2)$. Moreover S_i is the stroke size of the actuators connecting platform A and E (Tripod).

The Boolean condition for the Grassman condition which checks for coplanar, line-line join, line-line meet, plane-line meet and point-line join is presented here.

$$G_{GN} = \sum_{Iteration=0}^{n} \left(f(pos, limit, error) \wedge limit \rightarrow error_{a,b,c,d,e}\right) \tag{8.13.a}$$

Where $error_{\text{a,b,c,d,e}}$ represents the Grassman error condition described below and G_{GN} is a set of Grassman's error for a given set of iteration. The iteration is created by drawing a pencil line using the structure's line and edge. The limit is the threshold value for the error state.

For a case where $x = (x1, x2, x3)$ and $y = (y1, y2, y3)$ for line L, therefore displacement along L is found as scalar multiple of d=y-x. The point being displaced is known as moment, $m = x.y$.

$$x = (x1, x2, x3)\ , y = (y1, y2, y3)\ . \tag{8.13.b}$$

Where m is the moment for this point displaced from its origin.

$$m' = \begin{bmatrix} x_i' & y_i' \\ x_j' & y_j' \end{bmatrix} = \begin{bmatrix} x_i & y_i \\ x_j & y_j \end{bmatrix} \begin{bmatrix} \lambda_{00} & \lambda_{01} \\ \lambda_{10} & \lambda_{11} \end{bmatrix} \tag{8.13.c}$$

Where m' are the linear combinations of the columns of m, for some 2x2 nonsingular matrix .

The Grassman error, $error_{a,b,c,d}$ condition is described here as

a) coplanar condition, when d.m'+m.d'=0,

b) line-line joins condition, when$(m.d')_{x_0} + (dxd') = 0$,

c) line-line meets condition,

When,$(x_0 : x) = (d.m' : m \times m)$,

d) plane-line meets when given a plane with equation $0 = a^0 x_0 + a.x$. The point of intersection is given as$(x_0 : x) = (a.d : a \times m - a_0 d)$,

e) point-line join condition, when $0 = (y.m)x_0 + (y \times d - y_0 m).x$

Where displacement, d=(y-x) and Plucker coordinates= (d: m).

The developed methodology identified the singular points of the hexapod using the mathematical calculation. The singular points of the tripod were calculated using the Grassman error.

8.3 Simulation Results

The obtained data of the actuators were imported to the designed CAD model to track the position of the end-effector. The modified motor in the software follows the stroke size for the considered motions. The obtained data were then tested on both hexapod and hybrid parallel robots. Figures 8.2, 8.3, and 8.4 demonstrate the tracking data of the end-effector for the hexapod and are compared against the experimental data. The experimental data are the obtained motions of the foot. The results are compared over a continuous time range of 0.44 seconds of a full motion cycle.

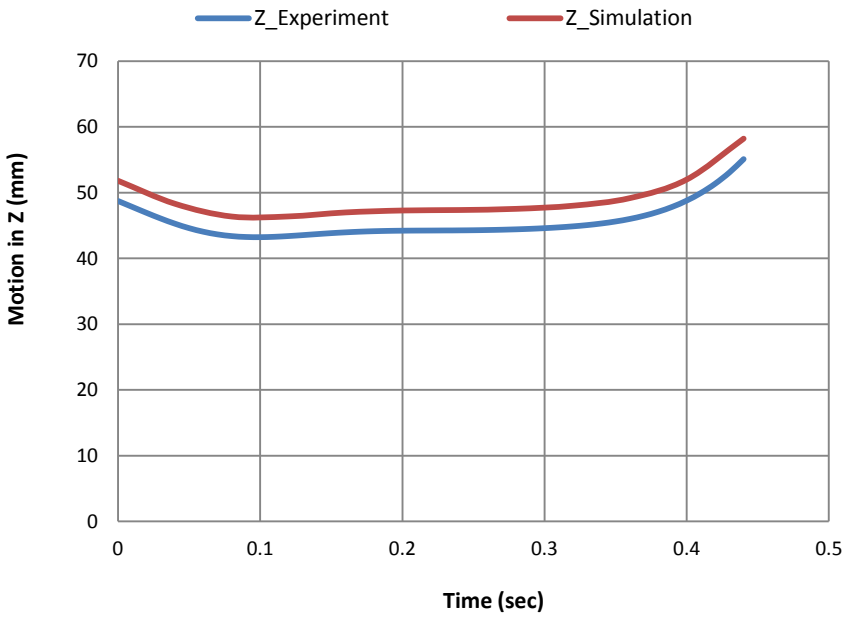

Figure 8-2: Hexapod Motion in Z-Axis for Activity 1

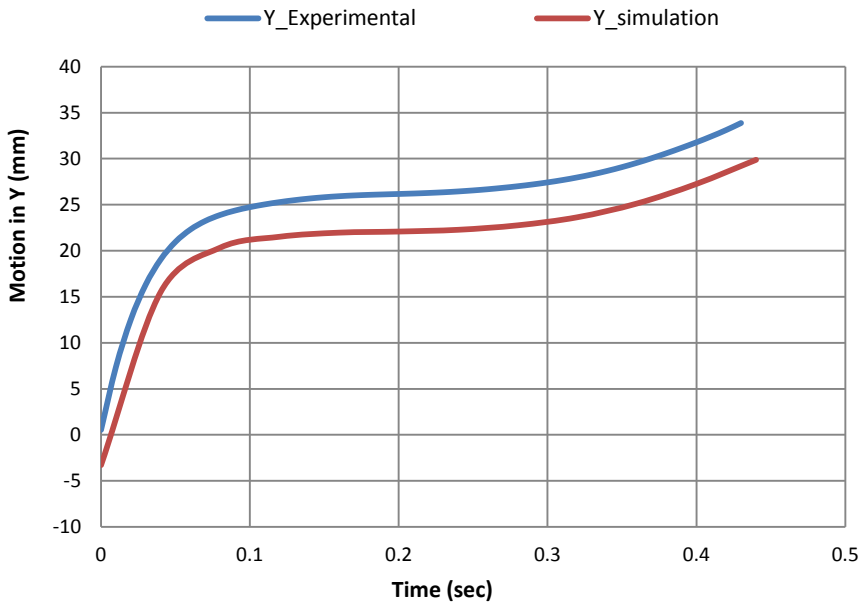

Figure 8-3: Hexapod Motion in Z-Axis for Activity 1

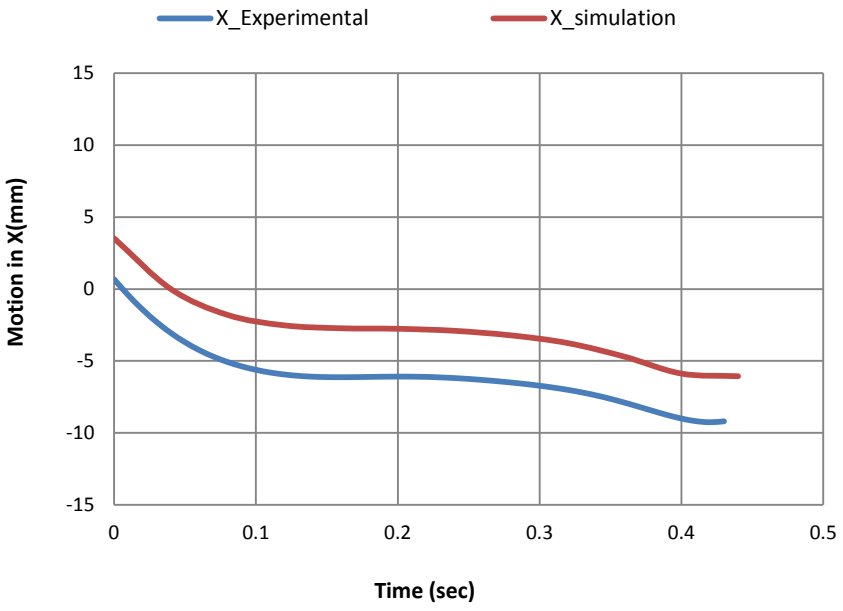

Figure 8-4: Hexapod Motion in Z-Axis for Activity 1

The obtained results of hexapod path planning for ankle motion illustrated the capability of parallel robots for the considered application. However there is some difference between the simulation and experiment results that could be due to method of tracing the position in simulation software. The software track the central mass of the end effector.

Tracking the position of platform E for the hybrid robot has been obtained using Matlab software as described in Figure 8.5.

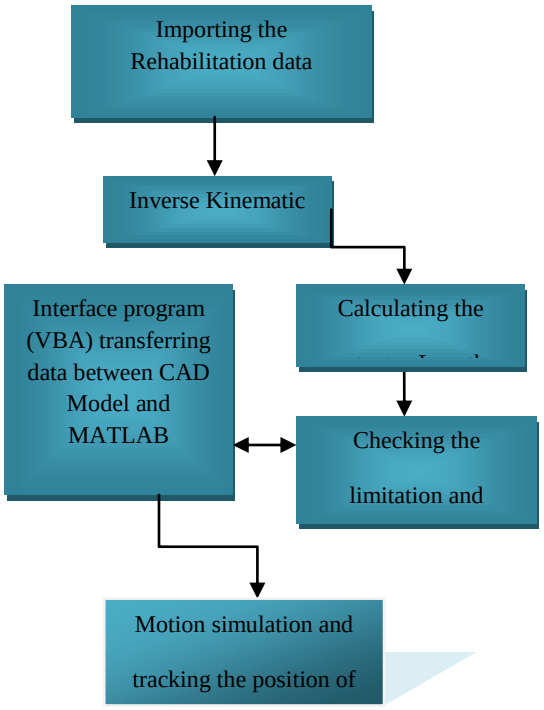

Figure 8-5: Program Modeled for Hybrid parallel robot

The considered motion has been applied to the developed inverse kinematic of the hybrid parallel robot. The results of the simulation motion are compared with the obtained data of the ankle rehabilitation in Figures 8.6, 8.7 and 8.8 for X, Y and Z axes respectively.

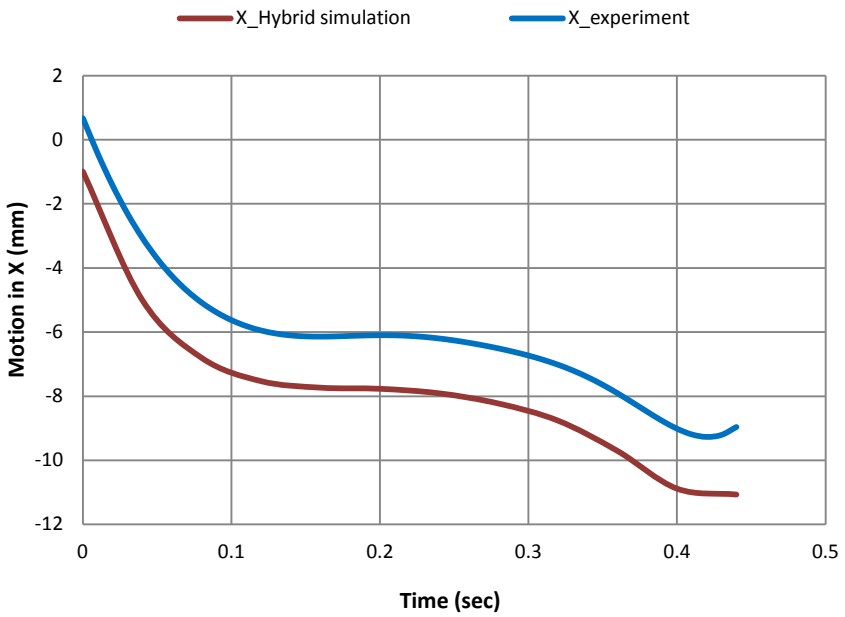

Figure 8-6: Hybrid Motion in X-axis Activity 1

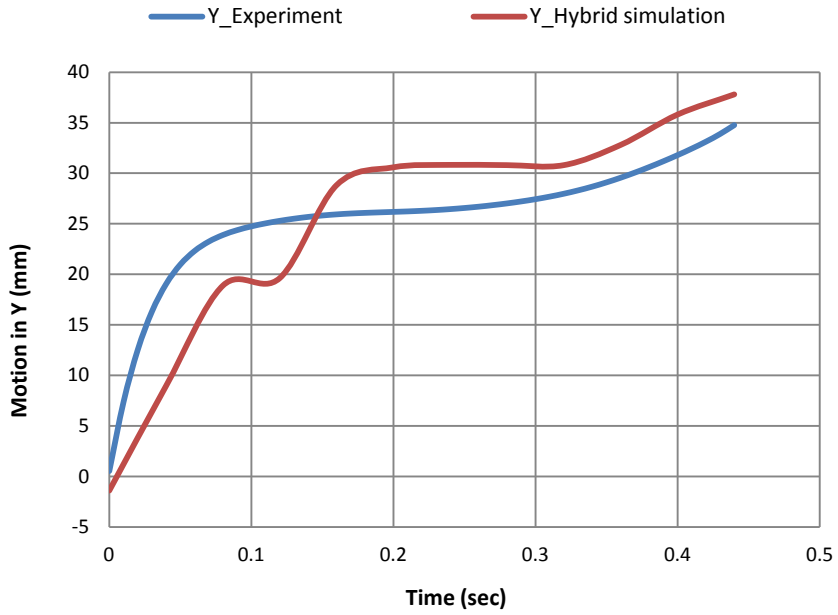

Figure 8-7: Hybrid Motion in Y-axis Activity 1

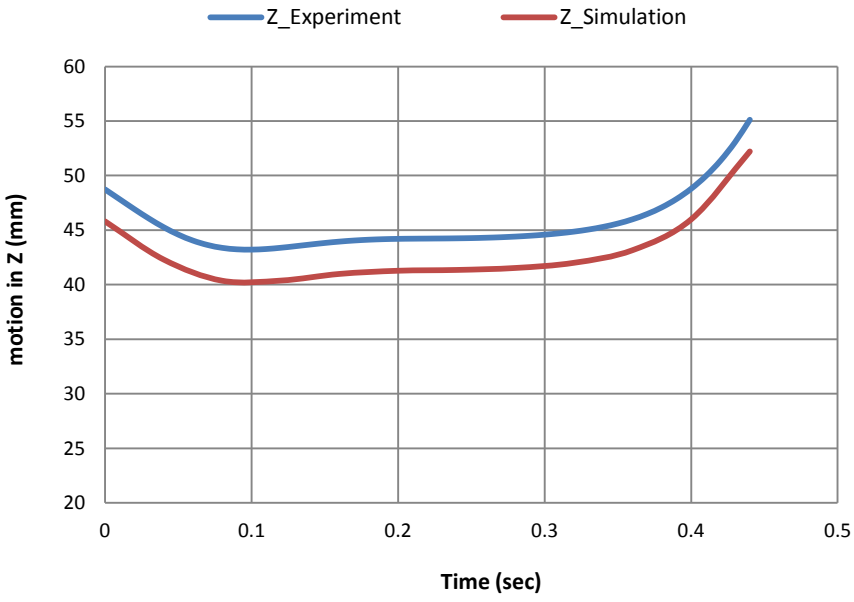

Figure 8-8: Hybrid Motion in Z-axis Activity 1

The obtained results of end-effector in hybrid parallel robot were validated the applied path planning strategy for the system. The maximum errors are 2 mm, 3mm and 1.5 mm in X, Y and Z direction respectively. In Figure 8.8 the trend of graphs in simulation and experimentation were different due to support the singular point in the path.

8.4 Theoretical Results of Ankle Motions simulation

Three different ankle rehabilitation motion ranges have been applied to the hexapod and hybrid robot models. The results demonstrate the capability of the new configuration to follow the desired path.

The end-effector positions of the hexapod and hybrid parallel for the applied paths are compared with the experimental rehabilitation data, as shown in Figures 8.9, 8.10, and 8.11. Here the length of each actuator stroke is 100 mm for both structures.

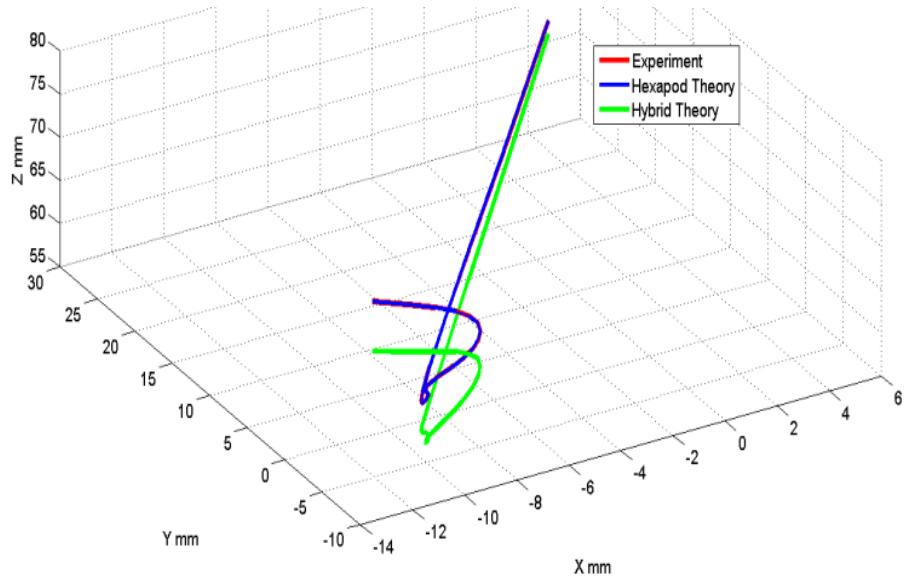

Figure 8-9: Hybrid Parallel Robot and Hexapod Path for Activity 1

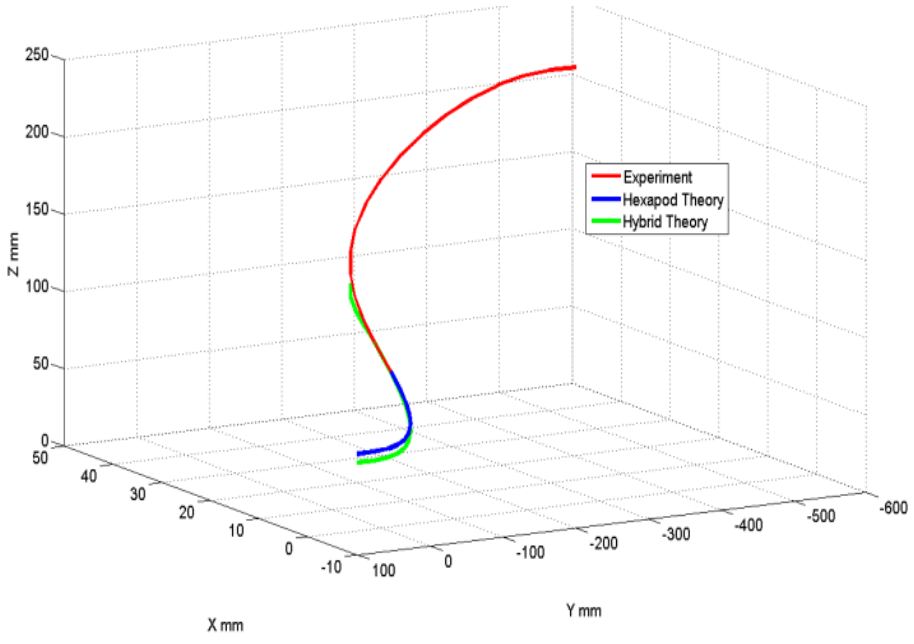

Figure 8-10: Hybrid Parallel Robot and Hexapod Path for Activity 2

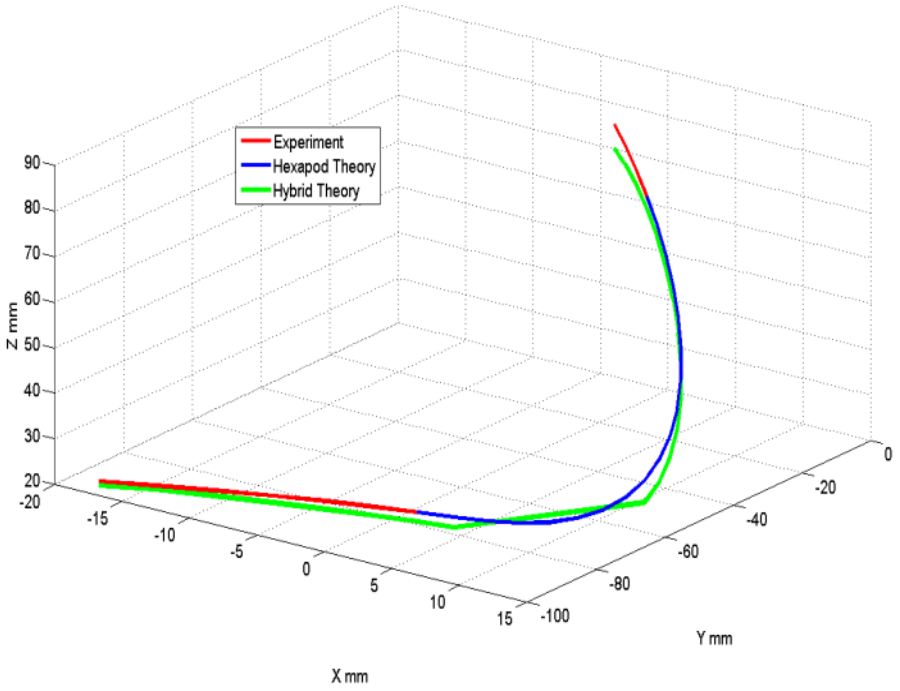

Figure 8-11: Hybrid Parallel Robot and Hexapod Path for Activity 3

It is shown that the hexapod exhibits singularity limitations and is not therefore, suitable for a certain range of activities required for ankle rehabilitation. However, the hybrid robot's trajectory can achieve the same range of motions without any singularity limitations. The comparisons of the obtained motion profile for the hexapod and hybrid robots reveal that the hexapod follows well the hybrid robot in the first motion activity. Furthermore, approximately 19% of the second activity can be simulated by the hexapod, while the corresponding value for the hybrid is 42%. The third activity is fully simulated by the hybrid robot, while the hexapod can successfully simulate approximately 41% of the path.

8.5 Methodology of Dynamics Experimentation

In order to obtain spatio-temporal parameters, rotation of the angles, trajectory of the markers and ground reaction forces, the motion signatures of healthy participants were measured and recorded as a skeletal model with joint characteristics and ranges, including links' displacement information and kinematics with force distribution, by the Vicon cameras in the gait laboratory of the West Midlands Rehabilitation Centre, Birmingham, United Kingdom.

Identification and measurement of leg segmental motion characteristics were performed for 30 participants who were selected by an advertisement at the University Of Birmingham; these included 15 males and 15 females, with the mean age of 27.05±7.32 years old, a mean height of 168.16±14.32 cm and a mean body mass of 68± 7.43 kg.

The laboratory was equipped with 12 infrared cameras (six MX T40 cameras and six MX3+ cameras) with a sampling frequency of 100 Hz. By using the Vicon cameras, the 3D spatial location of each marker was detected as the subject walked. Two digital cameras were used. One camera was located along the walkway to record the movements of the testers in the coronal plane. Another digital camera was located inside of the walkway to record the movements in the sagittal plane A Kistler force plate at a sampling rate of 1000Hz was embedded in the middle of the walkway, and it was leveled with the floor surface.

In order to run the plug-in gait lower body model with the Vicon Nexus software, some anthropometric measurements were measured and recorded, such as leg length, knee width, ankle width and inter ASIS distance. Two different sets of retro-reflective markers were used

for constructing the 3D model of the lower limb. The size of the markers were 9mm and the Oxford foot model was used for the left limb and the standard plug-in-gait model (including two posterior superior iliac spine (PSI) markers for the pelvis) was used for the right limb.

Participants were instructed to walk barefoot at a self-selected speed , looking towards the line of progression, during which data capture was completed. For each tester 12 dynamic trials recorded. The 3D gait data were collected and processed by the Vicon system and Vicon Nexus (version 1.7.1) software respectively.

After reconstruction of the segment`s motion of the 3D model by Vicon, the foot strike and toe off was defined for each leg with respect to the captured videos of the trials. With respect to the obtained data, the trajectories and orientation of the markers and joints have been exerted and normalized by the following Equation 8.14.

$$P_k = \frac{P_k - MinVal}{MaxVal - MinVal} \tag{8.14}$$

Where, P_k is the index of data, MinVal and MaxVel reveals minimum and maximum values respectively.

A specific pattern was defined based on the path motion of the left foot segment from the first foot strike to the second foot strike in a gait cycle. Due to the variety of ankle motions for different samples, the mean values for the X, Y and Z values in three different planes have been calculated for all of the 30 samples and trials.

With respect to the trajectories of the Toe marker (which was placed on the second metatarsal head), and the LCAL marker (which was placed on the lateral aspect of the calcaneus, at the same distance from the most posterior point as STAL), the path motion for the foot segment has been defined, and was applied to the hybrid mechanism so it followed this path.

This path motion would be a walking gait rehabilitation activity in which the ankle will be engaged with all of the rotations of dorsiflexion/plantar flexion, adduction/abduction and inversion/eversion

8.6 Force Analysis

The data obtained from the experiment of the human foot motions involved the force applied to the end-effector. Applied force by the foot for 0.5 seconds of the motion was studied. The imported force by each actuator was calculated for the considered motion. In general dynamic formulation is expressed in equations 8.15.a and 8.15.b.

$$\mathrm{Fa}_i - F = m_a i \in \{1 \dots 9\} \tag{8.15.a}$$

$$\mathrm{Fa}_i = \mathrm{Fas}_\mathrm{i} + \mathrm{Fad}_\mathrm{i} i \in \{1 \dots 9\} \tag{8.15.b}$$

The force entered by patients is applied to platform E of the system in the following study. Therefore, direction of applied force is calculated by the same transformation matrix which was developed for the end-effector while the initial direction of the platform is known.

$$U_{EZ} = U_Z \times R_T^O \times R_{\theta\emptyset\psi}^O \tag{8.16}$$

Where, U_{EZ} is direction of force after motion and U_Z is initial direction that is (0, 0, 1,1) while the end-effector is in the home position.

Therefore, the vector of applied force on platform E could be calculated by using Equation 8.17.

$$F(t) = f(t) \times U_{EZ} \tag{8.17}$$

Where, applied force by foot through the motion is a function respected to time. Moreover, the force F is defined as follows, $F(T) = [F_x \quad F_y \quad F_z]$.

$$\sum_{j=1}^{3} \frac{L_{Hj}}{\|L_{Hj}\|} \times (Fas_j) = F \tag{8.18}$$

Where, L_{Hj} and Fas_j are the position vector of the actuator and static force required for motion of the actuator for a particular activity, respectively.

The formulation is expanded in order to determine the applied force on six other actuators. By subtitling the obtained value of Fas_j in Equation 8.18, three linear equations can be developed. The developed formulations calculate the required force for the hexapod's actuators to overcome patient weight.

$$\sum_{j=1}^{3} \frac{L_{Hj}}{\|L_{Hj}\|} \times \mathrm{Fas_j} + \mathrm{M_T g} = \sum_{i=1}^{6} \frac{L_{Hi}}{\|L_{Hi}\|} \times \mathrm{Fas_i} \qquad (8.19)$$

$$\sum_{i=1}^{6} \frac{L_{Hi}}{\|L_{Hi}\|} \times \mathrm{Fas_i} \times (\mathrm{A_i} - \mathrm{O_A}) = 0 \qquad (8.20)$$

Where, M_T is the weight of all components on top of platform A, moreover L_{Hi} and Fas_i are position vector and applied force of actuators, respectively.

In order to find the force of the actuator for a particular motion, the velocity and acceleration of the actuator needs to be calculated. The stroke sizes of the actuators were calculated in inverse kinematics with respect to time of the motion in the previous section. Therefore, the changes of the velocity are obtainable through the experimental data. Thus, dynamic force that is needed for the ankle rehabilitation motion is calculated in equation 8.21.

$$\mathrm{Fad_i} = \frac{\mathrm{d^2 u_i}}{\mathrm{dt}} \times \mathrm{m_a} \qquad i \in \{1 \dots 9\} \qquad (8.21)$$

Where, Fad_i is the dynamic force for each actuator and m_a is the mass of the actuator. Moreover, u_i is the distance that the actuator needs to move with respect to time.

8.7 Simulation Results

The obtained data of the actuators are imported to the designed CAD model to track the position of the end-effector. The modified motor in the software follows the stroke size for the

considered motions. The obtained data are tested on both the hexapod and hybrid parallel robot. The figures below demonstrate the tracking data of the end-effector for the hexapod and are compared with the experimental data. The experiment data are the obtained motion of the foot. The results are compared in limited time (0.5 second).

However, tracking the position of platform E for the hybrid model is programmed. The developed modeled is demonstrated in Figure 8.12.

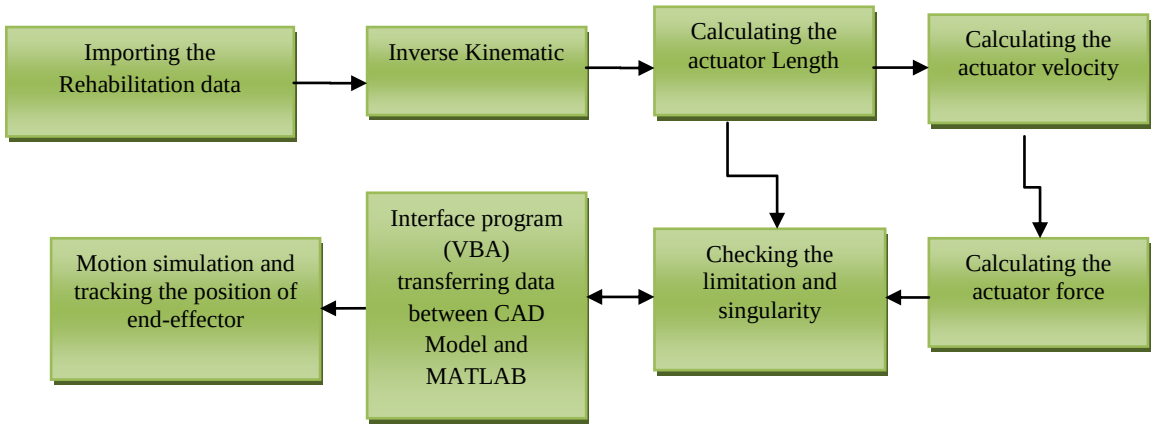

Figure 8-12: Program Modeled for Hybrid Parallel Robot

The experiment data and simulation of model is expressed in x, y and z direction in Figures 8.13, 8.14 and 8.15 respectively.

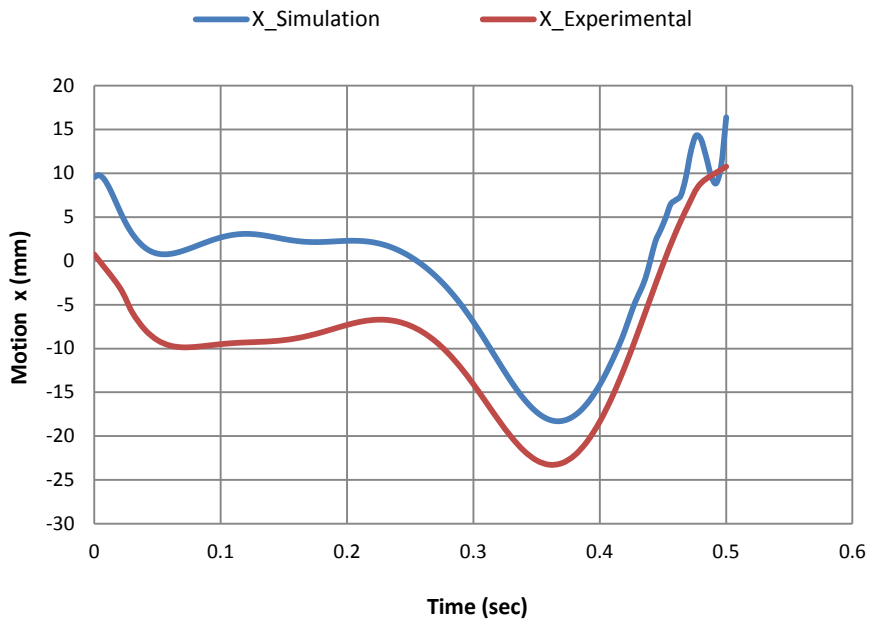

Figure 8-13: Comparison of Experiment and Simulation X-axis

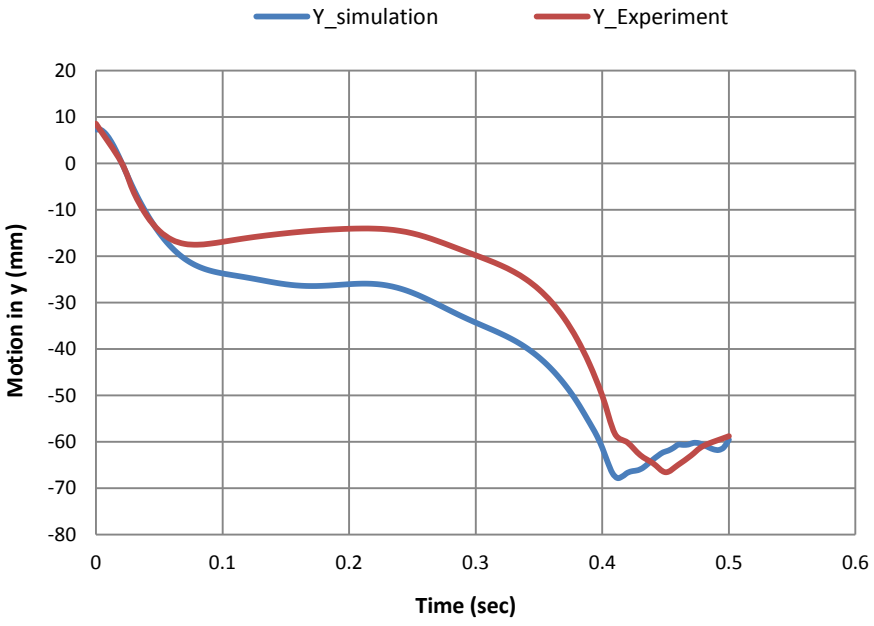

Figure 8-14: Comparison of Experiment and Simulation Y-axis

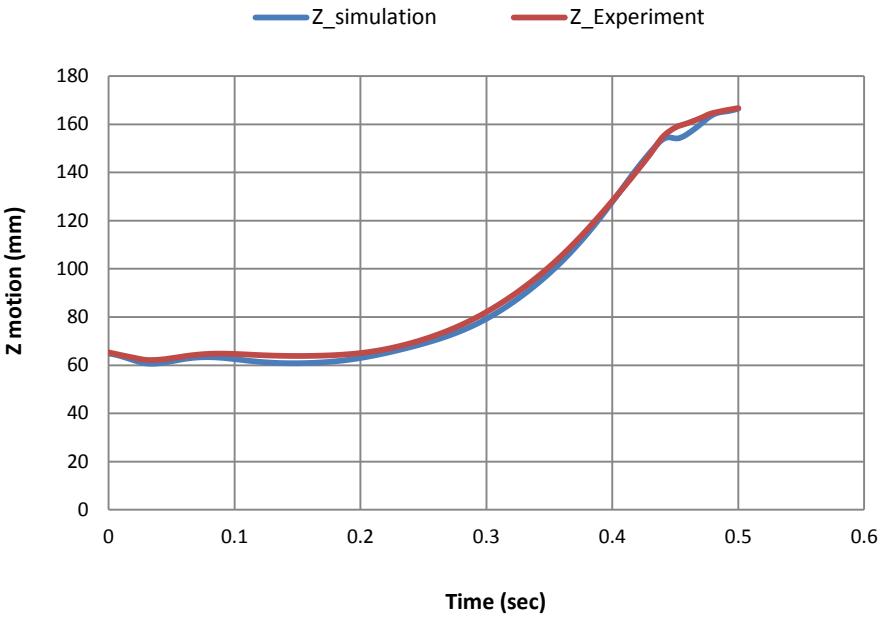

Figure 8-15: Comparison of Experiment and Simulation Z-axis

The results of simulation and ankle motions are compared in graphs depict the difference in results. The part of the path containing positions and orientations of the end-effector is not in the workspace of the system. That could force the model to find another path to reach to destination point.

8.8 Results and Discussion

The data from the rehabilitation experiments is imported to the control model strategy program in MATLAB software to track the position of the end-effector in the theory. The

results of the theory are compared with the foot motion in Figures 8.16. As it is demonstrated the foot motion is simulated by a hybrid parallel robot.

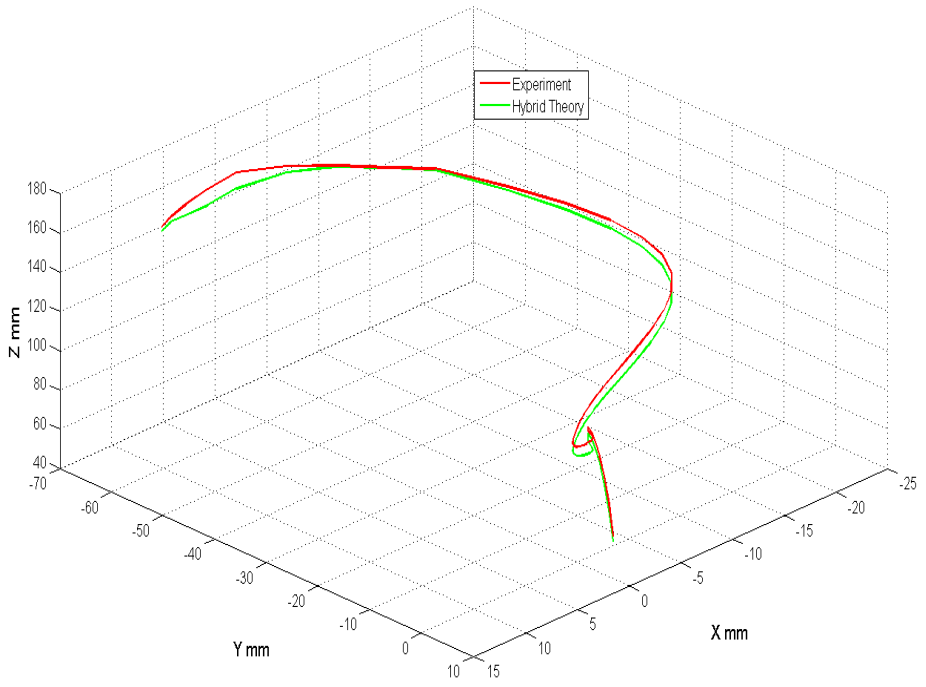

Figure 8-16: Obtained Path Motion of Theory and Experimental Data

The desired motions are applied to the kinematic program (Matlab) in order to find the length of the actuators for particular motions. The calculated lengths are transferred to the interface program (VBA) in order to modify the motors which were developed in the assembled CAD mode. The CAD software calculates the motor power based on the applied force and stroke size of each actuator. The applied force (by patient's foot) for 0.5 seconds of the motion is used in the software in order to calculate the required force needed by each actuator, as shown in the Figures 8.17 and 8.18.

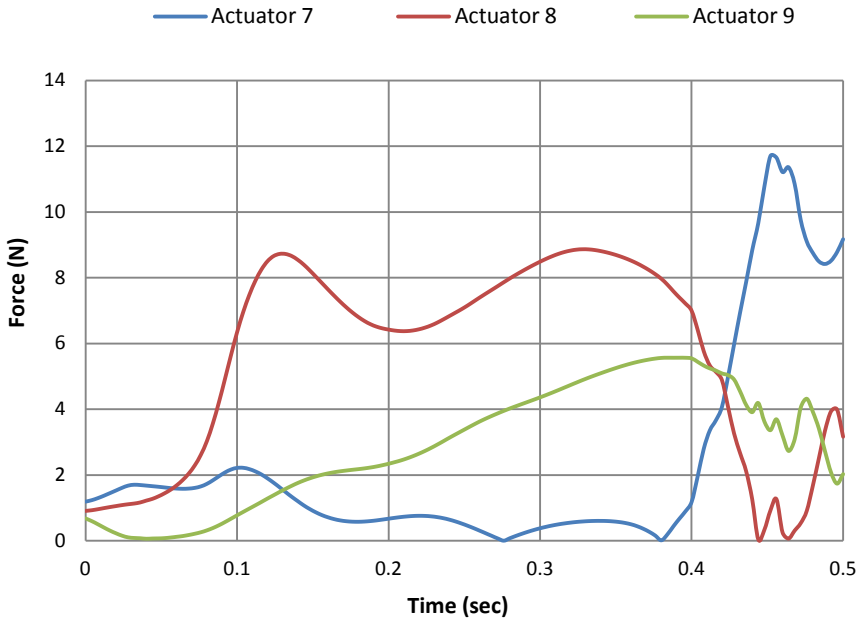

Figure 8-17: Applied Force on the Tripod's Actuators

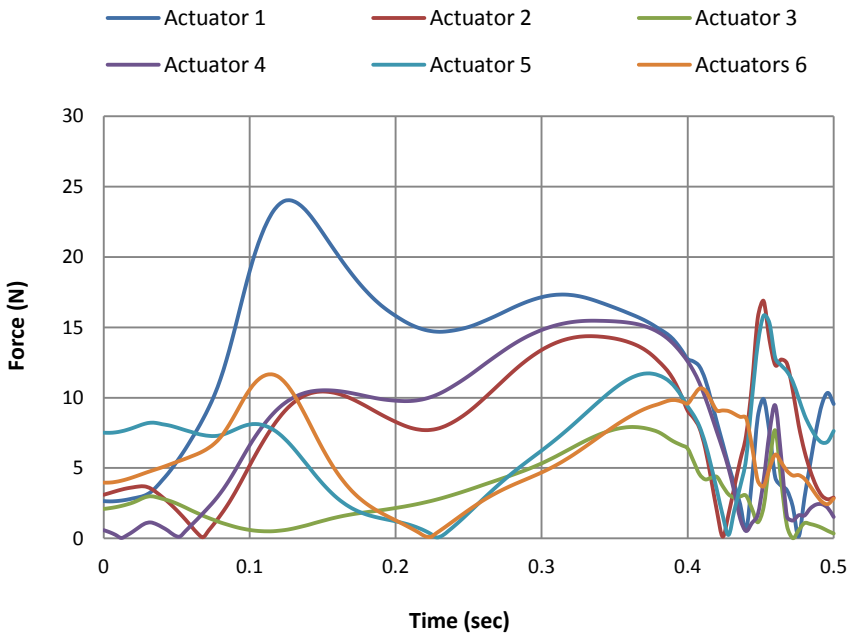

Figure 8-18: Applied Force on the Hexapod's Actuators

The forces required for path planning of the hybrid parallel robot were demonstrated In Figures 8.17 and 8.18. The input data of the force was supported for 0.5 second. The similarities of force behavior of the actuator force in this section and previous chapters validate the obtained data. The effect of the tripod's weight on the hexapod caused more pressure on the hexapod's actuators. The changes in the value of the input force were identified in the obtained results. All the actuators have the identified path for the considered motion simulation. The assumption of this study is that all actuators reach for the required motion at the same time in order to increase the efficiency of the motion. The considered assumption assists to calculate the velocity of the actuators. The changes in velocity in each 0.1 second causes the introduction of a nonlinear acceleration. It is proposed that the changes in the acceleration of the actuators cause the changes of the required force for the motion.

The accuracy of the path planning of the hybrid parallel robot is experimented. The results of error in the position system for the considered rehabilitation motion are demonstrated in Figures 8.19, 8.20 and 8.21.

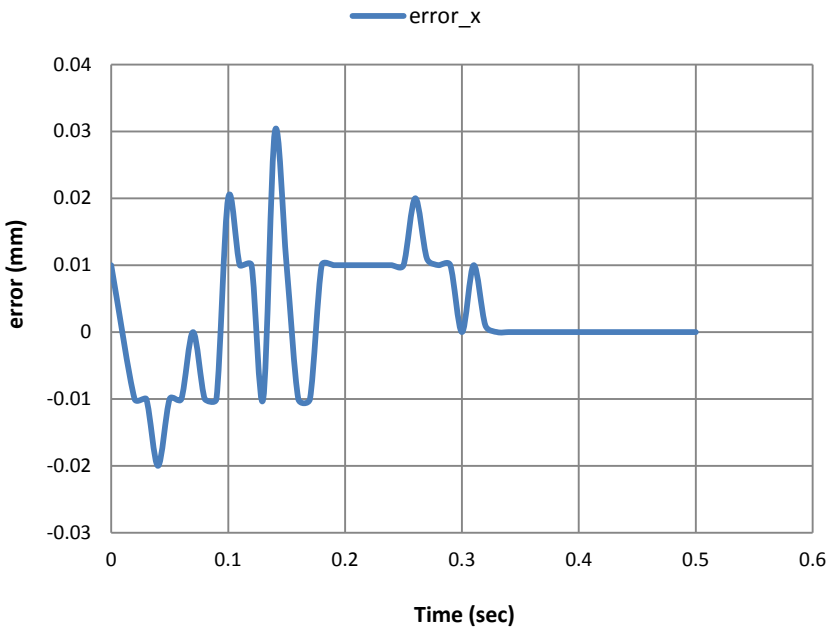

Figure 8-19: Error of the Motion in X Direction

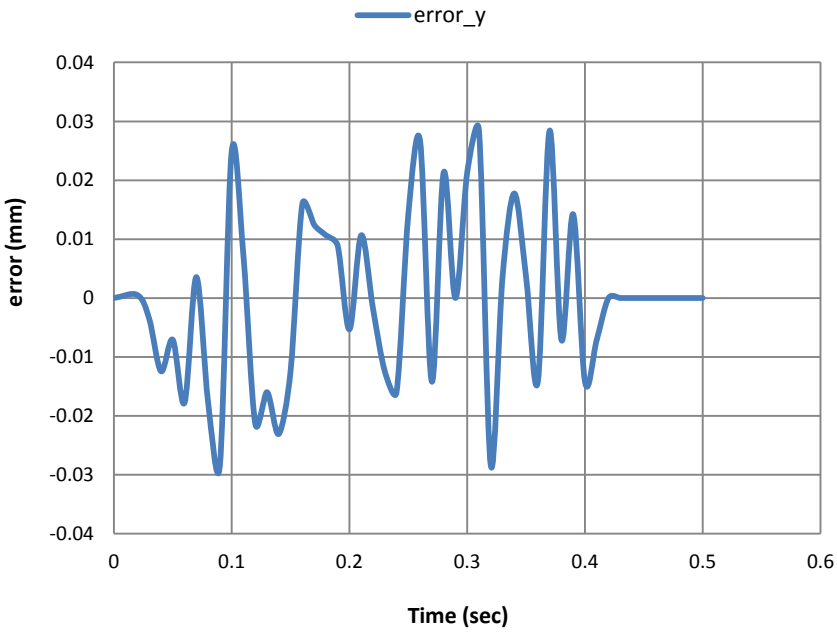

Figure 8-20: Error of the Motion in Y Direction

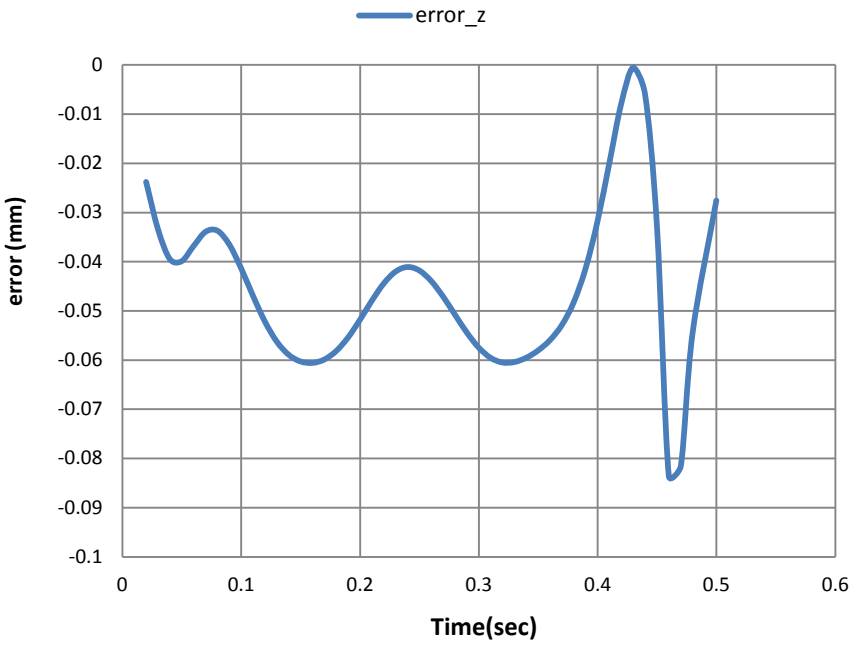

Figure 8-21: Error of the Motion in Z Direction

The obtained accuracy results for non singular path for ankle rehabilitation illustrated that the maximum errors are 0.029 mm, 0.03 mm and 0.08 mm in X, Y and Z direction respectively. The results raveled that hybrid parallel robot is very useful device for rehabilitation.

8.9 Conclusion

In this chapter the proposed hybrid parallel robot was tested for a robotic ankle rehabilitation application. Different ankle exercise ranges of motion were tested on able-bodied testers in order to obtain normalized data in a gait laboratory. The ankles' motions data were applied on a hexapod and a proposed hybrid parallel robot through a developed inverse kinematic model.

The actuators' lengths were applied in CAD software to track the positions of the end-effector. The comparisons of the hexapod and hybrid robots' motions demonstrate the singularity-related limitations of a hexapod to achieve the desired path, while the hybrid structure was successfully able to simulate the considered activities.

Chapter 9

Conclusion

9.1 Introduction

Parallel robots have been investigated due to high accuracy, stiffness rather than serial robots. They are used for flight simulation, machining and pick and place in small workspace. The proposed parallel-serial robot is a new approach to address the limited workspace weakness of a hexapod. The research aim is therefore achieved by developing a new design of a 9-DOF hybrid parallel robot in order to increase the workspace and supporting the singularities in structure. The main objectives of the research are as follows:

- Development and verification of inverse kinematic of hybrid parallel robot
- Development of dynamics analysis of the system
- Design of CAD model and analysis of robot stiffness
- Build physical prototype and perform static and dynamic experimentation
- Development of control strategy and algorithm
- Systems verification and industrial application evaluation

The new configuration of hybrid parallel robot provides opportunities to apply new ideas to kinematics, dynamics and control strategies in parallel robots. The design was successfully verified in a robotic ankle rehabilitation application.

9.1 Developed Methodologies and Main Results

This project proposed a new 9-DOF hybrid parallel robot. This hybrid parallel configuration includes nine actuators attached to one stationary and two moveable platforms. The aim of the developed design was to increase the workspace for the mentioned applications. The inverse kinematics of the model was developed (Chapter 3) in order to find the working area, limitations and singularities in the structure. According to the obtained results of the workspace of the hexapod, tripod and hybrid parallel robot, the workspace of the hybrid is increased by 362% and 804% compared to the tripod and the hexapod respectively. The inverse kinematic of the system was successfully validated with the other methods. The fully defined assembly was designed in a CAD model in order to be used for static and dynamic simulation. The components of the robot that required being prototyped, such as the road clevis, were designed to complete the model. The FEA results obtained from the SOLIDSIMULATION software were used to calculate the stiffness of the model. In the developed theoretical model the applied force on each actuator in a different pose and orientation was calculated.

The inverse dynamic formulation of the model was developed based on the Newton-Euler method. In this method the velocity of each actuator was calculated based on stroke size for particular motions. In the developed method, the angular and linear velocity and acceleration of platforms A and E were calculated for both hexapod and tripod. The developed work and energy equilibrium determined the whole energy which was applied by actuators. Then, the velocity and position of the end-effector were calculated. The stroke size data were transferred to the CAD model by a developed interface program to simulate the motion. The applied forces on the actuators for particular motions were simulated and demonstrated. The main result in Chapter 4 was the developed dynamic methodology to calculate the force applied on the actuators, and the linear and angular velocities of the end effector for particular motion.

The physical model was prototyped to test the robot and the proposed theories. The obtained results of the dynamic and static experimentation validate the theories developed for the system. The force sensors were placed between the joints and platforms in order to calculate the forces applied to the actuators. The force sensors were calibrated using the standard method. Each force sensor is placed between two flat platforms and identified weights applied on the plate. The force sensors were connected to a microcontroller in order to send digital data to the associated computer. The collected data of the applied weight and the measured value by force sensors were plotted in order to determine the linear relationship. The data obtained by force sensor verified the developed theory for dynamics formulation.

The control strategy which was developed was based on the capabilities of the system. An extra tripod with three degrees of freedom assisted the system to reach the same position and orientation with a different travelling stroke of each actuator. Therefore, the singularities of the system could be the supported motion of the end-effector. The Bezier curve was applied to the motion of the hexapod to smooth the travelling path. This method increased the efficiency of the motion. The obtained results of the different methods were demonstrated in theory and simulation.

The rehabilitation application was applied to the robot to test the capability of the system. The results of the foot motions were obtained from experimentation on the motions of healthy people. A 3D camera was used to capture the position and orientation of the markers attaching to the foot. Then 3D paths of the motions were developed with a MATLAB program. The obtained paths were applied to the hexapod and hybrid parallel robots' kinematics to test the capability of the systems. The obtained results depicted that the hybrid parallel robot could follow the path more efficiently than the hexapod. The data of the stroke size was transferred to the CAD model by an interface program (VB) to simulate the motion. The required forces for the actuators were calculated for the foot motions. The Results obtained in Chapter Eight verified the capability of the proposed parallel robot for tracking the path motion of the foot for rehabilitation purposes.

9.2 Contribution of this Thesis

A new hybrid parallel robot by developing new sets of formulation for kinematics and dynamics and control strategies for industry and rehabilitation applications is designed. The theories are validated by simulation studies and experimentations. The research contributions are listed as follow:

- Designing of new configuration of a nine DOF hybrid parallel robot

Within the designing of the system, this research addressed the inverse kinematics, workspace and stiffness development methodology of the hexapod, tripod and hybrid parallel robot.

- New methodology to investigate the dynamics of the model

In this research the Euler-Newton method is developed for hybrid parallel robot. The results of theory were validated by experimentations and simulations.

- New Methodology for developing non-singular path planning for hybrid parallel robot

The new strategies based on capability of structure were developed in order to support the singularities in workspace of the hexapod.

- The strong performance of the developed system in rehabilitation application can contribute in modern motion simulation

9.3 Future Direction

The positioning accuracy analysis of allocated application in this research can be extended for further development. The research concerned with the development of calculation of design, kinematics and dynamics of the proposed system can be applied to industrial application such as workholding and/or jigs and fixture operations in assembly of large aerospace components.

The close loop control model could be develop for the system in order to increase the accuracy of the motions. High resolution position sensor (camera or laser) will be needed to track the position of the end-effector. The captured end-effector's position data will be sent to the inverse kinematic program in order to reduce the position errors.

In addition, some of the relevant future directions are listed as follow:

- Calculating the system dynamics behavior with exact external force applied to end-effector for the particular application
- Improving the control model using closed-loop strategies
- Implementing the optimisation method to enhance accuracy
- Developing control strategy through using CAD model for Virtual manufacturing application

References

[1] J.P. Merlet, Parallel robots solid mechanics and its applications", Second Edition, Springer, 2006, Volume 128.

[2] Tian Huang, Xingyu Zhao, D.J Whitehouse, Stiffness estimation of a tripod-based parallel kinematic machine, IEEE Transactions on Robotics and Automation, 2002 ,vol.18, no.1, pp.50-58

[3] Zhenhua Wang, Liguo Chen, Lining Sun, An Integrated Parallel Micromanipulator with Flexure Hinges for Optical Fiber Alignment, International Conference on Mechatronics and Automation ICMA, 2007, pp.2530-2534.

[4] G. Kumar Satheesh, M Bikshapathi, T Nagarajan, Y. G Srinivasa, Stiffness analysis and kinematic modeling of Stewart Platform for machining applications, Poster, American Society for Precision Engineering, 2004

[5] Nabil Simaan, Moshe Shoham, Stiffness Synthesis of a Variable Geometry Six-Degrees-of-Freedom Double Planar Parallel Robot, The International Journal of Robotics Research, 2003,Vol 22, pp757-775.

[6] Fengfeng Xi, Dan Zhang, Chris M. Mechefske, Sherman Y.T. Lang, Global kinetostatic modelling of tripod-based parallel kinematic machine, Mechanism and Machine Theory, 2004 ,Volume 39, Issue 4, Pages 357-377.

[7] Bashar S. El-Khasawneh and Placid M. Ferreira, Computation of Stiffness and Stiffness Bounds for Parallel Link Manipulators, International Journal of Machine Tools and Manufacture, 1996 ,pp 321-342.

[8] Wang Zhongfei, Ji Shiming, Li Yanbiao and Wan Yuehua, A unified algorithm to determine the reachable and dexterous workspace of parallel manipulators, Robot. Computer Integrated Manufacturing, 2010, Vol 26, Issue 5, pp 454-460.

[9] Wenjie Chen, Guilin Yang, Wei Lin, A Tripod Mechanism for Parallelism Alignment: Kinematics Analysis and Application. IEEE/ASME International Conference on Advanced Intelligent Mechatronics, Singapore, 2009, pp 1047 - 1051.

[10] P. Dietmaier, The Stewart-Gough platform of general geometry can have 40 real postures, Advances in Robot Kinematics: Analysis and Control, Kluwer Academic Publishers, 1998, pp 1-10.

[11] Zhuang Hanqi, Yan Jiahua, Oren Masory, Calibration of Stewart platforms and other parallel manipulators by minimizing inverse kinematic residuals, J. Robotic Syst., 1998, Vol 15:7, pp 395-405.

[12] Yan Shi and Yi Lu, CAD Application to the Analysis about the Workspace of an Asymmetric Parallel Robot Influenced by the Joints' Distribution, International Conference on Computer and Electrical Engineering, 2008, pp 497-501.

[13] A.M. Hay, J.A. Snyman, Multidisciplinary Design Optimization Group (MDOG), The determination of nonconvex workspaces of generally constrained planar Stewart platforms, Comp. & Mathematics with Applications, 2000, Vol. 40: 8-9, pp 1043-1060.

[14] D. Lazard, J. P Merlet, The (true) Stewart platform has 12 configurations, Proceedings of IEEE International Conference on Robotics and Automation, 1994, vol.3, pp.2160-2165.

[15] Yu Wen Li, Jin Song Wang, Li Ping Wang, Stiffness analysis of a Stewart platform-based parallel kinematic machine, Proceedings of IEEE International Conference on Robotics and Automation ICRA, 2002, vol.4, pp. 3672- 3677.

[16] Dan Zhang , S. Patel, Zhen Gao, Yunjian Ge, Stiffness control for a 3-DOF parallel robot based machine tool, International Conference on Information and Automation ICIA, 2008, pp.1085-1090.

[17] Mehdi Tale Masouleh, Mohammad Hossein Saadatzi, A Geometrical Constructive Approach for the workspace Analysis of Symmetrical 5-PRUR parallel mechanism [3T2R], International Design Engineering Technical Conferences & Computers and Information in Engineering Conference, 2010, IDETC/CIE.

[18] J A Saglia. N G Tsagarakis, J S Dai. D G Caldwell, Inverse-kinematics-based control of a redundantly actuated platform for rehabilitation, IMechE. Part I: J. Systems and Control Engineering, 2009, Vol. 223, pp 53-70.

[19] Doina Pisla, Bogdan Gherman, Calin Vaida, Marius Suciu, Nicolae Plitea, An active hybrid parallel robot for minimally invasive surgery, Robotics and Computer-Integrated Manufacturing 29, 2013, pp 203–221.

[20] Y. Shneor, V.T. Portman, Stiffness of 5-axis machines with serial, parallel, and hybrid kinematics: Evaluation and comparison, CIRP Annals - Manufacturing Technology 59, 2010, pp 409–412.

[21] Zhen Gao, Dan Zhang , Yunjian Ge, Design optimization of a spatial six degree-of-freedom parallel manipulator based on artificial intelligence approaches, Robotics and Computer-Integrated Manufacturing 26 ,2010,pp 180–189.

[22] Jun Wu, Jinsong Wang, Liping Wang, Tiemin Li, Zheng You, Study on the stiffness of a 5-DOF hybrid machine tool with actuation redundancy, Mechanism and Machine Theory 44, 2009, pp 289–305.

[23] JunWu, Tiemin Li, Jinsong Wang, Liping Wang, Performance Analysis and Comparison of Planar 3-DOF Parallel Manipulators with One and Two Additional Branches, Springer, Journal of intelligent robotic system, 2013, Volume 72, Issue 1, pp 73-82.

[24] T. Huang, P.F. Wang, X.M. Zhao , D.G. Chetwynd, Design of a 4-DOF hybrid PKM module for large structural component assembly, CIRP Annals - Manufacturing Technology 59, 2010, pp 159–162.

[25] Yongbo Wang, Pekka Pessi, Huapeng Wu, Heikki Handroos, Accuracy analysis of hybrid parallel robot for the assembling of ITER, Fusion Engineering and Design 84 (2009) 1964–1968

[26] Bo Hua, Yi Lua, Qing Tan, Jianping Yu, Jianda Han, Analysis of stiffness and elastic deformation of a 2(SP+SPR+SPU) serial–parallel manipulator, Robotics and Computer-Integrated Manufacturing 27, 2011, pp 418–425.

[27] Wei Zhao, Bing Li, Ying Hu, Stiffness Analysis of a Hybrid Manipulator Applied to a Multi-dimensional Vibration Isolator ,Proceedings of IEEE International Conference on Mechatronics and Automation , 2012 August 5 - 8, Chengdu, China ,1874-1879.

[28] David F. Rogers, J. Alan Adams, Mathematical Elements for Computer Graphics, Edition 2, McGraw-Hill, 1990 ,pp101-151.

[29] Y. Li and Q. Xu, Design and development of a medical parallel robot for cardiopulmonary resuscitation, IEEE/ASME Trans. Mechatronics, 2007, vol. 12, no. 3, pp. 265–273.

[30] Liping Wang, Jun Wu, Jinsong Wang, and Zheng You, An Experimental Study of a Redundantly Actuated Parallel Manipulator for a 5-DOF Hybrid Machine Tool, IEEE/ASME Transactions on Mechatronics, 2009, VOL. 14, NO. 1, pp 72- 81.

[31] Sergiu-Dan Stan, Milos Manic, Vistrian Mătieş, Radu Bălan, Kinematics Analysis, Design, and Control of an Isoglide3 Parallel Robot (IG3PR), Conference Industrial Electronics,. 34th Annual Conference of IEEE, 2008, Orlando, FL, pp 2636 – 2641.

[32] Weiwei Shang, Shuang Cong, Yaoxin Zhang, and Yanyang Liang, Active Joint Synchronization Control for a 2-DOF Redundantly Actuated Parallel Manipulator, IEEE transactions on control systems technology, 2009, Vol. 17, NO. 2, pp 416-423.

[33] Jun Wu, Jinsong Wang, Liping Wang, Tiemin Li, Dynamics and control of a planar 3-DOF parallel manipulator with actuation redundancy ,Mechanism and Machine Theory, Volume 44, Issue 4, 2009, pp 647-872 .
[34] Stefan Staicu, Inverse dynamics of the 3-PRR planar parallel robot, ELSEVIER Robotics and Autonomous Systems 57, 2009, pp 556-563.
[35] Xiaocong Zhua, Guoliang Taoa, Bin Yaoa,b, Jian Caoa, "Adaptive robust posture control of a parallel manipulator driven by pneumatic muscles", Automatica ,Volume 44, Issue 9,2008 , pp 2248-2257.
[36] Hong Bo Guo,Yong Guang Liu, Gui Rong Liu, Hong Ren Li, Cascade control of a hydraulically driven 6-DOF parallel robot manipulator based on a sliding mode, Control Engineering Practice, 2008, Volume 16, Issue 9, pp 1055–1068.
[37] Dongmei Wu, Zhijiang Du, Heqiang Tian, Zhenyu Jiang, Lining Sun, FPGA-based Control System for 6-UPS Medical Parallel Robot, IEEE International Conference on Digital Manufacturing & Automation, 2010, Changsha, pp 744-748.
[38] M.J. Liu, C.0X. Li, and C.N. Li, Dynamics analysis of the Gough–Stewart platform manipulator, IEEE Trans. Robot. Automn, 2000, Vol.16, NO. 1, pp 94-98.
[39] Wisama Khalil and Sylvain Guegan, 2004, Inverse and Direct Dynamic Modeling of Gough–Stewart Robots, IEEE Transaction on Robotics and Automation 20, pp 754-762.
[40] A. Codourey, E. Burdet, A Body-oriented Method for Finding a Linear Form of the Dynamic Equation of Fully Parallel Robots, IEEE, International Conference on Robotics and Automation, Albuquerque,1997,New Mexico, pp 1612-1618.
[41] F. Pierrot, A. Fournier and P. Dauchez, Towards a Fully-Parallel 6 DOF Robot for High Speed Application, IEEE, International Conference on Robotics and Automation, 1991,California, pp 1289-1293.
[42] Andre´ s Vivas, Philippe Poignet, Predictive functional control of a parallel robot, ELSEVIER Control Engineering Practice, 2005, pp 863-874.
[43] G.Q. Cai, Q.M. Wang, M. Hu, M.C. Kang, N.K. Kim, A Study on Kinematics and Dynamics of a 3-DOF Parallel Machine Tools, ELSEVIER Journal of Materials Processing Technology, 2011, Volume 111, Issues 1–3, pp 269–272.
[44] F. Pierrot, A. Fournier and P. Dauchez, Towards a Fully Parallel 6 DOF Robot for High Speed Application, IEEE Conference on Robotics and Automation, 1991, California, pp 1289-1293.
[45] Fabrizio Caccavale, Bruno Siciliano, and Luigi Villani, The Tricept Robot: Dynamics and Impedance Control, IEEE/ASME Transaction on Mechatronic, 2003, VOL. 8, NO. 2, pp 263-269.
[46] J.P. Merlet, Parallel manipulators, (2nd edition), chapter 6: Singular configurations, Pressed by Springer, 402 p, 179-210,1988.
[47] Bhaskar Dasgupta, T. S. Mruthyunjaya, Singularity-free path planning for the Stewart platform manipulator, Mechanism and Machine Theory, 33 (6), 1998, pp 711–725.
[48] Shamik Sen, Bhaskar Dasgupta, Asok Kumar Mallik, Variational approach for singularity-free path-planning of parallel manipulators, Mechanism and Machine Theory 38, 2003, pp 1165–1183.
[49] Anjan Kumar Dash, I-Ming Chen, Song Huat Yeo, Guilin Yang, Workspace generation and planning singularity-free path for parallel manipulators, Mechanism and Machine Theory 40, 2005,pp 776–805.
[50] Reza N. Jazar, Theory of Applied Robotic, pressed by Springer, 2007, second edition, Chapter 13: Path Planning.
[51] S. Bellakehal, N. Andreff, Y. Mezouar, M. Tadjine, Force/position control of parallel robots using exteroceptive pose measurements, Meccanica 46, 2011, pp 195–205.

[52] Tae-Young Lee, Jae-Kyung ,Forwards Kinematics of General 6-6 Stewart platform using algebraic elimination, Mechanisms and Machine Theory 36, 2001 ,pp 1073-1085.
[53] Ping Ji and Hongtao Wu, A Closed-Form Forward Kinematics Solution for the 6–6 Stewart Platform, IEEE Transactions on Robotics and Automation, 2001,Vol. 17, no. 4.
[54] Xi Fengfeng , Dan Zhang, Chris M. Mechefske, Sherman Y.T. Lang, Global kinetostatic modelling of tripod-based parallel kinematic machine, Mechanism and Machine Theory, 2004, Volume 39, Issue 4, Pages 357-377.
[55] Wenjie Chen, Guilin Yang, Wei Lin, A Tripod Mechanism for Parallelism Alignment: Kinematics Analysis and Application, IEEE/ASME International Conference on Advanced Intelligent Mechatronics, 2009, pp 1047-1051.
[56] Yuan Yun, Yangmin Li, Design and analysis of a novel 6-DOF redundant actuated parallel robot with compliant hinges for high precision positioning, Springer Science+Business Media B.V, 2010,pp 829-845.
[57] D. Pisla, N. Plitea, C. Vaida, J. Hesselbach, A. Raatz, L. Vlad, F. Graur ,B. Gyurka, B. Gherman, M. Suciu, PARAMIS parallel robot for laparoscopic surgery, Chirurgia 105, 2010, pp 677-683.
[58] S. D'Angella, A. Khan, F. Cepolina, M. Zoppi, Modeling and control of a parallel robot for needle surgery, IEEE International Conference on Robotics and Automation, 2011, Shanghai, China
[59] Mohsen Moradi Dalvand, Bijan Shirinzadeh, Motion control analysis of a parallel robot assisted minimally invasive surgery/microsurgery system (PRAMiSS), Robotics and Computer-Integrated Manufacturing 29, 2013, pp 318–327.
[60] B. Achili, B. Daachi, Y. Amirat, A. Ali-cherif, A robust adaptive control of a parallel robot, International Journal of Control,2010 , Vol. 83, No. 10, pp 2107–2119.
[61] Philippe Begon, Franqois Pierrot and Pierre Dauchez, Fuzzy Sliding Mode Control of a Fast Parallel Robot, IEEE lnternatlonal Conference on Robotlcs and Autornatlon, 1995 , pp 1178-1183.
[62] Redwan Dahmouche , Nicolas Andreff , Youcef Mezouar and Philippe Martinet, Efficient High-speed Vision-based Computed Torque Control of the Orthoglide Parallel Robot, IEEE. International Conference on Robotics and Automation Anchorage Convention District, 2010, Anchorage, Alaska, USA.
[63] Houssem Abdellatif, Member, IEEE, and Bodo Heimann, Advanced Model-Based Control of a 6-DOF Hexapod Robot: A Case Study, IEEE/ASME Transactions On Mechatronics, Vol. 15, No. 2, April 2010, pp 269-279.
[64] Georg Rauter, Joachim von Zitzewitz, Alexander Duschau Wicke, Heike Vallery, and Robert Riener, A Tendon-Based Parallel Robot Applied to Motor Learning in Sports, Proceedings of the 3rd IEEE RAS & EMBS International Conference on Biomedical Robotics and Biomechatronics, 2010, the University of Tokyo, Tokyo, Japan,
[65] Yue-Qing Yu, Zhao-Cai Du, Jian-Xin Yang, and Yuan Li, An Experimental Study on the Dynamics of a 3-RRRFlexible Parallel Robot, IEEE Transactions on Robotics, 2011,Vol. 27, No.5, pp 992-996.
[66] Sung-Hua Chen, Chin-Teng Lin, and Li-Chen Fu, Second Order Sliding Mode Control on Task-Space of a 6-DOF Stewart Platform, IEEE, 2012 , pp 2482-2487.
[67] Hyun Min Do, Chan Hun Park, Byung In Kim, Gwang Jo Chung and Jin Ho Kyung, Design and Control of High-Speed Parallel Robot , 12th International Conference on Control, Automation and system, 2012, Jeju Island, Korea , pp 2139-2142 .
[68] Miguel G. Villarreal-Cervantes, Carlos A. Cruz-Villar, Jaime Alvarez-Gallegos and Edgar A. Portilla-Flores, Differential evolution techniques for the structure-control design of a five-bar parallel robot, Engineering Optimization, 2010, Vol. 42, No. 6, pp 535–565.

[69] Hongzhou Jiang, Jingfeng He, Zhizhong Tong, Modal Space Control for a Hydraulically Driven Stewart Platform, Journal of Control Engineering and Technology (JCET), 2012, Vol. 2 Iss. 3, pp 106-115.
[70] Yangjun Pi, Xuanyin Wang, Trajectory tracking control of a 6-DOF hydraulic parallel robot manipulator with uncertain load disturbances, Control Engineering Practice 19, 2011, pp 185–193.
[71] Chifu Yang, Qitao Huang, Junwei Han, Decoupling control for spatial six-degree-of-freedom electro-hydraulic parallel robot, Robotics and Computer-Integrated Manufacturing 28, 2012, pp 14–23.
[72] Yuan Yun, Yangmin Li, Optimal design of a 3-PUPU parallel robot with compliant hinges for micromanipulation in a cubic workspace, Robotics and Computer-Integrated Manufacturing 27, 2011, pp 977–985.
[73] Hamid Reza Hassanzadeha, Mohammad-R. Akbarzadeh-Ta, Alireza Akbarzadeh, Amir Rezaeib, An interval-valued fuzzy controller for complex dynamical systems with application to a 3-PSP parallel robot, Fuzzy Sets and Systems 2013, ELSEVIER.
[74] Farzin Piltan , Sh. Tayebi Haghighi, N. Sulaiman, I. Nazari & S. Siamak, Artificial Control of PUMA Robot Manipulator: A-Review of Fuzzy Inference Engine and Application to Classical Controller, International Journal of Robotic and Automation (IJRA), Volume 2, Issue 5, 2011, pp 401-425.
[75] Laurent Vermeiren, Antoine Dequidt, Mohamed Afroun, Thierry-Marie Guerra, Motion control of planar parallel robot using the fuzzy descriptor system approach, ISA Transactions 51, 2012, pp596–608.
[76] Andre´ s Vivas, Philippe Poignet, Predictive functional control of a parallel robot, ELSEVIER Control Engineering Practice 13, 2005, pp 863–874.
[77] Meysar Zeinali, Leila Notash, Adaptive sliding mode control with uncertainty estimator for robot manipulators, Mechanism and Machine Theory 45, 2010, pp 80–90.
[78] Yunfeng Wang, Gregory S. Chirikjian, A New Potential Field Method for Robot Path Planning, IEEE international Conference on Robotics and Automation, 2000, San Francisco, CA, pp 977-982.
[79] J. Corths, T. Simeon, J.P. Laumond, A Random Loop Generator for Planning the Motions of Closed Kinematic Chains using PRM Methods, IEEE international Conference on Robotics & Automation, 2002 , Washington, DC, pp 2141-2146.
[80] M. Almonacid, R. J. Saltarén, R. Aracil, and O. Reinoso, Motion Planning of a Climbing Parallel Robot, IEEE transactions on robotics and automation, 2003,vol. 19, no. 3, pp 485-489.
[81] Yanrong Hu and Simon X. Yang, A Knowledge Based Genetic A1gorithm for Path Planning of a Mobile Robot, IEEE international Conference on Robotics 8 Automation, 2004,pp 4350-4355.
[82] Patrick Grosch, Raffaele Di Gregorio, Javier L´opez, and Federico Thomas, Motion Planning for a Novel Reconfigurable Parallel Manipulator with Lockable Revolute Joints, IEEE International Conference on Robotics and Automation, 2010,pp 4697-4702.
[83] Dmitry Berenson, Pieter Abbeel, Ken Goldberg, A Robot Path Planning Framework that Learns from Experience, IEEE International Conference on Robotics and Automation, 2012, Minneapolis, pp 3671-3678.
[84] Bih-Yaw Shih, Hsiang Chang and Chen-Yuan Chen, Path planning for autonomous robots – a comprehensive analysis by a greedy algorithm, Journal of Vibration and Control, SAGE, 2012, vol 19, pp 130-142.
[85] Samir Lahouar, Erika Ottaviano, Said Zeghoul, Lotfi Romdhanec, Marco Ceccarelli, Collision free path-planning for cable-driven parallel robots, Robotics and Autonomous Systems 57, 2009, pp 1083_1093.

[86] Anjan Kumar Dash, I-Ming Chen, Song Huat Yeo, Guilin Yang, Workspace generation and planning singularity-free path for parallel manipulators, Mechanism and Machine Theory 40, 2005, pp 776–805.
[87] J. Stebbins , M. Harrington, N. Thompson, A. Zavatsky, T. Theologis, Repeatability of a model for measuring multi-segment foot kinematics in children, Gait & Posture 23, 2006, pp 401–410.
[88] Bo Hu, Chunping Sui, Jianda Han, Jingjing Yu and Yi Lu, Static and Stiffness Model of Serial-Parallel Manipulator Formed by K Parallel Manipulators Connected in Series, Journal of Mechanisms and Robotics ASME, 2012 , Volume 4, Issue 2, pp 1-8.
[89] Tanio K. Tanev, Kinematic of hybrid (parallel-serial) robot manipulator, Mechanism and Machine Theory 35, 2000, pp 1183-1196.
[90] Xin Jun Liu, Jinsong Wang and Gunter Pritschow, A new family of spatial 3-DoF fully-parallel manipulators with high rotational capability, Mechanism and Machine Theory 40, 2005, pp 475–494.
[91] Nicolás Rojas, Federico Thomas, On closed-form solutions to the position analysis of Baranov trusses, Mechanism and Machine Theory 50, 2012, pp 179–196.
[92] Yi Lua, Yan Shi , Zhen Huanga, Jianping Yub, Shihua Li, Xingbin Tiana, Kinematics/statics of a 4-DOF over-constrained parallel manipulator with 3 legs, Mechanism and Machine Theory 44, 2009, pp 1497–1506.
[93] M. Honegger, R. Brega, G. Schweitzer , Application of a Nonlinear Adaptive Controller to a 6 dof Parallel Manipulator, IEEE, International Conference on Robotics & Automation, 2000, San Francisco.
[94] David F. Rogers and J. Alan Adams, Mathematical Elements for Computer Graphics, second editions, McGraw-Hill company,1999, PP 101-200 .
[95] R.C.Hibbeler, Engineering Mechanics Dynamics, third editions, Prentice Hall, 2004, Chapter 21, Three-Dimensional Kinetics of rigid body, pp 553-600.
[96] Hamid Rakhodaei, Chengjian Ding, Mozafar Saadat, Alireza Rastegarpanah, Free Singularity Path Planning of Hybrid Parallel Robot, Proceeding of the 11th International Conference on Manufacturing Research, ICMR, 2013, pp 313-318.
[97] Available from: http:// http://www.firgelli.com [Accessed October 2011].
[98] N. M. Amato, M. T. Goodrich, and E. A. Ramos, Computing the arrangement of curve segments: Divide-and-conquer algorithms via sampling, in Proceedings of the eleventh annual ACM-SIAM symposium on Discrete algorithms, 2000, pp. 705–706.
[99] H. Simas, A. Dias and R. Guenther, A Scallop-Height Based Algorithm To Compute Parallel Paths On Parametric Surfaces, Abcm Symp. Ser. Mechatronics, 2008, vol. 3, pp. 326–335
[100] H. Shah, M. S. Narayanan, and V. N. Krovi, CAD-enhanced workspace optimization for parallel manipulators: A case study, in Automation Science and Engineering (CASE) , 2010.
[101] G. Farin and D. Hansford, Discrete coons patches, Comput Aided Geom, vol. 16, no. 7, IEEE Conference on, 1999, pp. 816–821.
[102] O. Shardt and J. C. Bowman, Surface parameterization of nonsimply connected planar Bézier regions, Comput. Aided Des, 2012, vol. 44, no. 5, pp. 484.e1–484.e10

Appendices

Appendix A: Stiffness Development

In this section, the stiffness of the hybrid parallel robot is investigated through the comparison of different models. The derived formulation is based on the stiffness matrix of the tripod and the hexapod. Here, all matrices are assumed invariable:

$$[F]=[K]\times[X] \tag{A.1}$$

The Stiffness of the hexapod and the tripod are derived using equations derived by Equation A.3. The displacement of the hybrid system is equivalent to the sum of the hexapod and the tripod displacements. In order to calculate the equation for the displacement, an inverse matrix of the system stiffness is multiplied and as a result, displacement of the system is as follows:

$$[X]=[x_H]+[x_T] \tag{A.2}$$

$$[K]^{-1}\times[F]=[X] \tag{A.3}$$

The displacement formulation of the hexapod and the tripod are given below:

$$[K_H]^{-1} \times [F] = [x_H] \tag{A.4.1}$$

$$[K_T]^{-1} \times [F] = [x_T] \tag{A.4.2}$$

The obtained formulae for the hexapod and the tripod are substituted in Equation A.2. Therefore, the stiffness of the system is obtained as follows:

$$[K]^{-1} = [K_H]^{-1} + [K_T]^{-1} \tag{A.5}$$

Appendix B: Simulation Results of the HPKM

In following tables the FEA simulation conditions for the hybrid parallel robot are explained in more detail.

Table 9: Fixture Position of the FEA Simulation

Restraint name	Selection set
Fixed-1 <Lower_Platform_Assem-1/Spherical1-1, Actuator for simulation 2-5, Lower_Platform_Assem-1/Spherical1-2, Actuator for simulation 2-4, Actuator for simulation 2-3, Lower_Platform_Assem-1/Spherical1-3, Lower_Platform_Assem-1/Spherical1-6, Actu...	on 21 Face(s) fixed.

Table 10: Load Position on Platform

Load name	Selection set	Loading type
Force-1 <End_Effector_assem-1/end effector-1>	on 1 Face(s) apply normal force 100 N using uniform distribution	Sequential loading
Gravity-1	Gravity with respect to Front Plane with gravity acceleration -9.81 m/s^2 normal to reference plane	Sequential loading

Table 11: Mesh Information

Mesh Characteristic	Mode
Mesh Type	Solid Mesh
Mesher used	Standard mesh
Automatic transition	Off
Smooth surface	On
Jacobian check	4 Points
Element size	3 mm
Tolerance	0.15 mm
Quality	High
Number of elements	459740
Number of nodes	774688
Time to complete mesh(hh;mm;ss)	00:10:12
Computer name:	USER-PC

The FEA results of the SOLIDSIMULATION software on the HPKM for two different configurations with different size of actuators are presented below. The configurations are 3-3UPU-3UPR and 6-3UPU-3UPR with a stroke size in the range of 30 to 170 mm.

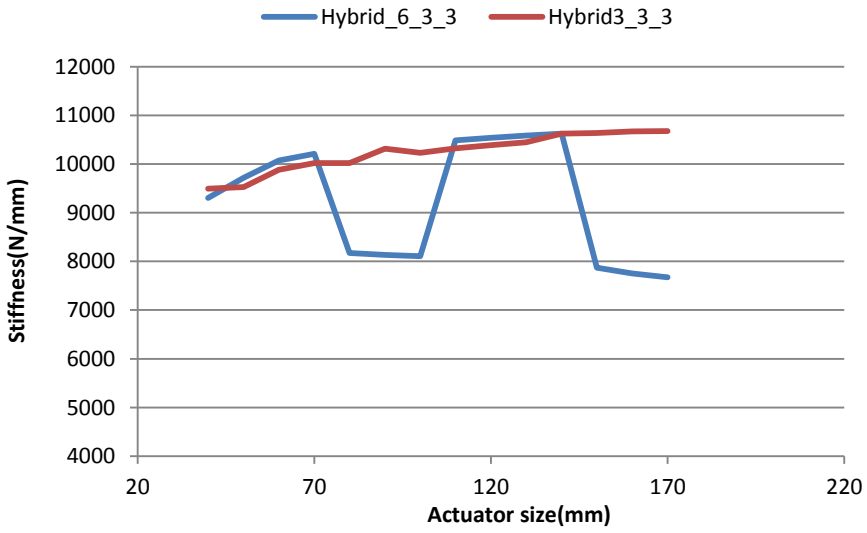

Figure A-1: The Stiffness Comparisons of Two Configuration of Hybrid Robot

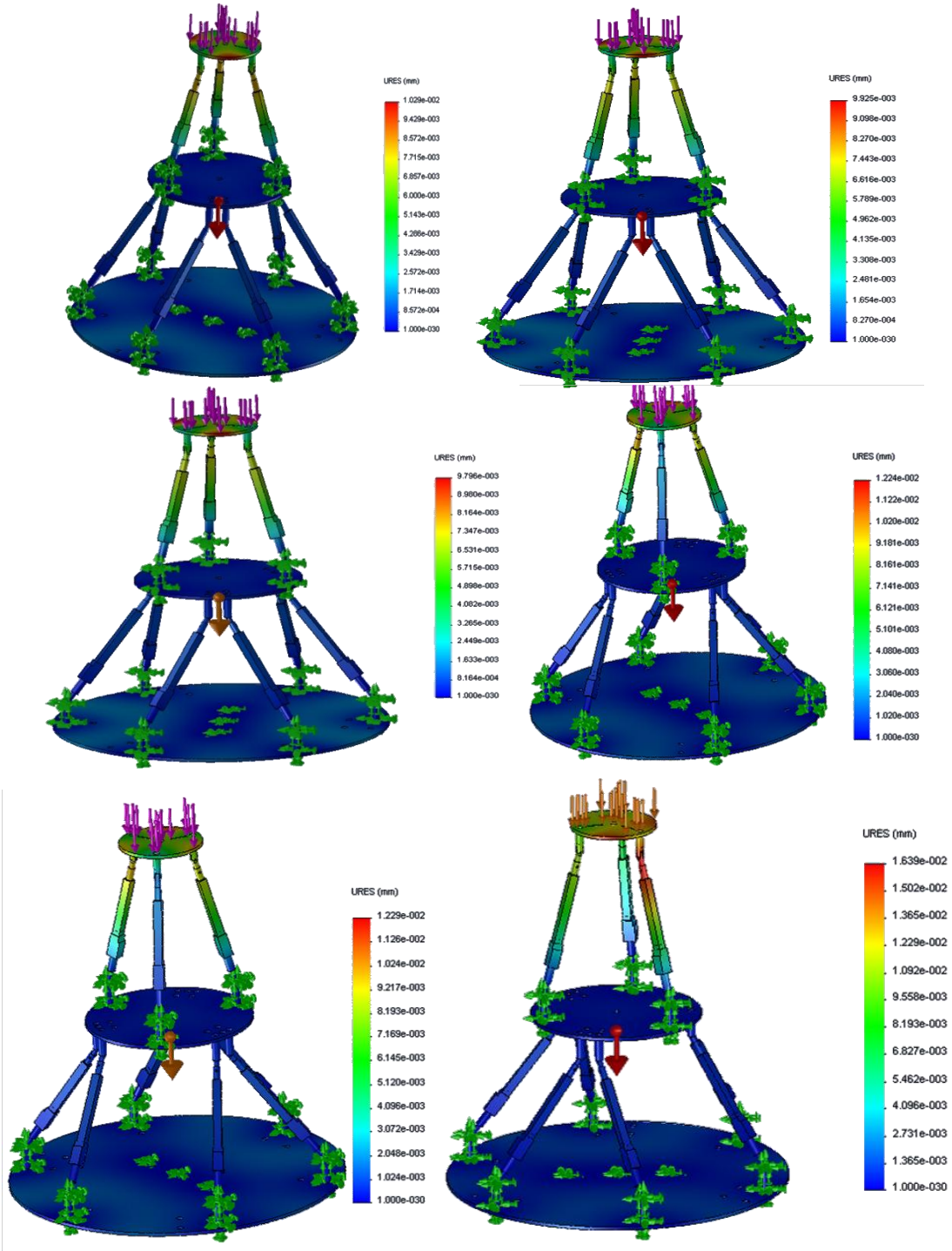

Figure A-2: FEA Results of the HPKM 6-3-3 with Different Stroke Sizes from 30mm- 200mm

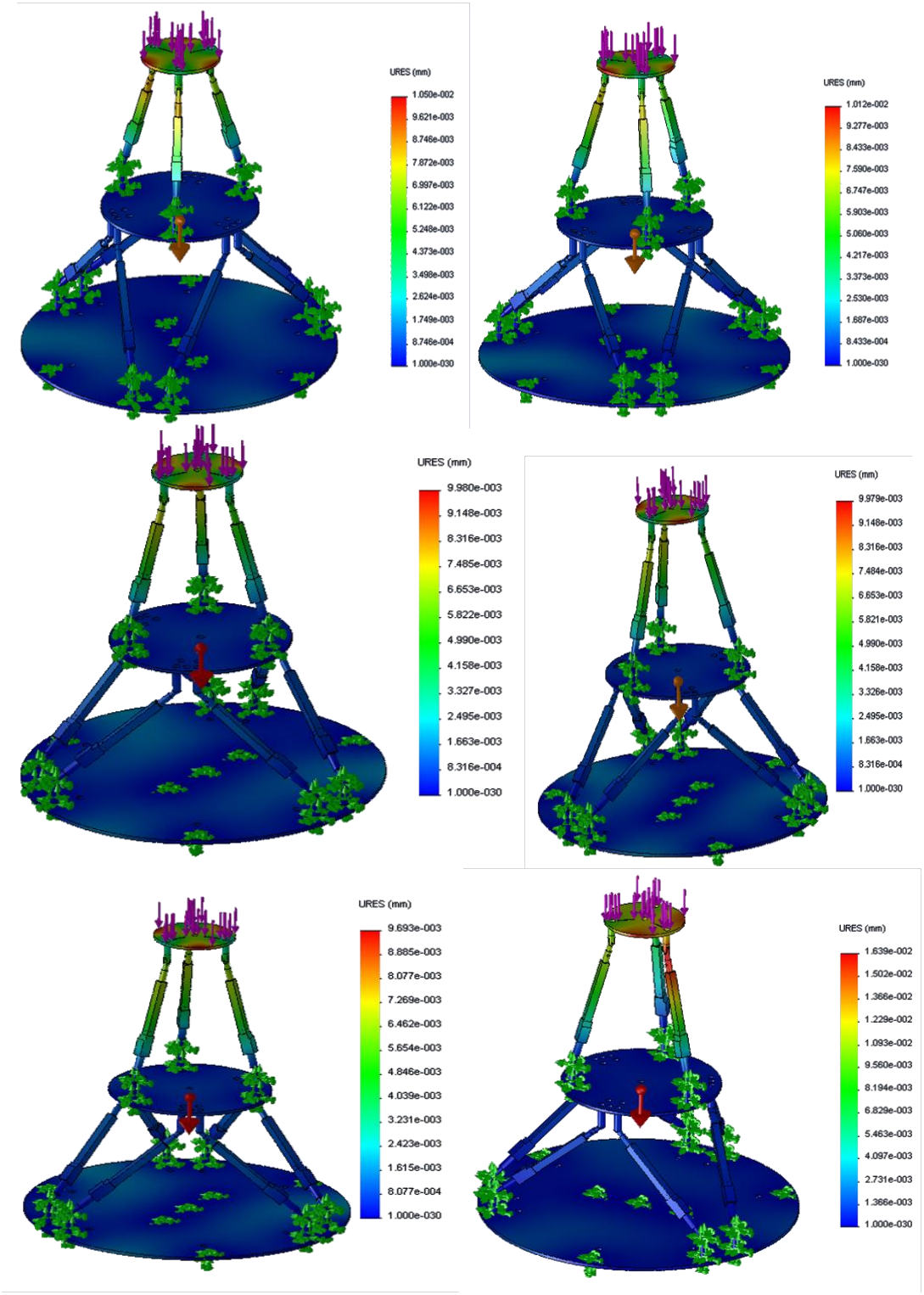

Figure A-3: FEA Results of the HPKM 3-3-3 with Different Stroke Sizes from 30mm- 200mm

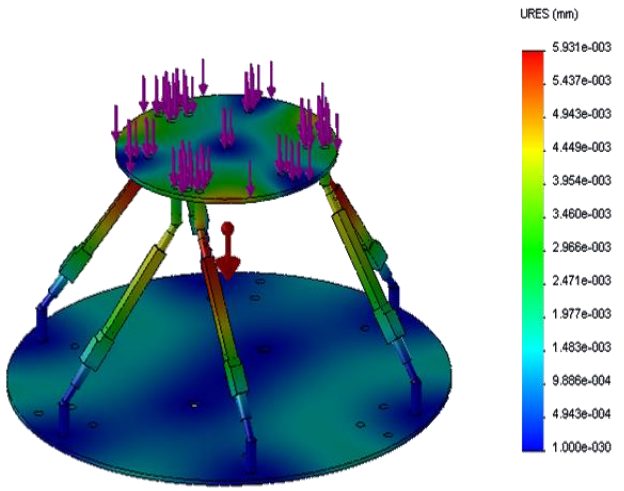

Figure A-4: Hexapod with a Stroke Size of 100mm FEA Results

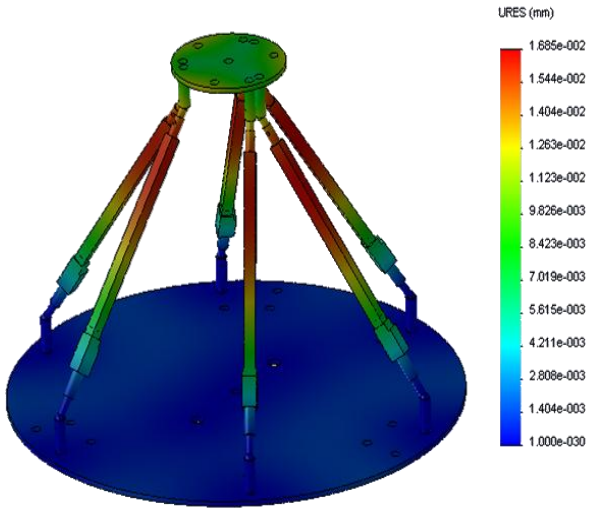

Figure A-5: Hexapod with a Stroke Size of 200mm FEA Results

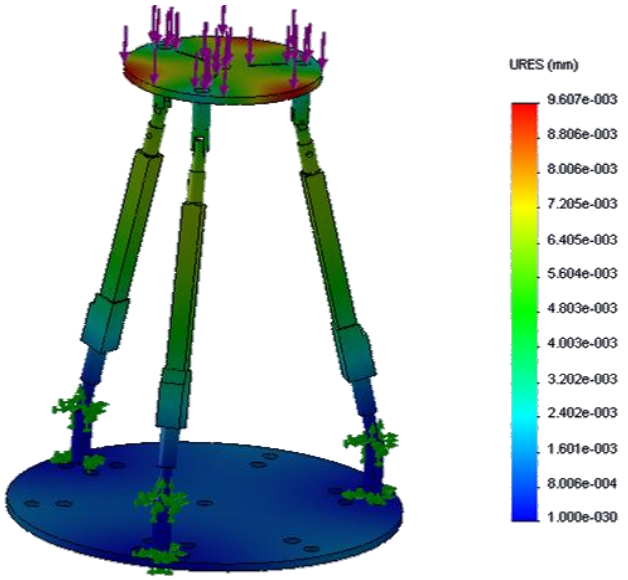

Figure A-6: Tripod with a Stroke Size of 100mm FEA Results

Appendix C: Sensors Calibration

The force sensors are used to identify the applied force to the actuators for static and dynamic validity of theoretical and simulation methods. Nine sensors are used in the HPKM structure. The sensors' calibration graphs are demonstrated in the figures below:

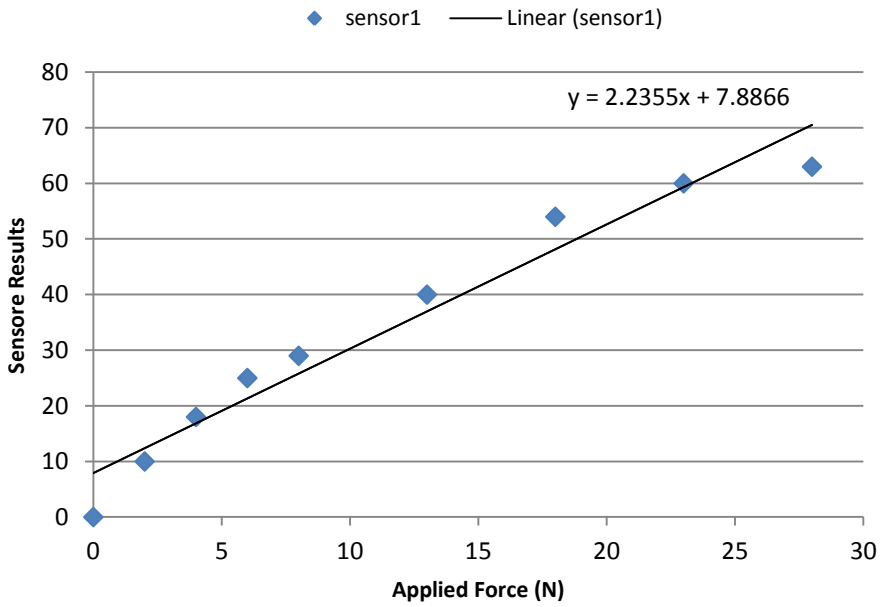

Figure A-7: Results for Calibration of Sensor 1

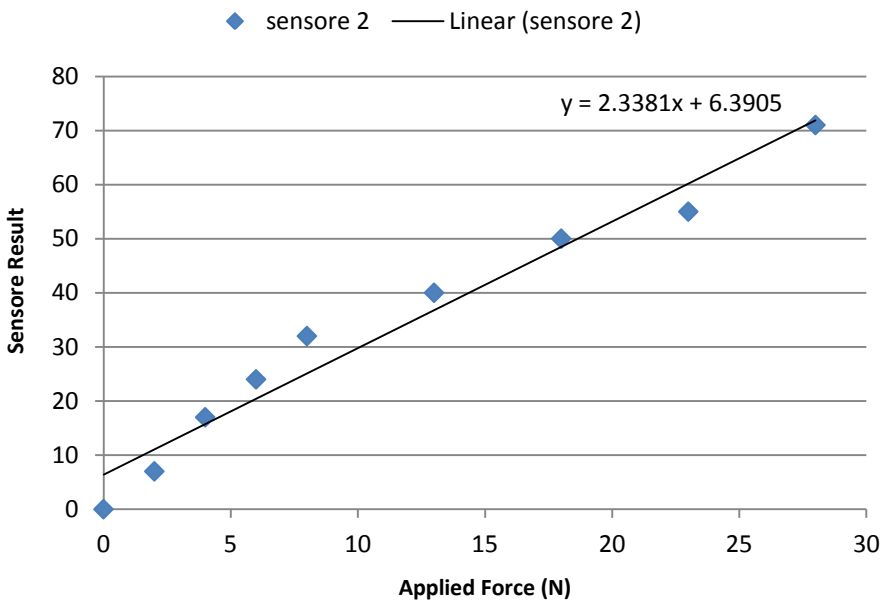

Figure A-8: Results for Calibration of Sensor 2

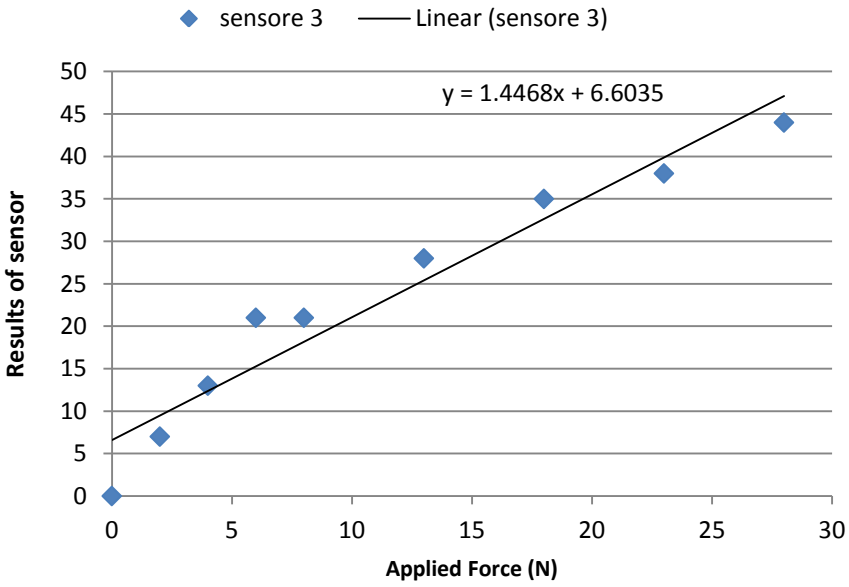

Figure A-9: Results for Calibration of Sensor 3

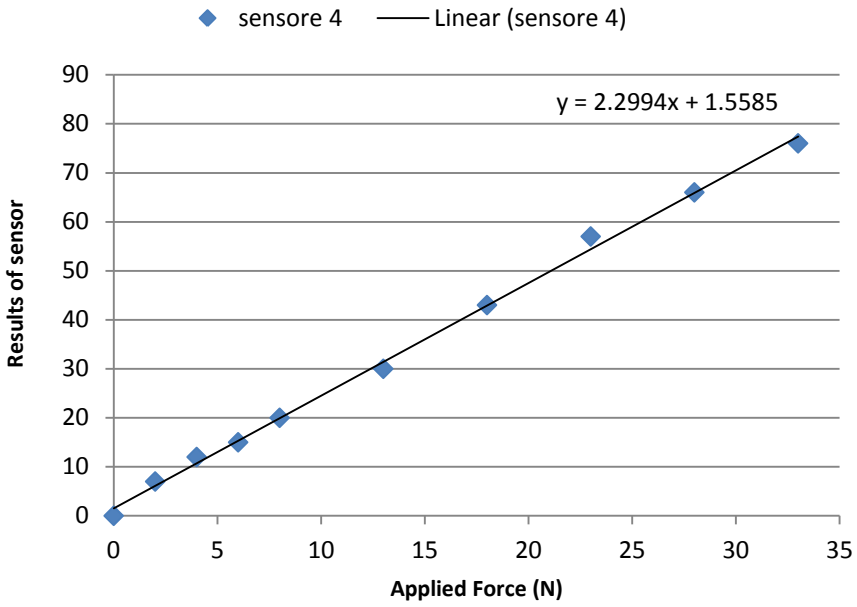

Figure A-10: Results for Calibration of Sensor 4

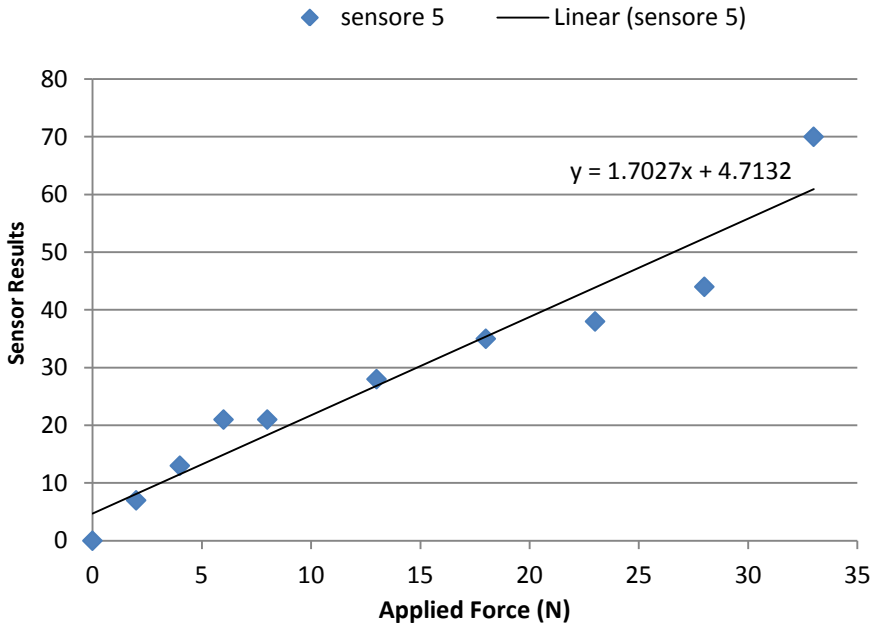

Figure A-11: Results for Calibration of Sensor 5

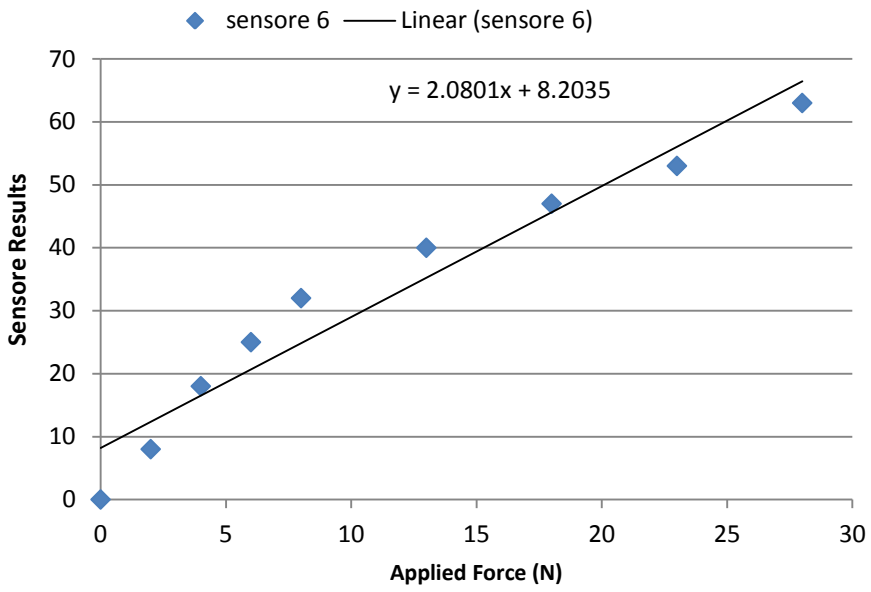

Figure A-12: Results for Calibration of Sensor 6

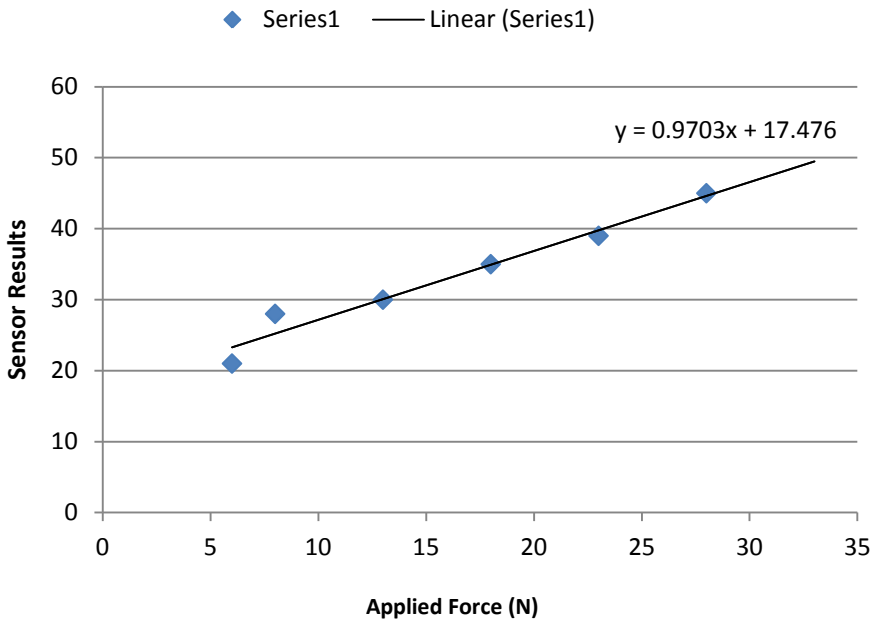

Figure A-13: Results for Calibration of Sensor 7

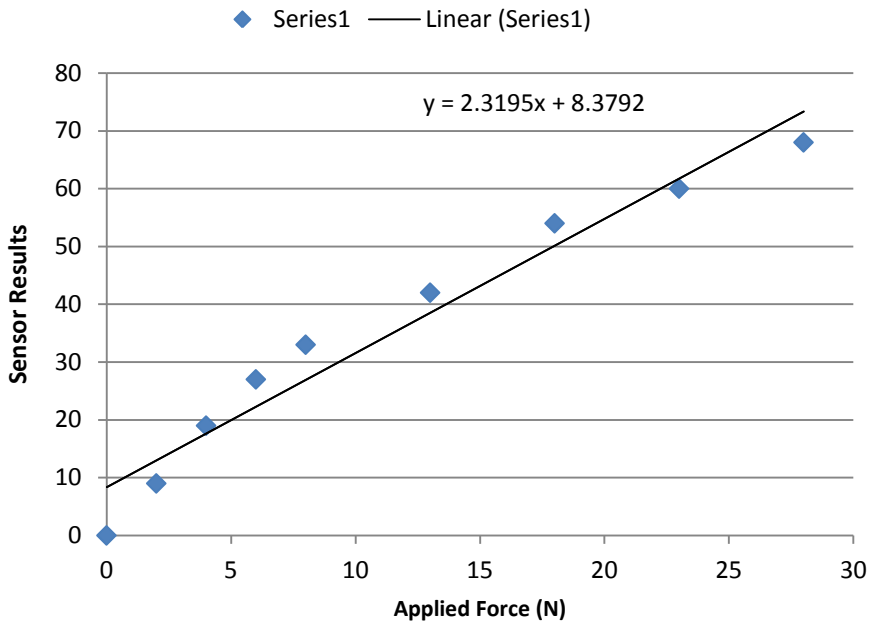

Figure A-14: Results for Calibration of Sensor 8

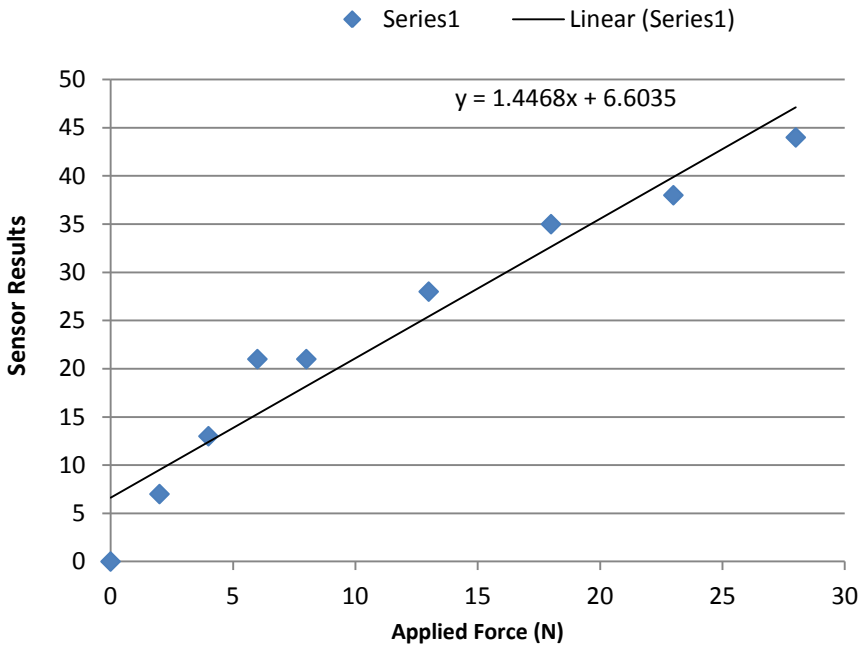

Figure A-15: Results for Calibration of Sensor 9

Appendix D: Interfacing Program for MATLAB and SOLIDWORKS

Different programs are developed for making the interface between Solidworks and Matlab software packages to increase the control variety for the HPKM. Stroke size of the actuators is transferred with the developed program to simulate FEA in the following position as well as the motion of the actuators. The program is able to capture the position of three points on the end-effector of the system. The data are transferred to Matlab to calculate the lengths of the actuators by using inverse kinematic formulation. The interface helps to control the physical model by moving the CAD model.

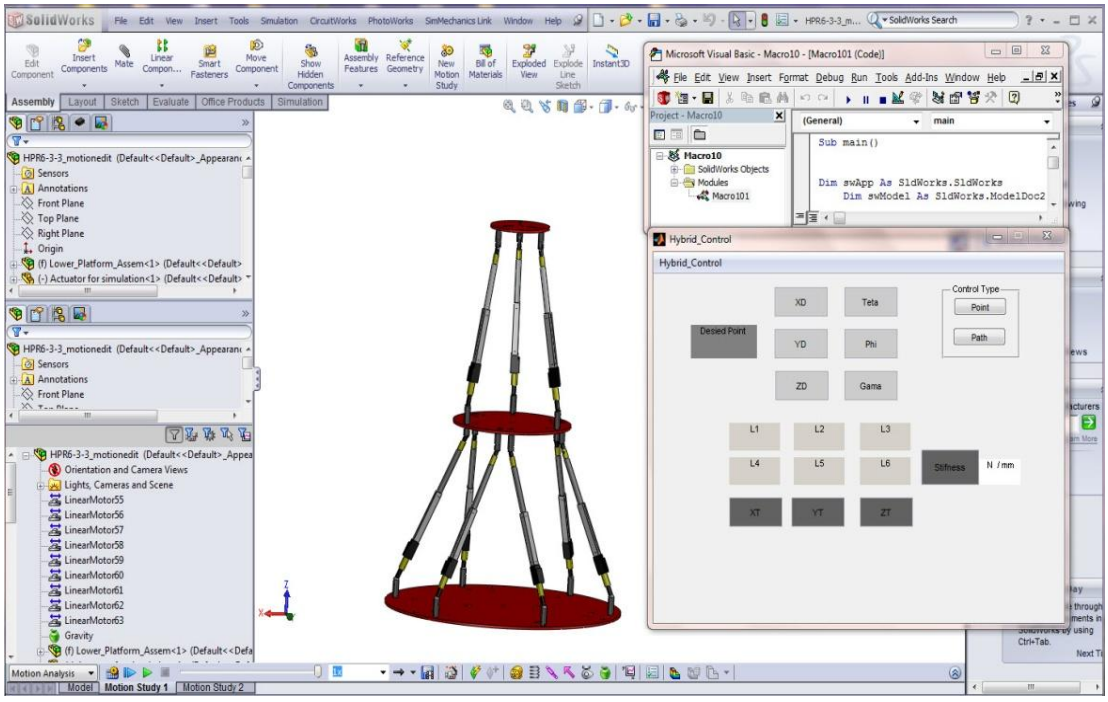

Figure A-16: GUID Control Model with Interface Program

Appendix E: Drawing of Designed Components

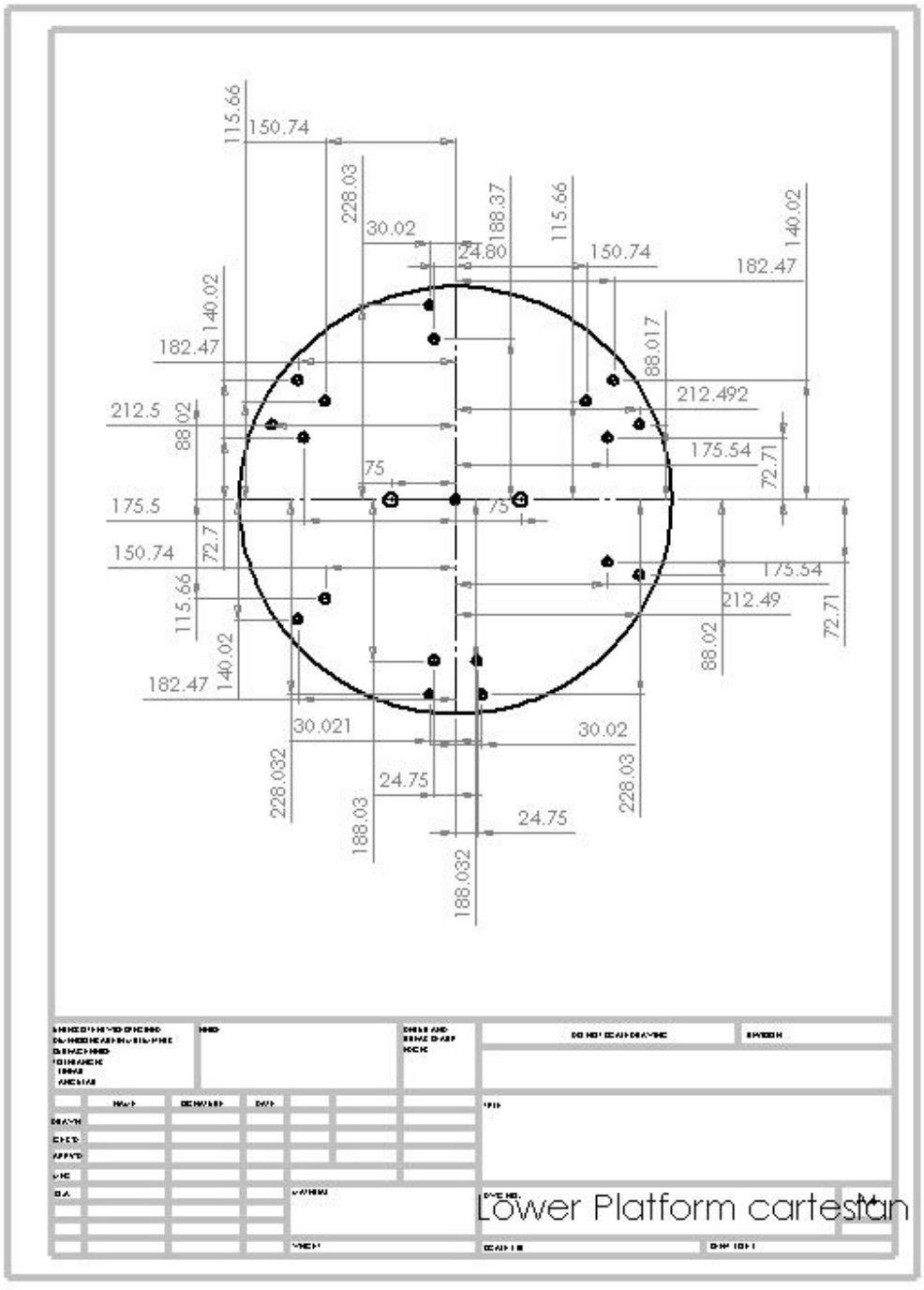

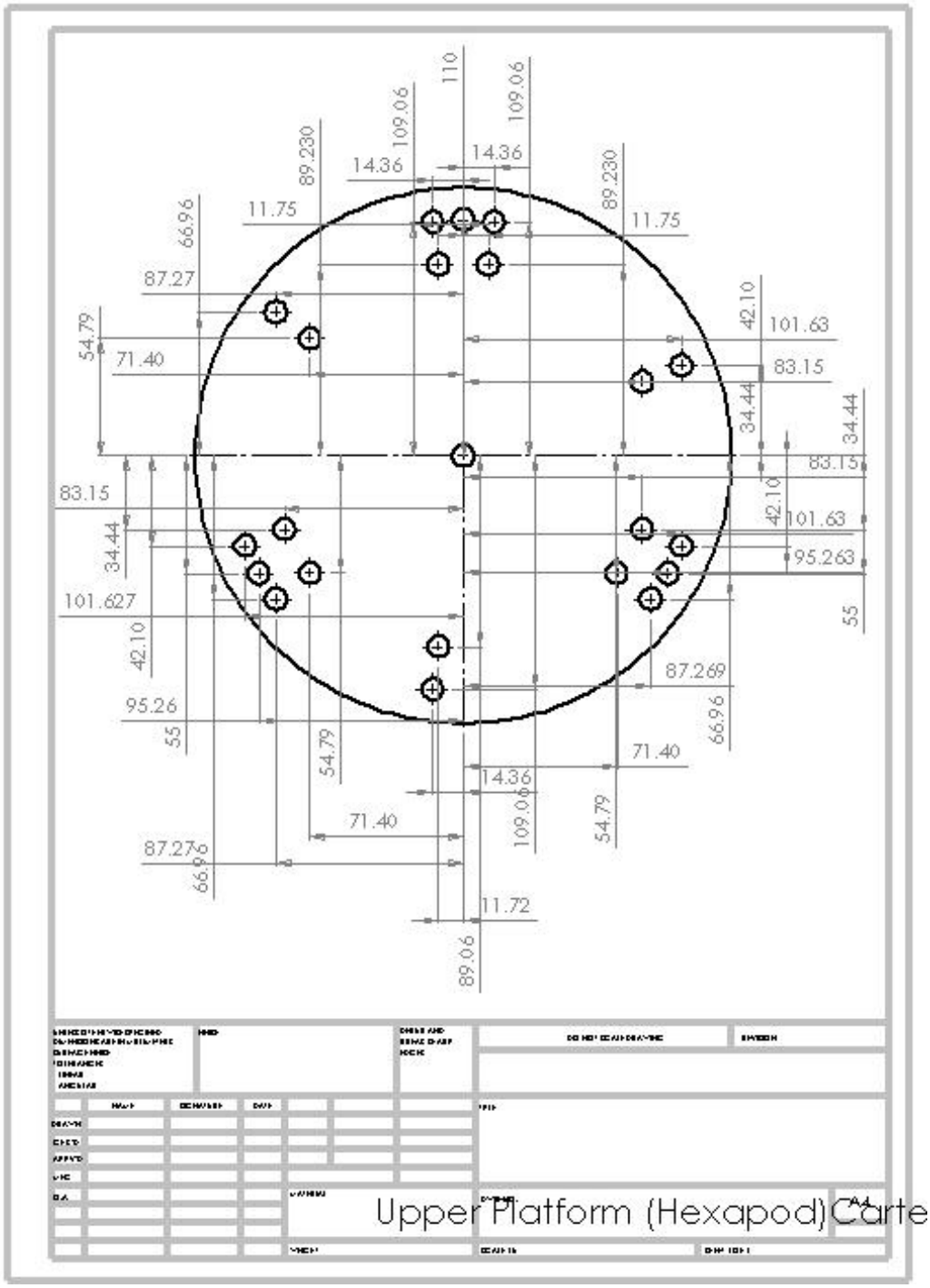
110
109.06
109.06
89.230
14.36
14.36
89.230
66.96
11.75
11.75
87.27
42.10
101.63
54.79
71.40
83.15
34.44
34.44
83.15
83.15
42.10
101.63
34.44
95.263
55
101.627
42.10
87.269
95.26
66.96
55
54.79
71.40
14.36
109.06
54.79
71.40
87.276
66.96
11.72
89.06
Upper Platform (Hexapod) Carte

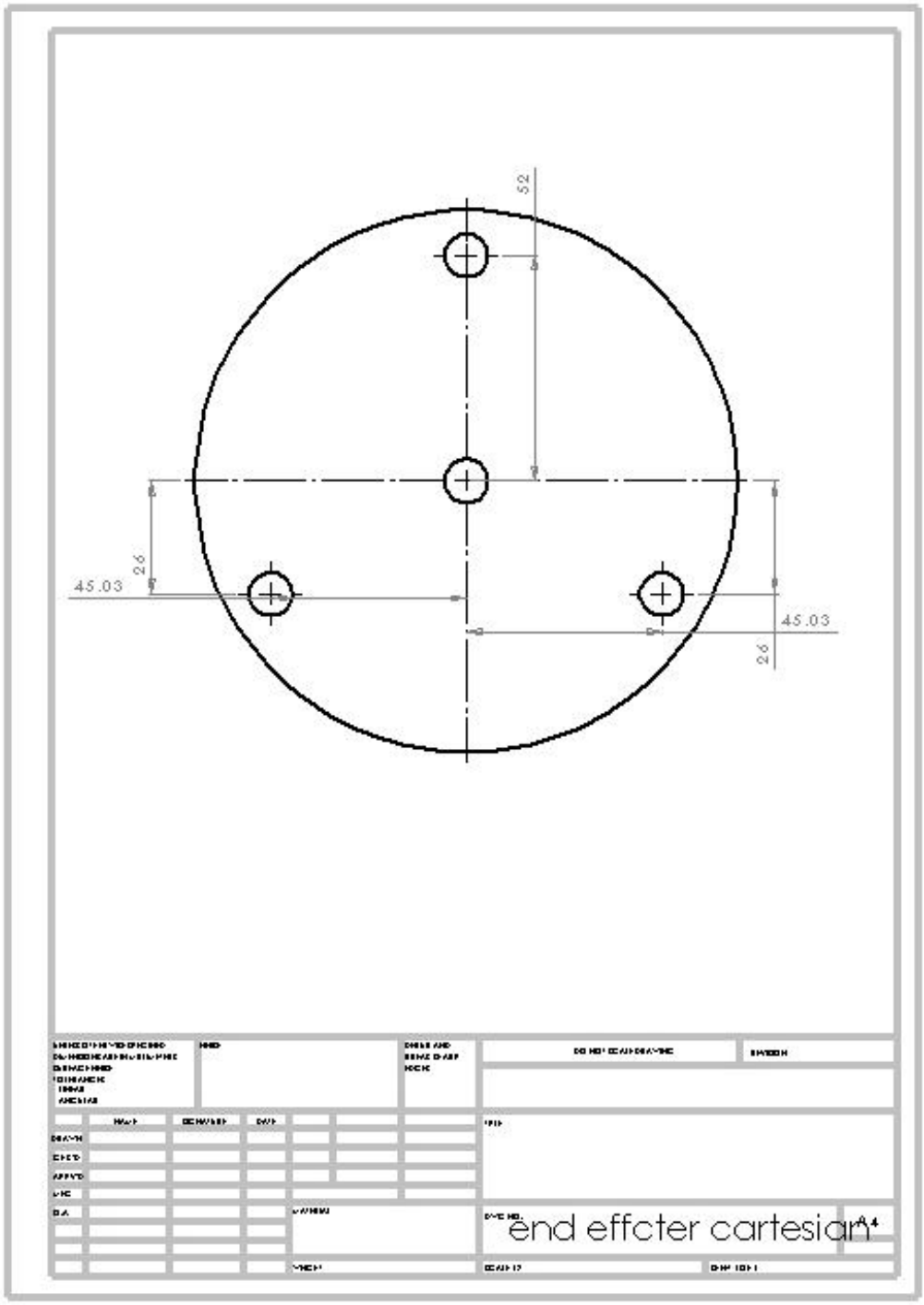
52
45.03
26
45.03
26
end effcter cartesian
A4

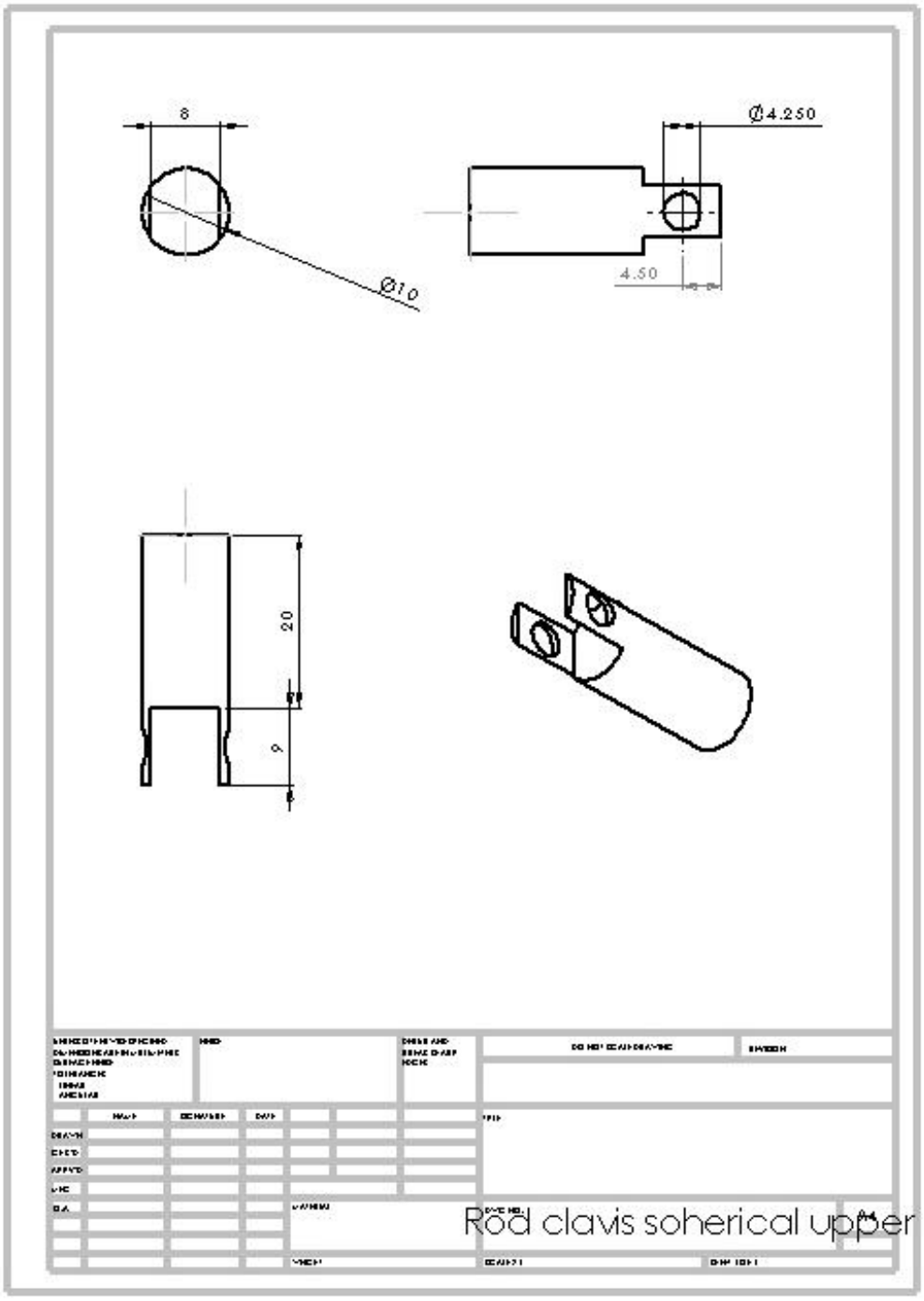
8
Ø10
Ø4.250
4.50
20
9
Rod clavis soherical upper